Vesicular and non-vesicular extracellular small RNAs direct gene silencing in a plant-interacting bacterium

Antinéa Ravet[1§], Jérôme Zervudacki[2,3§], Meenu Singla-Rastogi[1], Magali Charvin[1], Odon Thiebeauld[2], Alvaro L Perez-Quintero[1,4], Lucas Courgeon[1], Adrien Candat[1], Liam Lebeau[1], Antonio Emidio Fortunato[2, 3], Venugopal Mendu[1], Lionel Navarro[1]*.

[1] Institut de Biologie de l'Ecole Normale Supérieure (IBENS), 75005 Paris, France, Centre National de la Recherche Scientifique UMR8197, 75005 Paris France, Institut National de la Santé et de la Recherche Médicale U1024, 75005 Paris, France.

[2] IRT, 46 Rue d'Ulm, 75005 Paris, France.

[3]ENGreen, 21 Zac de Queyries, 33100 Bordeaux, France.

[4] Plant Health Institute of Montpellier (PHIM), University of Montpellier, CIRAD, INRAE, Institut Agro, IRD, Montpellier, France.

[§] These authors contributed equally to the work

*To whom correspondence should be addressed: lionel.navarro@ens.psl.eu

Abstract

Extracellular plant small RNAs (sRNAs) and/or double-stranded RNA (dsRNA) precursors act as triggers of RNAi in interacting filamentous pathogens[1–7]. However, whether any of these extracellular RNA species direct gene silencing in plant-interacting bacteria remains unknown. Here, we show that Arabidopsis transgenic plants expressing sRNAs directed against virulence factors of a *Pseudomonas syringae* strain, reduce its pathogenesis. This Antibacterial Gene Silencing (AGS) phenomenon is directed by Dicer-Like (DCL)-dependent antibacterial sRNAs, but not cognate dsRNA precursors. Three populations of active extracellular sRNAs were recovered in the apoplast of these transgenic plants. The first one is mainly non-vesicular and associated with proteins, whereas the second one is likely located inside Extracellular Vesicles (EVs). Intriguingly, the third population is unbound to proteins and in a dsRNA form, unraveling a novel class of functional extracellular free sRNAs (efsRNAs). Both Arabidopsis transgene- and genome-derived efsRNAs were retrieved inside bacterial cells. Finally, we show that salicylic acid (SA) promotes AGS, and that a substantial set of endogenous efsRNAs exhibits predicted bacterial targets that are down-regulated by SA biogenesis and/or signaling during infection. This study thus unveils an unexpected AGS phenomenon, which may have wider implications in the understanding of how plants regulate transcriptome, microbial community composition and genome evolution of associated bacteria.

Introduction

RNAi is a conserved gene regulatory mechanism that promotes antiviral defense by repressing translation, accumulation and replication of viral RNAs[8]. In plants, RNAi also orchestrates resistance against bacterial, fungal and oomycetal pathogens, partly by fine-tuning the expression of immune-responsive genes[9,10]. The core mechanism of RNAi involves the processing of double-stranded RNAs (dsRNAs) by DCL proteins, leading to the production of

52 20-25 nt long small RNAs (sRNAs). Small RNAs are then loaded into Argonaute (AGO)
53 proteins to direct post-transcriptional silencing of sequence-complementary mRNA targets,
54 through endonucleolytic cleavage and/or translational inhibition[11].

55 An important feature of plant sRNAs is their ability to trigger non-cell autonomous silencing
56 in adjacent cells as well as in distal tissues[12,13]. This phenomenon is essential to prime antiviral
57 response ahead of the infection front, but also to translocate silencing signals between plant
58 cells and their non-viral eukaryotic interacting (micro)organisms[1,14]. For example, plant sRNAs
59 are exported in the fungal pathogens *Verticillium dahliae*[2] and *Botrytis cinerea*[3], as well as in
60 the oomycetal pathogen *Phytophthora capsici*[4], to silence pathogenicity factors. The transfer
61 of sRNAs from plant cells towards *B. cinerea* and *P. capsici* cells is in part mediated by
62 extracellular vesicles (EVs)[1,4,5]. Conversely, fungal sRNAs from *B. cinerea*, and oomycetal
63 sRNAs from *Hyaloperonospora arabidopsidis*, are translocated into plant cells to silence
64 defense genes[15,16]. In addition, some transfer RNA-derived fragments (tRFs), produced by the
65 rhizobium *Bradyrhizobium japonicum*, can silence genes in the soybean *Glycine max* to
66 promote nodulation[17]. However, whether plant sRNAs could be transferred in interacting
67 bacteria, and in turn directly regulate bacterial gene expression, remains elusive.

68 Artificial trans-kingdom RNAi has long been employed to direct Host-Induced Gene Silencing
69 (HIGS), a technology used to characterize the function of virulence genes or to engineer disease
70 resistance in plants[3]. HIGS notably relies on *in planta* expression of dsRNAs bearing
71 homologies to essential and/or virulence genes, and can operate in insects, nematodes, parasitic
72 plants, oomycetes, and fungi[18]. For example, HIGS confers full protection against *Fusarium*
73 *graminearum*[6] and *B. cinerea*[3], a phenotype that can be recapitulated by spraying antifungal
74 dsRNAs and/or sRNAs onto wild-type plants prior to infection. The latter Spray-Induced Gene
75 Silencing (SIGS) phenomenon is reminiscent of environmental RNAi, a process that involves

76 the uptake of RNAs from the environment to trigger RNAi. However, so far, HIGS and SIGS
77 have been shown to be effective in eukaryotic (micro)organisms possessing canonical RNAi
78 factors. Indeed, there is no evidence indicating that the stable *in planta* expression, or the
79 external application, of artificial sRNAs and/or dsRNAs could trigger gene silencing in a plant-
80 interacting bacterium.
81
82 Here, we used the Gram-negative pathogenic bacterium *Pseudomonas syringae* pv. *tomato*
83 strain DC3000 (*Pto* DC3000), and the plant *Arabidopsis thaliana*, as a model interaction
84 system to address these questions. We show that the stable *in planta* expression of an inverted
85 repeat transgene generating sRNAs directed against two *Pto* DC3000 virulence factors can
86 dampen bacterial pathogenesis. Three populations of active extracellular sRNAs were
87 recovered from the apoplastic fluid. The first one is mostly associated with proteins that are
88 located outside PENETRATION1 (PEN1)-positive EVs, while the second one is likely located
89 inside TETRASPANIN8 (TET8)-positive EVs. Intriguingly, the third one is unbound to
90 proteins and exists in a dsRNA form. Importantly, a subset of these artificial extracellular free
91 sRNAs (efsRNAs) was found internalized by *Pto* DC3000 cells. This was also true for
92 endogenous efsRNAs produced from various Arabidopsis genomic origins. Finally, we show
93 that SA promotes AGS activity, and that a substantial set of internalized endogenous sRNAs
94 exhibits sequence-complementarity to *Pto* DC3000 mRNAs, whose cognate protein levels
95 were found down-regulated by SA biogenesis and/or signaling during infection. Overall, this
96 work unveils the vesicular and non-vesicular extracellular sRNAs that are causal for AGS. It
97 also highlights a potential for endogenous plant sRNAs in directly reprogramming gene
98 expression in plant-associated bacteria.
99
100

101 **Results**

102

103 **Stable expression of anti-*cfa6*/*hrpL* sRNAs in Arabidopsis reduces *Pto* DC3000 virulence**

104 *Pto* DC3000 is the causal agent of bacterial speck in tomato and can also infect *Arabidopsis*
105 *thaliana*[18]. This bacterium enters Arabidopsis leaf tissues through stomata, and subsequently
106 reaches the apoplast, where it multiplies at high population levels[19]. Upon detection of *Pto*
107 DC3000, Arabidopsis triggers stomatal closure within an hour of infection, which limits the
108 access of this bacterium into inner leaf tissues[20,21]. As a counter-defense, *Pto* DC3000 actively
109 reopens stomata at 3 hours post-inoculation (hpi), in part, by secreting the phytotoxin
110 coronatine (COR)[19,22]. Accordingly, a *Pto* DC3000 Δ*cfa6* (*Pto*Δ*cfa6*) strain that is deleted in
111 *Cfa6*, a gene encoding a structural component of COR[23], does not trigger stomatal reopening
112 on wild-type Columbia-0 (Col-0) leaf sections at 3 hpi (Fig. 1a). A similar phenotype is
113 observed in response to a *Pto* DC3000 Δ*hrpL* (*Pto*Δ*hrpL*) strain that is deleted in *HrpL* (Fig.
114 1b). The latter gene encodes an alternative sigma factor that directly controls the expression of
115 type III secretion system (TTSS)-associated genes, and indirectly the expression of *COR*
116 biosynthesis genes[24,25]. Both phenotypes are rescued upon exogenous application of COR (Fig.
117 1a, b), indicating that they are caused by the inability of these mutant strains to produce
118 COR[24,25]. Conversely, and as shown previously[20], a normal stomatal reopening phenotype
119 occurs during infection with a type III secretion-defective *Pto* DC3000 Δ*hrcC* mutant
120 (*Pto*Δ*hrcC*) (Fig. 1b).

121

122 Because both *Cfa6* and *HrpL* genes are critical for *Pto* DC3000 pathogenesis, and only
123 expressed during infection[23–25], we reasoned that they represent suitable targets to test the
124 possible occurrence and relevance of AGS. We thus decided to stably express anti-*cfa6* and
125 anti-*hrpL* sRNAs from Arabidopsis and first monitored their possible anti-virulence effects

126 through a stomatal reopening assay. More specifically, we generated Arabidopsis transgenic
127 lines expressing a chimeric inverted repeat, bearing homologies with the coding regions of both
128 *Cfa6* and *HrpL* genes (Fig. 1c). As a negative control, we generated Arabidopsis transgenic
129 lines expressing inverted repeats targeting three cytochrome P450 lanosterol C-14α-
130 demethylase (*CYP51*) genes of the fungus *F. graminearum*[6,7], or the luciferase (*LUC*) reporter
131 gene. All the engineered inverted repeat transgenes were driven by the Cauliflower Mosaic
132 Virus (CaMV) 35S promoter. The resulting stable transgenic lines, respectively referred to as
133 IR-*CFA6/HRPL*, IR-*CYP51* or IR-*LUC*, expressed the cognate engineered artificial sRNAs,
134 and did not exhibit developmental defects compared to Col-0 plants (Supplementary Fig. 1a-
135 c). Small RNA sequencing (sRNA-seq) from the IR-*CFA6/HRPL*#4 reference line revealed
136 typical peaks of 21 and 24 nt endogenous sRNAs mapping to the Col-0 genome
137 (Supplementary Fig. 1d), and a high accumulation of 21 nt anti-*cfa6*/*hrpL* sRNAs (Fig. 1d),
138 which were produced along the *CFA6*/*HRPL* regions of the hairpin (Fig. 1e). Further target
139 prediction analysis of anti-*cfa6*/*hrpL* sRNAs against the Col-0 and *Pto* DC3000 annotated
140 genes, coupled with the analysis of free energy of corresponding sRNA-target pairings,
141 indicated that off-target effects are unlikely (Supplementary Fig. 1e, Supplementary Table 1
142 and 2).
143
144 We further monitored *Pto* DC3000-induced stomatal reopening response in IR-*CFA6/HRPL*
145 transgenic lines. Importantly, these transgenic lines were found insensitive to the stomatal
146 reopening response triggered by *Pto* DC3000 at 3 hpi (Fig. 1f), thereby mimicking the
147 phenotypes observed during infection of Col-0 with the *Pto*Δ*cfa6* or *Pto*Δ*hrpL* strains (Fig. 1a,
148 b). By contrast, the *Pto* DC3000-induced stomatal reopening phenotype was unaltered in the
149 infected IR-*CYP51* and IR-*LUC* lines, compared to Col-0-infected plants (Fig. 1f), supporting
150 a sequence-specific effect. Furthermore, the compromised stomatal reopening phenotypes

151 detected in three independent IR-*CFA6/HRPL*-infected lines were rescued upon exogenous
152 application of COR (Fig. 1g). Therefore, these phenotypes are presumably caused by an altered
153 ability of the leaf-associated and/or surrounding *Pto* DC3000 cells to produce COR.
154
155 We next reasoned that, by suppressing stomatal reopening, anti-*cfa6*/*hrpL* sRNAs would limit
156 the entry of *Pto* DC3000 into leaf tissues, and consequently reduce its apoplastic colonization.
157 To test this, we dip-inoculated Col-0, IR-*CYP51* and three independent IR-*CFA6/HRPL* lines
158 with *Pto* DC3000 and monitored bacterial titers in those plants. It is noteworthy that *Pto*
159 DC3000 infection did not alter the accumulation of anti-*cfa6*/*hrpL* in these conditions
160 (Supplementary Fig. 1f). We found that *Pto* DC3000 was less effective in colonizing the
161 apoplast of IR-*CFA6/HRPL* lines compared to Col-0- and IR-*CYP51*-infected plants, thereby
162 mimicking the growth defect of *Pto*Δ*cfa6* on Col-0 plants (Fig. 1h). Altogether, these data
163 indicate that the expression of sRNAs directed against *Cfa6* and *HrpL* genes in Arabidopsis
164 plants can reduce the virulence functions of *Pto* DC3000 during infection.
165
166 **Antibacterial sRNAs, but not cognate dsRNA precursors, are biologically active**
167 To get a first insight into the active RNA entities responsible for AGS, we introduced the *dcl2-*
168 *1*, *dcl3-1* and *dcl4-2* mutations in a reference line expressing an IR-*HRPL* inverted repeat under
169 the control of the constitutive Ubi.U4 promoter[26]. It is noteworthy that this promoter was used
170 here, instead of the 35S promoter, to prevent co-suppression effect caused by the presence of
171 35S copies in the T-DNA insertional mutant lines[27,28]. A drastic reduction in the accumulation
172 of anti-*hrpL* sRNAs was observed in Ubi.U4::IR-*HRPL dcl234* compared to Ubi.U4::IR-*HRPL*
173 control plants, as revealed by northern blot analysis (Fig. 2a, left panel). Furthermore,
174 unprocessed forms of IR-*HRPL* precursors accumulated in Ubi.U4::IR-*HRPL dcl234* plants,
175 while they were barely detectable in the Ubi.U4::IR-*HRPL* parental line (Fig. 2a, right panel).

176 Collectively, these data support a DCL-dependent processing of *HRPL* dsRNAs into anti-*hrpL*
177 siRNAs. Importantly, when the Ubi.U4::IR-*HRPL dcl234* plants were used in a stomatal
178 reopening assay, we found that *Pto* DC3000 triggered a normal stomatal reopening phenotype,
179 similar to the effect observed in Col-0 and *dcl234* control plants (Fig. 2b). By contrast, a full
180 suppression of stomatal reopening events was achieved in the Ubi.U4::IR-*HRPL* reference line
181 (Fig. 2b), which produces abundant anti-*hrpL* sRNAs (Fig. 2a). Collectively, these data
182 provided evidence that long *HRPL* dsRNAs are unlikely responsible for the anti-virulence
183 effect, and rather suggested that sRNA species are the RNA entities responsible for AGS. To
184 further test this assumption, we decided to establish a semi-*in vitro* assay. Col-0 leaf sections
185 were pre-treated with IR-*CFA6*/*HRPL*#4 total RNA extracts for one hour and were
186 subsequently challenged with *Pto* DC3000, following which the stomatal aperture events were
187 monitored at 3 hpi. A full suppression of the *Pto* DC3000-induced stomatal aperture was
188 detected in response to these RNA extracts (Fig. 2c). However, the stomatal reopening
189 phenotype remained unaltered in response to RNA extracts derived from Col-0, IR-*CYP51* and
190 IR-*LUC* plants, supporting sequence-specificity (Fig. 2c). Therefore, the pretreatment of IR-
191 *CFA6*/*HRPL*#4 RNA extracts on Col-0 leaf sections recapitulates the anti-virulence effect
192 achieved by IR-*CFA6*/*HRPL*#4 leaf sections (Fig. 1f, g). We further conducted size separation
193 of the IR-*CFA6*/*HRPL*#4 total RNA extracts and tested the activities of the resulting RNA
194 fractions. The long RNA fraction (>200 nt), which presumably contains long *CFA6*/*HRPL*
195 dsRNAs, did not suppress *Pto* DC3000-triggered stomatal reopening (Fig. 2d; Supplementary
196 Fig. 2a, b). In contrast, the small RNA fraction (<200 nt), likely containing anti-*cfa6*/*hrpL*
197 sRNAs, was as active as IR-*CFA6*/*HRPL*#4 total RNA extracts (Fig. 2d). Collectively, these
198 data indicate that anti-*cfa6*/*hrpL* sRNAs must be the active RNA entities from the IR-
199 *CFA6*/*HRPL*#4 total RNA extracts. To confirm this, we made use of the viral protein p19,
200 whose property is to selectively bind sRNA duplexes[29,30]. Chitin magnetic beads coated with

201 p19 proteins were incubated with total RNA extracts from IR-*LUC* and IR-*CFA6/HRPL*#4
202 plants. The eluted bound sRNA duplexes were subsequently analyzed by northern blot. Large
203 amounts of pulled-down anti-*cfa6/hrpL* sRNAs, and anti-*luc* control sRNAs, were detected
204 through this approach (Fig. 2e). Bound sRNA species were mostly 21 nt in length, which is
205 consistent with the high affinity of p19 for 21 nt sRNA duplexes[29]. Importantly, pulled-down
206 anti-*cfa6*/*hrpL* sRNAs were fully capable of suppressing stomatal reopening, such as IR-
207 *CFA6*/*HRPL*#4 total RNA extracts (Fig. 2f). In contrast, the pulled-down anti-*luc* sRNAs were
208 found inactive (Fig. 2f). These data further support that anti-*cfa6*/*hrpL* sRNA duplexes, but not
209 anti-*luc* sRNAs, harbour anti-virulence activity against *Pto* DC3000. We finally synthesized
210 *CFA6*/*HRPL* dsRNAs and anti-*cfa6*/*hrpL* sRNA duplexes *in vitro* (Fig. 2g), and tested their
211 activities. *In vitro*-synthesized *CFA6/HRPL* dsRNAs did not alter the ability of *Pto* DC3000 to
212 reopen stomata, nor did *CYP51* control dsRNAs (Fig. 2h). In contrast, *in vitro*-synthesized anti-
213 *cfa6/hrpL* sRNAs suppressed stomatal reopening events, which was not the case with anti-
214 *cyp51* sRNAs (Fig. 2h). Altogether, these data provide solid evidence that sRNAs, but not their
215 unprocessed dsRNA precursors, are biologically active.
216
217 **Anti-*hrpL* sRNAs are causal for the suppression of stomatal reopening**
218 Although the above findings indicate that anti-*cfa6*/*hrpL* sRNAs are effective against *Pto*
219 DC3000, they do not firmly demonstrate that they are causal for this phenomenon. To address
220 this, we expressed, in the *Pto*Δ*hrpL* mutant, either a WT *HrpL* transgene or a mutated (mut
221 *HrpL*) version that contains as many silent mutations as possible in the sRNA targeted region
222 (Fig. 3a, b). These mutations are expected to alter the binding of anti-*hrpL* sRNAs, as revealed
223 by just a few predicted sRNA-mut *HrpL* interactions, whose free energy mean was higher
224 compared to the one of the numerous sRNA-*HrpL* interactions (Fig. 3c, Supplementary Table
225 3). Both transgenes were expressed under the constitutive neomycin phosphotransferase II

226 (*NPTII*) promoter (Fig. 3a). The resulting recombinant bacteria, referred to here as *Pto*Δ*hrpL*
227 WT *HrpL* and *Pto*Δ*hrpL* mut *HrpL*, restored the ability of *Pto*Δ*hrpL* strain to trigger the
228 reopening of stomata (Fig. 3d), indicating that both transgenes are functional in a stomatal
229 reopening assay. To assess the specific effect of sRNAs towards suppression of *HrpL*-mediated
230 stomatal aperture, we generated two independent Arabidopsis 35S::IR-*HRPL* transgenic lines,
231 referred to as IR-*HRPL*#1 and #4. These lines overexpressed anti-*hrpL* sRNAs (Supplementary
232 Fig. 3), and, expectedly, suppressed the ability of *Pto* DC3000 to reopen stomata (Fig. 3e).
233 Similar results were obtained in response to *Pto*Δ*hrpL* WT *HrpL* (Fig. 3e), supporting a
234 sensitivity of this bacterial strain to sRNA action. By contrast, the *Pto*Δ*hrpL* mut *HrpL* strain
235 was fully competent in reopening the stomata (Fig. 3e), indicating that anti-*hrpL* sRNAs no
236 longer exert their anti-virulence effects towards this bacterium. Altogether, these data
237 demonstrate that anti-*hrpL* sRNAs are causal for the suppression of *HrpL*-mediated stomatal
238 reopening function.
239
240 **Active apoplastic particles that co-purify with PEN1-positive EVs are likely composed of**
241 **protein-bound anti-*cfa6*/*hrpL* sRNAs located outside these EVs**
242 Since apoplastic EVs were previously shown to contribute to the trafficking of plant sRNAs
243 towards fungal and oomycetal pathogens[1,4], we investigated whether they could similarly
244 participate in the transfer of active sRNAs from Arabidopsis towards *Pto* DC3000. Two main
245 categories of plant EVs have been characterized so far. The first one is composed of vesicles
246 that are heterogenous in size, and that are notably marked by PEN1[31]. The second one, which
247 is required for the transfer of active sRNAs from Arabidopsis towards *B. cinerea*[1,5], is
248 composed of smaller EVs, which are less heterogenous in size, and that are marked by TET8[1].
249 We first characterized the APF fraction from IR-*CFA6*/*HRPL*#4 plants co-purified with PEN1-
250 positive EVs. To do so, we vacuum-infiltrated IR-*CFA6*/*HRPL*#4 plants with Vesicle-Isolation

251 Buffer (VIB, see methods), and further collected the apoplastic fluids (APFs) by low-speed
252 centrifugation (at 900 g for 15 min, at 4°C). To remove dead cells and cell debris, these APFs
253 were filtered (using a 0.2 µm filter), and the resulting filtered APFs further subjected to
254 ultracentrifugation (at 40,000 g for 60 min, at 4 °C), using a swing-out rotor (TST41.14).
255 Nanoparticle tracking analysis (NTA) from the recovered "P40" pellets revealed the presence
256 of particles in a size range between 50 to 400 nm (Supplementary Fig. 4a). Transmission
257 Electron Microscopy (TEM) further unveiled particles exhibiting a cup-shaped structure and/or
258 a round vesicle-like morphology, as previously described[32], and their diameters ranged between
259 16 to 409 nm with a mean of 90 nm +/- 4 nm (Supplementary Fig. 4b, c). Furthermore, and as
260 previously shown[31], the EV markers PEN1 and PEN3 were readily detected in these P40 pellets
261 (Supplementary Fig. 4d). Endogenous sRNAs sequenced from these APF fractions were
262 mostly composed of tiny RNAs (tyRNAs; 10-17 nt), and were deprived of typical 21 and 24 nt
263 peaks (Supplementary Fig. 4e)[33,34]. The sRNAs that mapped to the IR-*CFA6*/*HRPL* hairpin
264 were composed of both 21 nt sRNAs and tyRNAs (Fig. 4a), and their accumulation profiles
265 along the *CFA6*/*HRPL* regions of the hairpin were distinct from the ones of total sRNAs (Fig.
266 1e, 4b). The latter observation suggests that extracellular sRNAs are either selectively released
267 in this apoplastic fraction, and/or stabilized by specific RNA-binding proteins, as previously
268 proposed[5,34]. Furthermore, these anti-*cfa6*/*hrpL* sRNAs are unlikely derived from degraded
269 cells and/or debris from IR-*CFA6*/*HRPL*#4 leaves, because we were unable to detect the U6
270 small nuclear RNA (snRNA) in the P40 fractions (Fig. 4c), which is readily detectable from
271 total RNAs (Fig. 2a, e; Supplementary Fig. 1b, c, f; Supplementary Fig. 3).
272
273 We next investigated whether the anti-*cfa6*/*hrpL* sRNAs from the P40 pellets could be
274 functional. To this end, we made use of the previously described semi-*in vitro* stomatal
275 reopening assay (Fig. 2), performed here with P40 pellets instead of RNAs. The P40 pellets

276 from IR-*CFA6*/*HRPL*#4 APFs suppressed stomatal reopening triggered by *Pto* DC3000,
277 compared to the P40 pellets from IR-*CYP51* APFs (Fig. 4d). This response was also detected
278 upon incubation with the P40 pellets of IR-*HRPL*#4 APFs, but was almost fully abolished in
279 the presence of *Pto*Δ*hrpL* mut *HrpL*, but not *Pto*Δ*hrpL* WT *HrpL* (Supplementary 4f).
280 Collectively, these data not only provide evidence that anti-*cfa6*/*hrpL* sRNAs from the P40
281 pellets are biologically active, but also that the population of anti-*hrpL* sRNAs operates in a
282 sequence-specific manner in *Pto* DC3000 cells.
283
284 The Arabidopsis apoplastic P40 pellets are composed of a mixture of particles, including
285 PEN1-positive EVs[34]. To determine in which particles the active anti-*cfa6*/*hrpL* sRNAs could
286 be present, we subjected the P40 pellets from IR-*CYP51* and IR-*CFA6*/*HRPL*#4 APFs to
287 different enzymatic treatments and subsequently monitored their activities. It is noteworthy
288 that none of these enzymatic treatments alters the morphology, the concentration nor the size
289 distribution of apoplastic EVs (Supplementary Fig. 4a-c). The micrococcal nuclease (MNase)
290 treatment, which degrades unprotected RNAs that are outside EVs and/or in contact with EVs,
291 did not affect the ability of the P40 pellets to suppress stomatal reopening, nor the accumulation
292 of anti-*cfa6*/*hrpL* sRNAs, as revealed by northern blot analysis (Fig. 4c, d). These data
293 suggested that the active anti-*cfa6*/*hrpL* sRNAs from the P40 pellets are either inside EVs
294 and/or outside EVs but associated with proteins, and thus protected from MNase-mediated
295 degradation. Consistent with the latter hypothesis, we found that the combined MNase and
296 Proteinase K treatment led to a decrease in the accumulation of anti-*cfa6*/*hrpL* sRNAs, and
297 almost fully suppressed *Pto* DC3000-induced stomatal reopening (Fig. 4c, d; Supplementary
298 Fig. 4g). An extra Triton X-100 (TX100) treatment, which disrupts EVs integrity[31], led to an
299 enhanced reduction in anti-*cfa6*/*hrpL* sRNA levels (Fig. 4e). This suggests the additional
300 presence of intravesicular anti-*cfa6*/*hrpL* sRNAs that might mildly contribute to AGS.

301 Altogether, these data indicate that active anti-*cfa6*/*hrpL* sRNAs from the P40 pellets are
302 mainly associated with proteins that are located outside PEN1-positive EVs.
303
304 **The apoplasic fraction that co-purifies with TET8-positive EVs contains active anti-**
305 ***cfa6*/*hrpL* sRNAs that are mainly located inside EVs**
306 We next characterized the APF fraction from IR-*CFA6*/*HRPL*#4 plants co-purifying with
307 TET8-positive EVs. To this end, we collected the supernatants from the above P40 pellets and
308 subjected them to ultracentrifugation (at 100 000 g for 60 min, at 4°C), using the same swing-
309 out rotor. The resulting "P100-P40" pellets were subsequently washed and analyzed
310 microscopically, molecularly and functionally. An immunogold labeling approach, using
311 native antibody recognizing the large extravesicular loop (the EC2 domain) of TET8 and a
312 secondary antibody coating gold beads, confirmed the presence of TET8-positive EVs in these
313 P100-P40 pellets (Fig. 5a). It is noteworthy that this subclass of EVs represented 22% of the
314 whole vesicles analyzed from these APF fractions (Supplementary Fig. 5a). By contrast, none
315 of the EVs from the P100-P40 fractions analyzed were labeled with an anti-UGPase antibody
316 (Fig. 5a), indicating that the immunogold staining of TET8-positive EVs is specific. We next
317 sequenced sRNAs from the P100-P40 pellets of IR-*CFA6*/*HRPL*#4 APFs. As observed with
318 P40 pellets, endogenous sRNAs sequenced from P100-P40 pellets were mostly composed of
319 tyRNAs (Supplementary Fig. 5b). Furthermore, the sRNAs that mapped to the *CFA6*/*HRPL*
320 inverted repeat were composed of 21 nt sRNAs and tyRNAs (Fig. 5b), and their accumulation
321 profiles along the *CFA6*/*HRPL* regions of the hairpin were distinct from the ones of total
322 sRNAs (Fig. 1e, Fig. 5c). As previously observed with P40 fractions (Fig. 4c), we were unable
323 to detect U6 snRNA from P100-P40 fractions (Fig. 5d), indicating that the detected anti-
324 *cfa6*/*hrpL* sRNAs are unlikely derived from degraded cells and/or debris from IR-
325 *CFA6*/*HRPL*#4 leaves.

326

327 We further subjected the P100-P40 pellets from IR-*CFA6*/*HRPL*#4 APFs to different
328 enzymatic treatments and monitored their activities. Of note, none of these enzymatic
329 treatments markedly alter the size distribution of EVs from these APF fractions, as revealed by
330 TEM analysis (Supplementary Fig. 5c). Interestingly, in contrast with the results obtained with
331 P40 pellets, the combined MNase and Proteinase K treatment did not alter the biological
332 activity of P100-P40 pellets (Fig. 4d, 5e), nor the treatments with MNase or Proteinase K alone
333 (Supplementary Fig. 5d, e). The former combined treatment did not markedly alter the
334 accumulation of anti-*cfa6*/*hrpL* sRNAs either (Fig. 5d). These data indicate that anti-virulence
335 sRNAs from the P100-P40 pellets are protected from enzymatic degradation. They also suggest
336 that these active sRNAs are possibly protected inside the lumen of EVs from this APF fraction.
337 Consistent with this hypothesis, we found that a triple treatment with MNase, Proteinase K and
338 TX100, strongly altered the accumulation of anti-*cfa6*/*hrpL* sRNAs (Fig. 5d). In addition, it
339 fully abolished the ability of the IR-*CFA6*/*HRPL*#4 P100-P40 pellets to suppress *Pto* DC3000-
340 induced stomatal reopening (Fig. 5e). Altogether, these data demonstrate that the APF fraction
341 co-purifying with TET8-positive EVs contains active antibacterial sRNAs that are likely
342 located inside EVs.

343

344 **The apoplastic fraction exhibiting a substantial reduction in EVs is composed of active**
345 **extracellular free sRNAs**

346 We next investigated whether active anti-*cfa6*/*hrpL* sRNAs could additionally be present in the
347 APF fraction that does not co-purify with EVs. For this purpose, we collected the supernatants
348 from the above P100-P40 pellets. The recovered SN fractions exhibited a substantial reduction
349 in canonical extracellular particles, as observed by NTA (Supplementary Fig. 6a), and were
350 notably deprived of the PEN1 and PEN3 markers (Supplementary Fig. 4d). RNAs from the SN

351 fraction of IR-*CFA6/HRPL*#4 APFs were further precipitated and subjected to sRNA-seq.
352 Small RNAs that mapped to the Col-0 genome were almost exclusively composed of tyRNAs
353 (Supplementary Fig. 6b). Anti-*cfa6*/*hrpL* sRNAs were represented by small amounts of 21 nt
354 sRNAs and large amounts of tyRNAs (Fig. 6a). However, a more pronounced accumulation of
355 21 nt anti-*cfa6*/*hrpL* sRNAs, compared to cognate tyRNAs, was detected by northern blot
356 analysis (Fig. 6b, Supplementary Fig. 6c). This suggests that biases occurring during sRNA
357 library preparation (e.g. adapter ligation), coupled with yet-unknown post-transcriptional
358 sRNA modifications, might hamper the retrieval of all 21 nt long anti-*cfa6*/*hrpL* sRNAs from
359 these SN fractions. As observed for P40 and P100-P40 fractions, we also found that the
360 accumulation profiles of SN-derived anti-*cfa6*/*hrpL* along the *CFA6*/*HRPL* regions of the
361 hairpin were different from the ones of total sRNAs (Fig. 1e; Fig. 6b). Furthermore, we were
362 unable to detect U6 snRNA from SN fractions (Fig. 6b), indicating that the detected anti-
363 *cfa6*/*hrpL* sRNAs are unlikely derived from degraded cells and/or debris from IR-
364 *CFA6*/*HRPL*#4 leaves.
365
366 We further monitored the activity of the SN fraction from IR-*CFA6*/*HRPL*#4 APFs. This APF
367 fraction was found to suppress stomatal aperture triggered by *Pto* DC3000, compared to the
368 one derived from IR-*CYP51* plants (Fig. 6d). The same phenotype was detected in response to
369 the SN fraction from IR-*HRPL*#4 APFs, but was impaired in the presence of *Pto*Δ*hrpL* mut
370 *HrpL*, but not *Pto*Δ*hrpL* WT *HrpL* (Supplementary Fig. 6d). Collectively, these data indicate
371 that anti-*cfa6*/*hrpL* sRNAs in the SN fraction are biologically active and that anti-*hrpL* sRNAs
372 function in a sequence-specific manner in *Pto* DC3000 cells. To characterize in more depth the
373 active sRNAs from the IR-*CFA6*/*HRPL*#4 SN fraction, we treated it with MNase or Proteinase
374 K, and subsequently monitored its activity. The Proteinase K treatment did not alter the *Pto*
375 DC3000-induced stomatal reopening phenotype (Fig. 6d), despite a substantial decrease in the

376 accumulation of ~21 nt anti-*cfa6*/*hrpL* sRNAs, and of the control microRNA miR167-5p
377 (Supplementary Fig. 6c). Collectively, these results indicate that the majority of ~21 nt anti-
378 *cfa6*/*hrpL* sRNAs from the SN fraction is associated with proteins and not functional. To our
379 surprise, we found that the MNase treatment alone fully abolished the ability of the IR-
380 *CFA6*/*HRPL*#4 SN fraction to suppress *Pto* DC3000-induced stomatal reopening (Fig. 6d).
381 Nevertheless, we were unable to detect, at the resolution of northern blot analysis, a significant
382 decrease in the accumulation of anti-*cfa6*/*hrpL* sRNAs upon MNase treatment (Supplementary
383 Fig. 6c). This effect was not due to a partial efficacy of the MNase treatment on sRNAs,
384 because a full degradation of anti-*cfa6*/*hrpL* sRNAs was observed when RNA extracts from
385 IR-*CFA6*/*HRPL*#4 plants were treated with this enzyme (Supplementary Fig. 6e). Collectively,
386 these data suggest that a low-abundant pool of active anti-*cfa6*/*hrpL* sRNAs, and/or discrete
387 sRNA species from the IR-*CFA6*/*HRPL* hairpin, must be unbound to proteins in the SN
388 fraction, and thus sensitive to MNase action. We named these novel and functional extracellular
389 sRNA species "extracellular free sRNAs" or efsRNAs.
390
391 **Anti-*cfa6*/*hrpL* efsRNA duplexes are recovered in the apoplast and are biologically active**
392 The fact that i) anti-*cfa6*/*hrpL* duplexes, purified from IR-*CFA6*/*HRPL*#4 plants or *in vitro*-
393 synthesized, were found functional (Fig. 2e-h), and ii) sRNA duplexes are typically more stable
394 than single-stranded RNAs[35], prompted us to investigate whether active anti-*cfa6*/*hrpL*
395 efsRNA duplexes could be present in the apoplast. To purify sRNA duplexes from SN
396 fractions, p19-chitin magnetic beads were incubated with the SN fractions from IR-*LUC* and
397 IR-*CFA6/HRPL*#4 APFs, and the eluted bound sRNA duplexes were further analyzed by
398 northern blot. We consistently retrieved comparable amounts of anti-*cfa6*/*hrpL* and anti-*luc*
399 sRNAs in the p19 pulled-down RNAs from IR-*CFA6/HRPL*#4 and IR-*LUC* SN fractions,
400 respectively (Fig. 6b). These data demonstrate the presence of both anti-*cfa6*/*hrpL* and anti-*luc*

401 efsRNA duplexes in these APF fractions. Importantly, the p19 pulled-down sRNAs from the
402 IR-*CFA6/HRPL*#4 SN fraction specifically suppressed the ability of *Pto* DC3000 to reopen
403 stomata, to the same extent as total sRNAs from this apoplastic fraction (Fig. 6e). Collectively,
404 these data provide evidence that the SN fraction of IR-*CFA6/HRPL*#4 APFs contains active
405 efsRNAs, which are, at least in part, in a free and dsRNA form.
406
407 **A subset of SN-derived anti-*hrpL* sRNAs, including a functional 21 nt sRNA, is**
408 **internalized by *Pto* DC3000 cells**
409 Although anti-*hrpL* efsRNAs were found to be causal for AGS (Supplementary Fig. 6d), it was
410 not experimentally shown whether they could be transferred in the cytoplasm of *Pto* DC3000
411 cells. To test this, we incubated *Pto* DC3000 cells with SN fractions from IR-*CFA6/HRPL*#4
412 APFs for 2 hours. Bacterial cells were further collected, and their outer membrane lysed using
413 a buffer containing Ethylenediaminetetraacetic acid (EDTA) prior to washing and RNA
414 isolation (Fig. 7a)[36]. This stringent condition ensured that sRNAs adhering onto the bacterial
415 surface were removed from our samples. Consistent with an effective degradation of the
416 bacterial outer membrane, the EDTA treatment substantially increased the uptake of propidium
417 iodide in *Pto* DC3000 cells (Supplementary Fig. 7a). Nevertheless, it also altered *Pto* DC3000
418 survival (Supplementary Fig. 7b), which could account for an under-representation of
419 sequenced sRNAs inside bacterial cells. We then prepared sRNA sequencing libraries
420 corresponding to mock- and SN-treated conditions. To retrieve anti-*hrpL* sRNAs that were
421 specifically derived from these SN fractions, rather than from bacterial *hrpL* transcripts (e.g.
422 RNA degradation products), we established a first bioinformatic filter. Briefly, this filter only
423 keeps reads that were not present in the control samples, which were untreated with SN
424 fractions. In comparison to anti-*hrpL* sRNAs derived from the SN fractions of IR-
425 *CFA6*/*HRPL*#4 APFs (Fig. 6a), an over-representation of tyRNAs, in a 10-12 nt size window,

426 was recovered inside *Pto* DC3000 (Fig. 7b, c). This suggests that *Pto* DC3000 either
427 preferentially takes-up tyRNAs and/or that longer sRNAs are internalized by *Pto* DC3000 and
428 further processed inside this bacterium. Nevertheless, we still detected a small peak of 21 nt
429 long sRNAs that was constantly observed across the biological replicates (Fig. 7c). We further
430 isolated the most represented 21 nt anti-*hrpL* internalized sequence in both replicates, and
431 chemically-synthesized the corresponding sRNA duplex labeled with the fluorescent dye
432 ATT0 565, positioned on the 5' end of the sRNA strand that is complementary to the *HrpL*
433 mRNA sequence (Fig. 7d, Supplementary Fig. 7c). Furthermore, because active anti-*hrpL*
434 sRNAs were found to be dependent on DCLs for their biogenesis (Fig. 2a, b), we designed this
435 synthetic sRNA duplex with 2 nt-3' overhangs, to mimic a DCL product (Fig. 7d,
436 Supplementary Fig. 7c). Confocal imaging of *Pto* DC3000-GFP cells incubated with this
437 ATTO 565-labeled anti-*hrpL* sRNA duplex, confirmed its internalization by, and/or association
438 with, bacterial cells (Fig. 7e, white arrows). Importantly, the cognate unlabeled sRNA duplex
439 (WT *hrpL*) exhibited full functionality in a stomatal reopening assay, which was not the case
440 of its cognate mutated version (mut *hrpL*), which behaved as a non-functional anti-*cyp51* sRNA
441 duplex control (Fig. 7f). Altogether, these data demonstrate that anti-*hrpL* sRNAs are
442 transferred from the SN fractions of IR-*CFA6*/*HRPL*#4 APFs to the cytoplasm of *Pto* DC3000
443 cells. They also show that a chemically-synthesized 21 nt sRNA duplex, corresponding to a
444 *bona fide* internalized anti-*hrpL* sRNA, is functional inside *Pto* DC3000.
445
446 **Salicylic acid-treated IR-*CFA6*/*HRPL* plants trigger silencing of *HrpL* in *Pto* DC3000 cells**
447 To monitor the silencing effect of anti-*hrpL* sRNAs on the *HrpL* target, we developed an
448 experimental set-up, whereby *Pto* DC3000 cells expressing an epitope-tagged version of *hrpL*
449 were exposed to extra-cellular/organismal sRNAs from IR-*CFA6*/*HRPL*#4 leaf sections (Fig.
450 8a). These conditions are reminiscent of the ones used in the stomatal reopening assay (Fig.

451 1f), with the exception that IR-*CFA6*/*HRPL*#4 plants were pre-treated with SA. It is noteworthy
452 that SA promotes the expression and/or activity of RNAi factors[37–43], as well as the release of
453 Arabidopsis EVs, and of silencing factors, in the apoplast[31], and was thus included here to
454 eventually optimize the silencing effect mediated by anti-*hrpL* sRNAs. More specifically, IR-
455 *CYP51* and IR-*CFA6/HRPL*#4 plants were pre-treated 48 hours before incubation with either
456 mock or SA, and the corresponding leaf sections were further challenged for 2 hours with the
457 *Pto* DC3000 strain expressing a functional C-terminal FLAG-tagged version of *hrpL* under its
458 native promoter (Fig. 8a)[44]. The mRNA and protein levels produced by *HrpL* were
459 subsequently monitored by RT-qPCR and western blot analyses, respectively. With this assay,
460 we did not observe a consistent and significant decrease in the accumulation of *HrpL* mRNAs
461 across different biological replicates, upon incubation of bacterial cells with mock or SA-
462 pretreated IR-*CFA6*/*HRPL*#4 leaves (Supplementary Fig. 8). On the contrary, although leaf
463 sections from IR-*CYP51* plants pretreated with SA exhibited a negative effect on HrpL protein
464 accumulation, a more substantial reduction was always detected in the presence of IR-
465 *CFA6/HRPL*#4 leaves treated in the same condition (Fig. 8b, c). Altogether, these data
466 demonstrate that leaf sections of IR-*CFA6/HRPL*#4 plants pretreated with SA trigger the
467 silencing of *HrpL* in *Pto* DC3000 cells. They also indicate that SA enhances HIGS efficacy
468 from stable transgenic plants expressing antibacterial sRNAs.
469

470 **Endogenous sRNAs, from various genomic origins, are internalized by *Pto* DC3000 and**
471 **exhibit predicted targets, some of which being repressed by SA biogenesis/signaling**

472 We next assessed the potential contribution of endogenous Arabidopsis extracellular sRNAs
473 on the targeting, and possibly silencing, of *Pto* DC3000 genes. To identify the putative *Pto*
474 DC3000 targets of Arabidopsis sRNAs, we focused our analysis on SN-derived sRNAs that
475 were found internalized by *Pto* DC3000 cells. For this purpose, we established a second

476 bioinformatic filter, designed to retrieve, exclusively, Arabidopsis sRNAs inside *Pto* DC3000.
477 Briefly, the sRNA sequences recovered from our first filter were selected, and those exhibiting
478 multimapping between the Arabidopsis TAIR10 reference genome and the *Pto* DC3000
479 genome, further discarded. The size distribution analysis of these stringently filtered sRNAs
480 unveils a majority of tyRNAs, which were derived from various genomic origins (Fig. 9a, b).
481 This observation is consistent with an over-representation of this sRNA category from the SN-
482 derived sRNAs mapping to the Arabidopsis genome (Supplementary Fig. 6b). It might
483 additionally involve a further processing of SN-derived sRNAs inside bacterial cells. In
484 agreement with the results obtained on transgenic lines expressing the artificial inverted repeat
485 *CFA6*/*HRPL*, sRNAs produced from two well-described endogenous inverted repeats, namely
486 IR71 and IR2039[45], were also retrieved inside *Pto* DC3000 (Fig. 9b-f). However, in this case,
487 only tyRNAs were recovered (Fig. 9c, d). The remaining internalized endogenous sRNAs were
488 produced from other genomic regions, including mRNAs, transposable elements (TEs), rRNAs
489 and tRNAs (Fig. 9b). In addition, because plant and mammalian tRNA-derived sRNAs
490 (tsRNAs) i) are commonly retrieved in extracellular compartments and biofluids [33,34,46,47], and
491 ii) have recently been shown to be transferred bidirectionally between host and microbes[17,48–
492 52], we investigated whether Arabidopsis tsRNAs could be part of the most represented sRNAs
493 inside *Pto* DC3000. To do so, we extracted the top 100 most represented internalized sRNA
494 sequences that are over 17 nt long in both replicates and examined the Arabidopsis tRNA
495 database tRex[53], for the presence of tsRNAs. We found that some of the top over-represented
496 sRNA sequences are tRFs, derived from various tRNA precursors, including ProAGG.17 (Fig.
497 9g). Furthermore, we noticed that the corresponding tRF sequence displays plausible sequence-
498 complementary targets in *Pto* DC3000 (Fig. 9h). Therefore, some Arabidopsis tRFs are taken-
499 up by *Pto* DC3000 and exhibit a potential for targeting transcripts in this bacterium.
500

501 Finally, because SA was found here to promote AGS (Fig. 8), we analyzed whether SA
502 biogenesis and/or signaling contribute to the possible silencing of sRNA predicted targets in
503 *Pto* DC3000. To do so, we made use of *Pto* DC3000 proteomic datasets generated from
504 infected Col-0, the SA biogenesis mutant *sid2*, the SA signaling mutant *pad4*, and the double
505 *sid2 pad4* mutant[54]. By cross-referencing the list of predicted *Pto* DC3000 targets from the
506 whole set of internalized sRNAs, with the one of SA-responsive proteins, we found that 209
507 (68.1%), 213 (69.4%), 214 (69.7%), out of the 307 SA-responsive predicated sRNA targets,
508 were less expressed in Col-infected plants compared to *sid2*-, *pad4*- and *sid2 pad4*-infected
509 plants, respectively (Fig. 9i, Supplementary Table 4). A similar proportion of under-expressed
510 targets, represented by 63.6% in Col-0 vs. *sid2*, 68.2% in Col-0 vs. *pad4* and 68.2% in Col-0
511 vs. *sid2 pad4*, was observed when the same analysis was performed on the predicted targets of
512 the top 100 most represented internalized sRNAs, which are above 17 nt in size (Fig. 9j).
513 Among those, we recovered functionally relevant *Pto* DC3000 genes, whose cognate mRNAs
514 exhibit plausible Watson-Crick base-pairing with specific internalized sRNAs, including the
515 type III effector HopE1, TonB dependent siderophore receptors, a type I restriction-modifying
516 enzyme as well as the cell division-related gene *ftsk* (Fig. 9k). Altogether, these data indicate
517 that the uptake of sRNAs by *Pto* DC3000 is not restricted to artificial sRNAs, but also occurs
518 with endogenous sRNAs. They also highlight a potential for Arabidopsis endogenous sRNAs
519 in targeting, and possibly silencing, *Pto* DC3000 genes, in part through SA biogenesis and/or
520 signaling.
521
522
523
524
525

526 **Discussion**

527

528 **Arabidopsis-encoded anti-*cfa6*/*hrpL* sRNAs are externalized from plant cells and dampen**
529 ***Pto* DC3000 pathogenesis**

530 We show here that Arabidopsis-encoded artificial sRNAs can target *Pto* DC3000 virulence-
531 associated genes, resulting in the dampening of bacterial pathogenesis. In particular, we found
532 that host-encoded sRNAs directed against the *Pto* DC3000 *Cfa6* and *HrpL* genes, fully
533 suppressed bacterial-induced stomatal reopening (Fig. 1). Furthermore, we showed that, in
534 Arabidopsis plants expressing anti-*hrpL* sRNAs, this phenotype no longer occurred in response
535 to the *Pto*Δ*hrpL* mut *HrpL* strain (Fig. 3). Altogether, these findings indicate that antibacterial
536 sRNAs act in a sequence-specific manner and can operate at the pre-invasive stage of infection,
537 presumably by limiting COR biosynthesis in *Pto* DC3000 cells that come in contact with the
538 leaf surface. In addition, we found that anti-*cfa6*/*hrpL* sRNAs reduced the ability of *Pto*
539 DC3000 to multiply in the leaf apoplast of Arabidopsis upon dip-inoculation (Fig. 1). This
540 phenotype might be caused by the inability of *Pto* DC3000 to reopen stomata in IR-
541 *CFA6*/*HRPL* lines, thereby limiting its access to inner leaf tissues and thus to the apoplast,
542 which is its main replicative niche. Collectively, these data imply that antibacterial sRNAs
543 must be externalized from plant cells towards the surface of Arabidopsis leaves to reach
544 epiphytic *Pto* DC3000 populations.

545

546 **Anti-*cfa6*/*hrpL* sRNA duplexes, but not their dsRNA precursors, are biologically active**

547 By using genetic and molecular biology approaches (Fig. 2), we demonstrated that DCL-
548 dependent antibacterial sRNAs, but not cognate dsRNA precursors, are the RNA entities
549 responsible for AGS (Fig. 10). These data imply that *Pto* DC3000 must be capable of taking-
550 up –passively and/or actively– anti-*cfa6*/*hrpL* sRNAs, despite the presence of a cell wall and

551 an intricate double membrane structure. This assumption was confirmed by showing that
552 artificial anti-*hrpL* sRNAs from the non-vesicular apoplastic fraction of IR-*CFA6*/*HRPL*#4
553 plants, but also a chemically synthesized 21 nt anti-*hrpL* sRNA duplex with 2-nt 3' overhangs,
554 were transferred into the cytoplasm of *Pto* DC3000 cells (Fig. 7). These results thus unveil
555 major differences with environmental RNAi in eukaryotic organisms, such as *C. elegans* and
556 plant herbivores, which specifically rely on long dsRNAs, or filamentous pathogens, which are
557 dependent on both dsRNAs and sRNAs[55]. They also suggest that the industrial dsRNA
558 production platforms, currently designed to produce long dsRNAs against pathogens and
559 parasites, are not adapted to produce RNA-based biocontrol agents against bacterial pathogens.
560

561 **A pool of active apoplastic protein-bound sRNAs is located outside PEN1-positive EVs**

562 We found here that a large proportion of apoplastic anti-*cfa6*/*hrpL* sRNAs is associated with
563 proteins, and thus protected from MNase-mediated degradation (Fig. 4). This feature was
564 notably observed for the apoplastic fraction that co-purified with PEN1-positive EVs (*i.e.* the
565 P40 pellet), as well as the fraction exhibiting a substantial reduction in EVs and a depletion in
566 PEN1 (*i.e.* the SN fraction). Nevertheless, only the protein-bound anti-*cfa6*/*hrpL* sRNAs from
567 the P40 pellet, but not those from the SN fraction, were found active (Fig. 4; Fig. 6). In addition,
568 protease and RNase protection assays from the P40 pellet revealed that these protein-bound
569 antibacterial sRNAs are likely located outside PEN1-positive EVs. Based on these
570 observations, we propose two possible non-mutually exclusive scenarios by which
571 extravesicular protein-bound sRNAs from the P40 fraction could be transferred to, and/or
572 effective in, *Pto* DC3000 cells (Fig. 10). The first one, which does not implicate EVs, would
573 involve yet-unknown plant factor(s) from the protein-bound sRNAs complex(es) that would be
574 specifically present in the P40 pellet, but not in the SN fraction. Potential candidates include
575 the RNA-binding protein GRP7, as well as AGO2, which are both known to bind sRNAs[56–59],

576 and have been recovered in the apoplastic P40 fractions, in extravesicular forms[34]. The second
577 one would involve PEN1-positive EVs, decorated with these protein-bound sRNAs complexes
578 at their surface, which would act as carriers of these RNA-associated particles. The latter
579 hypothesis is supported by the relatively large surface of EVs compared to their volume, which
580 notably contains exposed phospholipids that can bind specific proteins from the extracellular
581 environment[60].
582
583 **A pool of active apoplastic sRNAs is likely located inside TET8-positive EVs**
584 By characterizing the apoplastic fraction from IR-*CFA6*/*HRPL*#4 plants co-purifying with
585 TET8-positive EVs (*i.e*. the P100-P40 fraction), we found that the MNase and Proteinase K
586 combined treatment did not alter its antibacterial activity (Fig. 5). In contrast, an extra detergent
587 treatment led to a substantial reduction in the accumulation of anti-*cfa6*/*hrpL* sRNAs, as well
588 as a loss in AGS activity (Fig. 5). Collectively, these data indicate that a pool of active anti-
589 *cfa6*/*hrpL* sRNAs is likely located inside TET8-positive EVs (Fig. 10). They are thus congruent
590 with former studies showing that intravesicular plant antifungal sRNAs are delivered into *B*.
591 *cinerea* through TET8-positive EVs[1,5]. They are also consistent with recent studies showing
592 that i) antibacterial miRNAs, located inside ginger exosome-like nanoparticles (GELNs), can
593 be delivered and active in the periodontal pathogen *Porphyromonas gingivalis* and the
594 commensal intestinal bacterium *Lactobacillus rhamnosus*[61,62], and (ii), let-7b-5p, embedded in
595 EVs from human airway epithelial cells, is translocated in the opportunistic human pathogen
596 *Pseudomonas aeruginosa*, to reduce its ability to form biofilm and to enhance its antibiotic
597 sensitivity[36]. These findings also pave the way for the development of novel EV-based delivery
598 systems for antibacterial sRNAs.
599
600

601 **A pool of active apoplastic sRNAs is unbound to protein and in a dsRNA form**

602 Intriguingly, we found that anti-*cfa6*/*hrpL* sRNAs from the SN fraction harbour anti-virulence
603 activity, which was found abolished upon MNase treatment alone (Fig. 6). Furthermore, by
604 pulling-down anti-*cfa6*/*hrpL* sRNA duplexes from these apoplastic fractions, we showed that
605 these extracellular sRNA species were functional in a stomatal aperture assay (Fig. 6). These
606 data indicate that a third pool of anti-*cfa6*/*hrpL* efsRNAs, which is unbound to protein, and in
607 a free and dsRNA form, is biologically active (Fig. 10). Although our findings do not exclude
608 the possibility that extracellular single-stranded RNA species (ssRNAs) could also be present
609 and functional in the apoplast, they suggest that the dsRNA structure of the above characterized
610 efsRNAs might represent a structural feature that favors their stability in the apoplast. This
611 hypothesis would provide an explanation for why artificial sRNA duplexes, exogenously
612 applied on different plant species, were transmitted through, and stable in, xylem vessels, which
613 are part of the apoplast[63]. It is also possible that yet-unknown post-transcriptional modifications
614 of these functional efsRNAs contribute to their stability in the Arabidopsis apoplast.

615

616 **Salicylic acid-treated IR-*CFA6*/*HRPL* plants trigger *hrpL* silencing in *Pto* DC3000**

617 To monitor the potential effect of anti-*hrpL* sRNAs on the silencing of the *HrpL* gene, we
618 incubated the *Pto* DC3000 strain expressing an epitope-tagged version of *HrpL*, with leaf
619 sections of IR-*CFA6*/*HRPL*#4 plants. Using this assay, we found a substantial reduction in the
620 accumulation of HrpL proteins in *Pto* DC3000, which was specifically detected when the above
621 transgenic plants were challenged with SA (Fig. 8). Our findings thus provide insights into
622 strategies that can be further developed to improve HIGS efficacy. In addition, we observed
623 that the levels of *HrpL* mRNAs were not consistently and significantly reduced in the presence
624 of SA-pretreated IR-*CFA6*/*HRPL*#4 leaf sections across different biological replicates
625 (Supplementary Fig. 8). Although these findings do not exclude the possibility that internalized

626 anti-*hrpL* RNAs direct mRNA cleavage and/or degradation of *HrpL* mRNAs in *Pto* DC3000,
627 they suggest that extra-cellular/organismal anti-*hrpL* sRNAs, produced from SA-challenged
628 IR-*CFA6*/*HRPL* plants, predominantly dampen the translation of *HrpL* mRNAs in these
629 experimental settings (Fig. 10). This regulatory process might involve the internalization by
630 *Pto* DC3000 cells of vesicular and/or non-vesicular plant factors that are secreted in the
631 apoplast in response to SA[34,64], and/or SA-induced plant signals, which would enhance anti-
632 *hrpL* sRNA-directed translational repression of *HrpL* mRNAs in *Pto* DC3000. Although the
633 detailed mechanism remains unknown, various sRNA-directed translational inhibition
634 processes are known to operate in animals, plants and bacteria[65–68,68–73]. For instance, some
635 RNA-based antisense oligonucleotides (ASOs), which are in the same size range as tyRNAs,
636 siRNAs and miRNAs, but also longer bacterial small non-coding RNAs, which are typically
637 between 50 to 500 nt in size, have been shown to trigger translational inhibition of their mRNA
638 targets through different mechanisms in prokaryotic cells [68,73–75]. Altogether, these data suggest
639 that *Pto* DC3000 must have evolved a machinery to take charge of the internalized plant sRNAs
640 and direct gene silencing. It will thus be appealing to identify such machinery and elucidate the
641 principles of plant sRNA target recognition and mode of action in bacterial cells.
642
643 **Endogenous efsRNAs, including tRNA-derived sRNAs, are taken-up by *Pto* DC3000 cells**
644 By sequencing SN-derived sRNAs from IR-*CFA6*/*HRPL* plants that are transferred into the
645 cytoplasm of *Pto* DC3000 cells, we did not only retrieve artificial sRNAs from the *CFA6*/*HRPL*
646 hairpin but also Arabidopsis endogenous sRNAs. The latter sRNAs were derived from various
647 genomic origins, including endogenous inverted repeats, mRNAs, TEs, rRNAs and tRNAs
648 (Fig. 9; Fig. 10). Interestingly, among the most abundant sRNAs internalized by *Pto* DC3000
649 cells, we recovered tRFs, some of which exhibiting plausible bacterial mRNA targets (Fig. 9).
650 Transfer RNA-derived sRNAs have previously been shown to be transferred bidirectionally in

651 host-bacteria interactions[17,48–52]. More specifically, an abundant tRF was recovered inside outer
652 membrane vesicles (OMVs) from *P. aeruginosa*, and transferred into human airway cells[48].
653 Furthermore, this tRF displays predicted targets encoding kinases from the lipopolysaccharide
654 (LPS)-stimulated MAPK signaling pathway, and was shown to dampen the LPS-mediated
655 induction of interleukin-8 (IL-8) secretion in primary human airway epithelial cells, as well as
656 keratinocyte-derived chemokine production in mouse lung. Interestingly, tRFs produced from
657 the rhizobium strain *B. japonicum* have also more recently been shown to be transferred inside
658 soybean cells and further loaded into host AGO1, thereby silencing negative regulators of
659 nodulation[17]. Inversely, two human 5' tRNA halves from oral keratinocytes, were shown to be
660 secreted outside these cells and further taken-up from the saliva by the Gram-negative
661 pathobiont *Fusobacterium nucleatum*[49,50]. Importantly, these tsRNAs were able to reduce the
662 growth of different *F. nucleatum* strains *in vitro*, presumably by interfering with the ribosome-
663 related function of endogenous bacterial tRNAs[50]. Based on these collective findings, we
664 speculate that the abundant Arabidopsis tRFs recovered inside *Pto* DC3000 might either silence
665 sequence-complementary mRNA bacterial targets, and/or dampen protein biogenesis by acting
666 as decoys of bacterial tRNAs. In addition, we found that a large set of Arabidopsis sRNAs
667 recovered inside *Pto* DC3000 exhibits predicted bacterial mRNA targets, whose protein levels
668 were reduced by SA signaling and/or biogenesis during infection (Fig. 9). Although these
669 analyses have not been conducted in the natural host of *Pto* DC3000, they highlight a potential
670 for endogenous plant sRNAs in directly reprogramming bacterial gene expression during
671 infection. However, further studies are necessary to test whether plant sRNAs can indeed
672 regulate gene expression in natural host-bacteria interactions, and also shape plant
673 microbiomes composition as well as bacterial genomes evolution in these contexts.
674
675
676

677 **Figure legends**
678
679
680 **Figure 1. Stable expression of the IR-*CFA6/HRPL* transgene in Arabidopsis reduces *Pto***
681 **DC3000 virulence during infection.**
682 **a.** The coronatine (COR)-defective *Pto*Δ*cfa6* strain is impaired in its ability to reopen stomata
683 and this phenotype is rescued upon exogenous application of COR. Leaf sections of Col-0
684 plants were treated with mock (water), WT *Pto* DC3000 (*Pto* WT) or *Pto*Δ*cfa6* –with or
685 without COR– and the stomatal aperture response was analyzed at 3 hours post-inoculation
686 (hpi). The concentrations of bacterial strains and of COR were of 10^8 cfu mL^{-1} and 1μM,
687 respectively. The number of stomata analyzed per condition is written underneath each
688 condition and statistical significance was assessed using a one-way ANOVA test (ns: p-value
689 ≥ 0.05; ****: p-value < 0.0001). Similar results were obtained in three independent
690 experiments and are pooled in a single plot. **b.** The *Pto*Δ*hrpL* strain, but not the *Pto*Δ*hrcC*
691 strain, is impaired in its ability to reopen stomata and this phenotype is rescued upon exogenous
692 application of COR. The stomatal aperture assay was conducted as in a. with leaf sections of
693 Col-0 inoculated with *Pto* WT, Δ*hrpL* –with or without COR– and Δ*hrcC* strains. **c.** Schematic
694 representations of the IR-*CFA6*/*HRPL* chimeric hairpin construct stably expressed in
695 Arabidopsis transgenic plants (upper panel), and of the 250 bp regions of the *Cfa6* (1-250 nt,
696 blue box) and *HrpL* (99-349 nt, green box) genes that are targeted by sRNAs in *Pto* DC3000
697 (bottom panel). **d.** Size distribution and abundance of anti-*cfa6*/*hrpL* sRNA reads along the
698 *CFA6/HRPL* inverted repeat, sequenced from the IR-*CFA6*/*HRPL*#4 plants. **e.** Total sRNA
699 reads that map to the IR-*CFA6*/*HRPL* inverted repeat are depicted. Anti-*cfa6* and anti-*hrpL*
700 sRNAs are shown in blue and green, respectively. **f.** *Pto* DC3000 WT no longer induces
701 stomatal reopening in Arabidopsis IR-*CFA6*/*HRPL* transgenic lines. Stomatal aperture
702 measurements were conducted on leaf sections of IR-*CFA6/HRPL*#4, IR-*CYP51* and IR-*LUC*
703 lines infected with *Pto* WT, as described in a. **g.** The impaired stomatal reopening phenotypes

704 observed in IR-*CFA6*/*HRPL* lines are rescued upon application of exogenous COR. Stomatal
705 aperture measurements were conducted on leaf sections of IR-*CFA6/HRPL*#4, #5, #10 lines
706 infected with *Pto* WT, as described in a., with or without COR. **h.** Arabidopsis IR-*CFA6/HRPL*
707 lines exhibit reduced *Pto* WT titers when compared to Col-0 and IR-*CYP51*-infected plants at
708 2 days post-infection (dpi). Five to six-week-old Col-0, IR-*CYP51* and IR-*CFA6/HRPL*#4, #5
709 and #10 plants were dip-inoculated, at a concentration of 5 x 10^7 cfu mL^{-1}, with *Pto* WT-GFP.
710 As a control condition, Col-0 plants were treated at the same concentration with *Pto*Δ*cfa6*-
711 GFP. Number of leaf disc analyzed is written underneath each condition. Data from three
712 independent experiments are pooled in a single plot. Statistical significance was assessed using
713 a two-way ANOVA test (ns: p-value>0.05; ****: p-value<0.0001).
714
715 **Figure 2. Antibacterial sRNA species, but not unprocessed dsRNAs, are causal for the**
716 **suppression of *Pto* DC3000-triggered stomatal aperture.**
717 **a.** Accumulation level of anti-*hrpL* sRNAs in Col-0, Ubi.U4 IR-*HRPL*, *dcl2-1 dcl3-1 dcl4-2*
718 (*dcl234*), and Ubi.U4 IR-*HRPL* in *dcl234* mutant background (Ubi.U4 IR-*HRPL dcl234*) was
719 assessed by low molecular weight northern blot analysis. The northern blot results, obtained
720 from the same membrane, are shown at two different expositions: short (left) and long (right).
721 The long exposition was depicted to better visualize unprocessed forms of dsRNA precursors,
722 referred to as "sRNA precursors" in the panel. Because the same membrane was used to obtain
723 the results shown in panel a, the same U6 loading control This is one representative experiment
724 out of the three independent experiments performed. **b.** Ubi.U4 IR-*HRPL dcl234* plants do not
725 suppress *Pto* DC3000-induced stomatal reopening response. The stomatal reopening assay was
726 conducted on leaf sections of the same genotypes detailed in a. and as described in Fig 1a.
727 Similar results were obtained in three independent experiments and are pooled in a single plot.
728 The number of stomata analyzed per condition is written underneath each condition and

729 statistical significance was assessed using a one-way ANOVA test (ns: p-value ≥ 0.05; ****:
730 p-value < 0.0001). **c.** Twenty ng μl^{-1} of total RNA from IR-*CFA6/HRPL#4* but not IR-*LUC*
731 and IR-*CYP51* prevents stomatal reopening. Col-0 leaf sections were incubated with total RNA
732 from Col-0, IR-*CFA6/HRPL#4,* IR-*LUC* or IR-*CYP51* and stomatal reopening assay was
733 performed as in b. Similar results were obtained in two independent experiments and are pooled
734 in a single plot. **d.** Small RNA species, but not corresponding long RNA species, from IR-
735 *CFA6/HRPL*#4 plants suppress *Pto* DC3000-induced stomatal reopening. The stomatal
736 reopening assay was conducted with *Pto* DC3000 and by incubating Col-0 leaf sections with
737 total, long (> 200 nt) or small (< 200 nt) RNA fractions, separated from total RNAs of IR-
738 *CFA6/HRPL*#4 plants. Similar results were obtained in three independent experiments and are
739 pooled in a single plot. **e.** Accumulation of anti-*cfa6*/*hrpL* sRNAs in IR-*CFA6/HRPL*#4 and
740 IR-*LUC* total RNAs before or after p19 pull-down was detected by low molecular weight
741 northern blot analysis. U6 was used as a control of intracellular RNAs. This is one
742 representative experiment out of the three independent experiments performed. **f.** P19 pulled-
743 down sRNAs from the IR-*CFA6/HRPL*#4 total RNAs suppress the ability of *Pto* DC3000 to
744 reopen stomata. Stomatal aperture assay was conducted as in b. Statistical significance was
745 assessed using Student's *t*-test (****: p-value<0.0001). Similar results were obtained in three
746 independent experiments and are pooled in a single plot. **g.** Agarose gel picture of ethidium
747 bromide-stained *in vitro* synthesized (IVS) long dsRNAs and sRNA duplexes. **h.** *In vitro*
748 synthesized anti-*cfa6*/*hrpL* sRNAs*,* but not cognate unprocessed dsRNA precursors, suppress
749 *Pto* DC3000-triggered stomatal reopening. The stomatal reopening assay was conducted as in
750 b. Similar results were obtained in three independent experiments and are pooled in a single
751 plot.
752
753

754 **Figure 3. Anti-*hrpL* sRNAs are causal for the suppression of stomatal reopening**

755 **a.** Schematic representation of *Pto*Δ*hrpL* and of the recombinant strains expressing either the
756 WT *HrpL* or mut *HrpL* constructs, under the control of the constitutive *NPTII* promoter. **b.** The
757 sequence of WT *HrpL* (99-349 nt) selected to generate the inverted repeat transgene
758 (highlighted in green) was aligned with the sequence of mutated *HrpL* (mut *HrpL*) designed to
759 contain as many silent mutations as possible in the sRNA targeted region (highlighted in
760 purple). **c.** Thermodynamic energy analysis of sRNA-target interactions between anti-*hrpL*
761 sRNAs and the WT or mutated *HrpL* sequence versions. **d.** Both the WT *HrpL* and mut *HrpL*
762 constructs fully complemented *PtoΔhrpL* for its ability to reopen stomata. Col-0 leaves were
763 incubated with *PtoΔhrpL*, *PtoΔhrpL* WT *HrpL* and *PtoΔhrpL* mut *HrpL* bacterial strains.
764 Stomatal reopening response was assessed as described previously. Statistical significance was
765 assessed using a one-way ANOVA test (ns: p-value ≥ 0.05; ****: p-value < 0.0001). Similar
766 results were obtained from three independent experiments and the data are pooled in a single
767 plot. **e.** The *Pto*Δ*hrpL* mut *HrpL* strain is refractory to anti-*hrpL* sRNAs action at 3 hpi. The
768 stomatal reopening assay was conducted as in d., IR-*HRPL*#1 and #4 leaf sections were treated
769 with mock (water) or the indicated bacteria at a concentration of 10^8 cfu mL^{-1}. Results of two
770 independent experiments are pooled in a single plot. Statistical significance was assessed using
771 a one-way ANOVA test (ns: p-value>0.05; ****: p-value<0.0001).

772

773 **Figure 4. A pool of anti-*cfa6*/*hrpL* sRNAs, associated to proteins that are located outside**
774 **EVs, suppresses *Pto* DC3000-triggered stomatal reopening.**

775 **a.** Size distribution and abundance of anti-*cfa6*/*hrpL* sRNA reads from MNase-treated P40
776 pellets of IR-*CFA6/HRPL*#4 plants. **b.** Small RNA reads from the P40 pellets of IR-
777 *CFA6*/*HRPL*#4 plants that map to the *CFA6*/*HRPL* inverted repeat are depicted. Anti-*cfa6* and
778 anti-*hrpL* sRNAs are shown in blue and green, respectively. **c.** Anti-*cfa6*/*hrpL* sRNAs

accumulation is reduced when the P40 pellets of IR-*CFA6*/*HRPL*#4 plants were treated with MNase and ProtK. The P40 pellets from IR-*CFA6*/*HRPL*#4 plants were treated with mock, MNase or MNase plus ProtK, and the accumulation of anti-*cfa6*/*hrpL* sRNAs was analyzed by northern blot analysis. P40 pellets from untreated IR-*CYP51* plants were used as a negative control. The membrane was also probed with U6 to make sure that the P40 fractions were not contaminated by intracellular RNAs. The band intensities of *cfa6 /hrpL* siRNAs were quantified using ImageJ. Band intensities were normalized to the expression level of the mock condition. The results are shown above each blot. This is one representative experiment out of the three independent experiments performed. **d.** The ability of *Pto* DC3000 to reopen stomata is impaired in response to P40 pellets from IR-*CFA6*/*HRPL*#4 plants, and this effect is compromised in the presence of P40 pellets treated with MNase and Proteinase K (ProtK). The stomatal reopening assay was performed on Col-0 leaf sections incubated with IR-*CFA6/HRPL*#4 or IR-*CYP51*-derived P40 pellets that were subjected to different enzymatic treatments. Statistical significance was analyzed using a one-way ANOVA test (ns: p-value ≥ 0.05; *: 0.05 > p-value ≥ 0.01; ****: p-value < 0.0001). Similar results were obtained in three independent experiments and are pooled in a single plot. **e.** Anti-*cfa6* and anti-*hrpL* sRNAs accumulation is significantly reduced after MNase, ProtK and Triton X100 (TX100) treatments. Accumulation of sRNAs in IR-*CFA6/HRPL*#4- and IR-*CYP51*-derived P40 pellets was detected by northern blot analysis. The band intensities of *cfa6/hrpL* siRNAs were quantified using ImageJ. Band intensities were normalized to the expression level of the mock condition. The results are shown above each blot. This is one representative experiment out of the two independent experiments performed.

803 **Figure 5. A pool of anti-*cfa6*/*hrpL* sRNAs, likely located inside TET8-positive EVs,**
804 **suppresses *Pto* DC3000-triggered stomatal aperture**
805 **a.** P100-P40 pellets contain TET8-positive EVs. EVs were visualized through TEM analysis,
806 using native anti-TET8 (PhytoAB, PHY2750A) or UGPase (Agrisera) primary antibodies,
807 followed by detection with a gold-conjugated secondary antibody. White arrows indicate the
808 presence of gold beads. Scale bar: 50 nm. **b.** Size distribution and abundance of anti-*cfa6*/*hrpL*
809 sRNA reads from MNase-treated P100-P40 pellets of IR-*CFA6/HRPL*#4 plants. **c.** Small RNA
810 reads from the P100-P40 pellets of IR-*CFA6*/*HRPL*#4 plants that map to the *CFA6*/*HRPL*
811 inverted repeat are depicted. Anti-*cfa6* and anti-*hrpL* sRNAs are shown in blue and green,
812 respectively. **d.** Anti-*cfa6*/*hrpL* sRNAs accumulation is reduced when P100-P40 pellets of IR-
813 *CFA6*/*HRPL*#4 plants were treated with TX100, MNase and ProtK. The P100-P40 pellets from
814 IR-*CFA6*/*HRPL*#4 plants were treated with mock, MNase plus ProtK, or TX100 plus MNase
815 plus ProtK and the accumulation of anti-*cfa6*/*hrpL* sRNAs was detected by northern blot
816 analysis. P40 pellets from untreated IR-*CYP51* plants were used as a negative control. The
817 membranes used were hybridized with either the *cfa6* probe (upper panel) or the *hrpL* probe
818 (bottom panel). Of note, it was not possible to sequentially probe the same membrane with the
819 *cfa6* and *hrpL* probes because of low abundance of these sRNAs from P100-P40 pellets. The
820 band intensities of *cfa6/hrpL* sRNAs were quantified using ImageJ. Band intensities were
821 normalized to the expression level of the mock condition. The results are shown above each
822 blot. The membranes were also probed with U6 to make sure that the P100-P40 fractions were
823 not contaminated by intracellular RNAs. **e.** The ability of *Pto* DC3000 to reopen stomata is
824 impaired in response to P100-P40 pellets from IR-*CFA6*/*HRPL*#4 plants, and this effect is
825 compromised when these P100-P40 pellets were treated with MNase, ProtK and TX100.
826 Stomatal aperture measurements were performed on Col-0 leaf sections incubated with IR-
827 *CFA6/HRPL*#4 or IR-*CYP51*-derived P100-P40 pellets that were subjected to different

828 enzymatic treatments. Statistical significance was analyzed using a one-way ANOVA test (ns:
829 p-value ≥ 0.05; ****: p-value < 0.0001). Similar results were obtained in three independent
830 experiments and are pooled in a single plot.
831
832 **Figure 6. Extracellular free anti-*cfa6*/*hrpL* sRNA duplexes are recovered from SN**
833 **fraction and harbour anti-virulence activity**
834 **a.** Size distribution and abundance of anti-*cfa6*/*hrpL* sRNA reads from the SN fraction of IR-
835 *CFA6/HRPL*#4 plants. **b.** Accumulation of anti-*cfa6*/*hrpL* sRNAs in IR-*CFA6/HRPL*#4 and
836 IR-*LUC*-derived SN fractions before or after p19 pull-down assay was detected by northern
837 blot analysis. U6 was used as a control of intracellular RNA. The membrane was also probed
838 with U6 to make sure that the SN fractions were not contaminated with intracellular RNAs.
839 This is one representative experiment out of the two independent experiments performed. **c.**
840 Small RNA reads from the SN fraction of IR-*CFA6*/*HRPL*#4 plants that map to the
841 *CFA6*/*HRPL* inverted repeat are depicted. Anti-*cfa6* and anti-*hrpL* sRNAs are shown in blue
842 and green, respectively. **d.** The SN fraction from IR-*CFA6*/*HRPL*#4 plants prevents *Pto*
843 DC3000-induced stomatal reopening, and this effect is abolished upon treatment of this APF
844 fraction with MNase. Statistical significance was assessed using a one-way ANOVA test (ns:
845 p-value ≥ 0.05; ****: p-value < 0.0001). Similar results were obtained in three independent
846 experiments and are pooled in a single plot. **e.** P19 pulled-down sRNAs from the IR-
847 *CFA6/HRPL*#4 SN fraction suppress *Pto* DC3000-induced stomatal reopening. The stomatal
848 reopening assay was conducted as in c. Statistical significance was assessed using Student's t-
849 test (****: p-value<0.0001). Similar results were obtained in three independent experiments
850 and are pooled in a single plot.
851
852

853 **Figure 7. A subset of SN-derived anti-*hrpL* sRNAs is internalized by *Pto* DC3000 cells**

854 **a.** Schematic representation of the experimental set-up employed to sequence sRNAs that are
855 internalized by *Pto* DC3000. Bacterial cells were either incubated in VIB or in SN, derived
856 from SA-treated IR-*CFA6/HRPL*#4 plants (see methods), for two hours before collection of
857 the cells and washing with EDTA. Total RNAs were further extracted and used for sRNA-seq.
858 **b.** Internalized sRNA reads that map to the *CFA6*/*HRPL* inverted repeat are depicted. Anti-
859 *cfa6* and anti-*hrpL* sRNAs are shown in blue and green, respectively. **c.** Size distribution and
860 abundance of anti-*cfa6*/*hrpL* sRNA reads. **d.** The most represented 21nt anti-*hrpL* sequence is
861 framed in blue on top of the panel, with occurrence numbers for both replicates shown above
862 it. Below is depicted the corresponding duplex version labeled with ATTO 565 (red star) in the
863 5' end of the anti-*hrpL* sRNA strand that is complementary to *HrpL* mRNAs. **e.** Imaging of *Pto*
864 DC3000-*GFP (*green) incubated with the *hrpL* duplex labeled with ATTO 565 (red). White
865 arrows highlight examples of signals co-localization between ATTO 565 and GFP. Scale bar:
866 5 µm. **f.** WT *hrpL* duplexes but not *CYP51*, nor mut *hrpL* duplexes, suppress *Pto* DC3000-
867 induced stomatal reopening. The stomatal aperture measurements were performed on Col-0
868 leaf sections incubated with sRNA duplexes. Statistical significance was analyzed using a one-
869 way ANOVA test (ns: p-value ≥ 0.05; ****: p-value < 0.0001). Similar results were obtained
870 in three independent experiments and are pooled in a single plot.

871

872 **Figure 8. The accumulation of HrpL proteins is reduced in *Pto* DC3000 cells incubated**
873 **with leaf sections of salicylic acid-treated IR-*CFA6*/*HRPL*#4 plants**

874 **a.** Schematic representation of the experimental set-up employed to expose *Pto* DC3000 cells
875 to plant-derived extra-cellular/organismal sRNAs. IR-*CFA6/HRPL*#4 or IR-*CYP51* plants
876 were sprayed with SA (2 mM) for 48 hours prior to the experiment, and leaf sections from
877 those plants were further incubated with a *Pto* DC3000 strain expressing a Flag-tagged version

878 of *HrpL*, namely the *Pto* DC3000 *hrpL-FLAG* strain[44]. Some possible extra-cellular/organismal
879 sRNA populations are illustrated in the circle. RBPs, EVs, dsRNA and ssRNA, stand for RNA-
880 Binding Proteins, Extracellular Vesicles, double-stranded RNA and single-stranded RNA,
881 respectively. **b**. Western blot analysis showing the reduction in the accumulation of HrpL
882 proteins upon incubation of the *Pto* DC3000 *hrpL-FLAG* strain with leaf sections of SA-treated
883 IR-*CFA6/HRPL*#4 plants, compared to leaf sections of IR-*CYP51* plants treated in the same
884 condition. The accumulation of the elongation factor EF-Tu served as loading control. *Pto*
885 DC3000 pBS181 contains the empty expression vector pBS181 and served as a negative
886 control. This is one representative experiment out of the six independent experiments
887 performed. **c.** Plot depicting the band intensity of *Pto* DC3000 *hrpL-FLAG* protein levels
888 normalized to corresponding EF-Tu bands. IR-*CYP51* or IR-*CFA6/HRPL*#4 SA-treated ratios
889 were then further normalized to IR-*CYP51* and IR-*CFA6*/*HRPL*#4 mock condition ratios,
890 respectively. Similar results were obtained in six independent experiments and the data are
891 pooled in a single plot. Statistical significance was assessed using Student's paired t-test (ns:
892 p-value ≥ 0.05).
893
894 **Figure 9. Endogenous sRNAs, from the SN of SA-treated IR-*CFA6/HRPL*#4 plants, are**
895 **transferred into the cytoplasm of *Pto* DC3000 cells**
896 **a.** Size distribution of all the endogenous sRNAs that were recovered in *Pto* DC3000 cells. SN
897 fractions from SA-treated IR-*CFA6*/*HRPL*#4 plants were incubated for 2 hours with *Pto*
898 DC3000 cells (*Pto* DC3000 + SN 2h), and the internalized endogenous sRNAs analyzed using
899 the second stringent filter (see methods). **b.** Class repartition of reads after the second filtering
900 step. **c.** Size distribution of reads mapping to IR71 after the second filtering step. **d.** Size
901 distribution of reads mapping to IR2039 after the second filtering step. **e, f.** Coverage of sRNAs
902 on IR71 (e) and IR2039 (f) after the second filtering step. **g.** RNA-fold structure of ProAGG.17.

903 The most represented tRNA sequence from our filtered samples is highlighted in orange. **h.**
904 Examples of predicted *Pto* DC3000 targets of the tRF highlighted in g. The three best
905 predictions according to the minimal free energy value are represented. **i.** Three hundred seven
906 *Pto* DC3000 SA-responsive proteins were predicted to be targets of internalized sRNAs. The
907 heatmap depicts their accumulation in Col-0, *sid2*, *pad4* and *sid2 pad4* that were infected for
908 48 hours with *Pto* DC3000[54]. Z-score normalized (by row) values based on
909 protein accumulation values reported in Nobori *et al*.[54] **j.** Twenty-two of the SA-responsive
910 proteins corresponded to targets of the top 100 most represented internalized sRNA reads.
911 Their accumulation in Col-0-, *sid2*-, *pad4*- and *sid2 pad4*-infected plants is shown in the
912 heatmap. **k.** Representation of some candidate sRNA-Target pairings corresponding to
913 internalized sRNAs predicted to target mRNAs, whose protein levels are down-regulated in
914 Col-0-infected plants but no longer repressed in *sid2*-, *pad4*-, and/or *pad4*/*sid2*-infected plants
915 (from the 5 purple framed candidates depicted in j.).
916
917 **Figure 10. Model depicting the extracellular sRNA populations that are active against *Pto***
918 **DC3000 and/or internalized by these bacterial cells**
919 Model depicting the characterized Arabidopsis-encoded artificial sRNA species directing gene
920 silencing in interacting *Pto* DC3000 cells. The Arabidopsis IR-*CFA6/HRPL*#4 transgenic
921 plants produce an inverted repeat transcript that is processed by DCL proteins into anti-
922 *cfa6/hrpL* sRNAs (in green). The cytoplasmic anti-*cfa6/hrpL* sRNA species are further
923 incorporated into protein complexes containing RNA Binding Proteins (RBPs), or potentially
924 present in a free and dsRNA form in the cytosol, or in EVs. Both sRNA species are then
925 exported in the apoplast through unknown mechanisms (dashed arrows). Three populations of
926 active anti-*cfa6/hrpL* sRNAs have been characterized in this study: a first pool that is bound to
927 proteins, which are either non-associated to PEN1-positive EVs, or potentially located on their

928 surface. A second pool of sRNAs that is presumably located inside TET8-positive EVs, and a
929 third pool that is unbound to proteins and in a free and dsRNA form, named efsRNAs. Active
930 plant extracellular-sRNA species (*e.g*. anti-*hrpL* sRNAs), are subsequently transferred towards
931 *Pto* DC3000 cells (dashed arrows), to direct sequence-specific gene silencing of *hrpL* through
932 as-yet unknown mechanisms. Finally, the model depicts the endogenous sRNAs (in red),
933 produced from various Arabidopsis endogenous genomic origins, including specific tRFs,
934 which are internalized by *Pto* DC3000 cells.

935
936 **Supplementary figure legends**
937

938 **Supplementary Figure 1. Characterization of IR-*CFA6*/*HRPL*, IR-*CYP51* and IR-*LUC***
939 **transgenic lines**

940 **a.** Representative pictures of five-week-old Arabidopsis Col-0 plants and of independent
941 homozygous transgenic plants expressing the 35S::IR-*CYP51* or the 35S::IR-*CFA6/HRPL*
942 transgenes. **b.** Accumulation of anti-*cfa6*/*hrpL* sRNAs from two-week-old Arabidopsis
943 seedlings was detected by low molecular weight northern blot analysis. U6 was used as a
944 loading control. **c.** Accumulation of anti-*cyp51* or anti-*luc* sRNAs respectively from the
945 Arabidopsis plants IR-*CYP51*#1 or #2 and IR-*LUC* was detected by low molecular weight
946 northern blot analysis. U6 was used as a loading control. IR-*CYP51* line #2 or IR-*LUC* were
947 further used as reference lines in subsequent assays. **d.** Size distribution and abundance of
948 sRNA reads from the IR-*CFA6/HRPL*#4 transgenic line. Data from two biological replicates
949 are presented, and the same replicates are used in Fig. 1d. **e.** Thermodynamic energy analysis
950 revealed that the free energy of sRNA-*Pto* DC3000 target interactions (Kcal/mol), which are
951 almost exclusively composed of sRNA/*cfa6* and sRNA/*hrpL* pairs (see Table S2), is
952 significantly lower than that from sRNA-Arabidopsis transcript interactions (see Table S1),
953 indicating that off-targets in Arabidopsis are unlikely (see also Table S2 depicting the high e-

954 values for all the interactions between the anti-*cfa6* and anti-*hrpL* sRNAs and Arabidopsis
955 genes). **f.** Anti-*cfa6/hrpL* sRNAs accumulation remains unchanged upon bacterial dipping
956 assay. Anti-*cfa6*/*hrpL* sRNAs were detected by low molecular weight northern blot analysis.
957 U6 was used as a loading control. Anti-*cfa6/hrpL* sRNAs and U6 band intensities were
958 measured with ImageJ. The ratio of sRNAs to U6 was calculated, and the results were
959 normalized to the expression level of the mock condition. The results are shown above each
960 blot.
961
962 **Supplementary Figure 2. Characterization of the RNA entities after size separation.**
963 **a.** Size distribution of total, long and sRNAs from IR-*CFA6/HRPL*#4 plants was obtained with
964 an Agilent Bioanalyzer 2100 equipped with an RNA Nano chip. Low molecular weight RNA
965 fractions are encircled for each sample. 18S and 25S ribosomal peaks are highlighted. **b.**
966 Agarose gel picture of ethidium bromide-stained total, long and sRNAs from IR-
967 *CFA6/HRPL#4* plants.
968
969 **Supplementary Figure 3. Molecular characterization of 35S::*HRPL* transgenic lines.**
970 Accumulation of anti-*hrpL* sRNAs was assessed by low molecular weight northern blot
971 analysis using total RNA extracts from the Arabidopsis stable transgenic lines IR-*HRPL*#1 and
972 #4, expressing the 35S::IR-*HRPL* transgene. U6 was used as a loading control.
973
974 **Supplementary Figure 4. Impact of MNase, Proteinase K, and MNase plus Proteinase K**
975 **treatments on PEN1-positive EVs integrity, anti-*cfa6*/*hrpL* sRNAs accumulation and *Pto***
976 **DC3000-triggered stomatal reopening.**
977 **a.** Nanoparticle Tracking Analysis (NTA) showing that enzymatic treatments do not affect
978 particles size nor abundance in P40 pellets. Size distribution and abundance of nanoparticles

979 in IR-*CFA6/HRPL*#4-derived P40 pellets after different treatments; results from untreated
980 (Mock), MNase-treated or MNase and Proteinase K (ProtK)-treated were similar. Similar
981 results were obtained in three independent experiments. This is one representative experiment
982 out of the three independent experiments performed. **b.** Transmission Electron Microscopy
983 (TEM) analysis also revealed that enzymatic treatments do not alter neither the size nor the
984 morphology of EVs recovered in P40 pellets. IR-*CFA6/HRPL*#4-derived P40 pellets were
985 observed after different treatments: untreated, MNase-treated or MNase and ProtK-treated.
986 Scale bar: 100 nm. **c.** Pictures of representative EVs in b. were measured using ImageJ
987 software. The number of vesicles measured is written underneath each condition and statistical
988 significance was assessed using the ANOVA test (ns: p-value ≥ 0.05). This is one
989 representative experiment out of the two independent experiments performed. **d.** PEN1 and
990 PEN3 protein accumulations were detected by western blot analysis in IR-*CFA6/HRPL*#4 total
991 protein, P40 pellet or Supernatant fraction (SN). UGPase was used as a control in both western
992 blot experiments. These are one representative experiment out of the three independent
993 experiments performed. **e.** Size distribution and abundance of sRNA reads from IR-
994 *CFA6/HRPL*#4 MNase-treated P40 pellets. Data from two biological replicates are presented,
995 and the same replicates are used in Fig. 4b. **f.** The sRNAs from the P40 pellet of IR-*HRPL*#4
996 plants suppress *Pto* DC3000-induced stomatal aperture in a sequence-specific manner.
997 Stomatal reopening measurements were conducted on Col-0 leaf sections incubated with IR-
998 *HRPL*#4 or IR-*CYP51*-derived P40 pellets that were subjected to MNase treatment. The
999 stomatal aperture assay was conducted as in Fig 2c. Similar results were obtained in three
1000 independent experiments and are pooled in a single plot **g.** Anti-*cfa6* and anti-*hrpL* sRNAs
1001 accumulation remains stable after MNase treatment but decreases after MNase plus ProtK
1002 treatment. Small RNAs band signal intensity was assessed using ImageJ. This molecular
1003 analysis was performed in three independent experiments. Signal was normalized relative to

1004 the untreated condition and statistical significance was assessed using Student's *t*-test (ns: p-
1005 value ≥ 0.05, ****: p-value<0.0001).
1006
1007 **Supplementary Figure 5. Characterization of the P100-P40 pellet, anti-*cfa6*/*hrpL* sRNAs**
1008 **accumulation and impact of MNase and Proteinase K treatments on TET8-positive EVs**
1009 **integrity.**
1010 **a.** Percentage of EVs in the P100-P40 sample labeled with TET8 antibody. Immunolabeling
1011 was performed using TET8 antibodies and secondary antibodies coupled with gold beads. EVs
1012 were observed through TEM. **b.** Size distribution and abundance of sRNA reads from IR-
1013 *CFA6/HRPL*#4 MNase-treated P100-P40 pellets. Data from two biological replicates are
1014 presented, and the same replicates are used in Fig. 5b. **c.** Pictures of representative EVs were
1015 measured using ImageJ software. The number of vesicles measured is written above each
1016 condition and statistical significance was assessed using the ANOVA test (ns: p-value ≥ 0.05;
1017 *: 0.05 > p-value ≥ 0.01). Similar results were obtained in three independent experiments and
1018 the data are pooled in a single plot. **d.** MNase treatment alone does not affect P100-P40 pellet
1019 activity against *Pto* DC3000. Stomatal aperture measurements were conducted in Col-0 pre-
1020 treated with IR-*CFA6/HRPL*#4- or IR-*CYP51*-derived P100-P40 pellets that were subjected to
1021 enzymatic treatments. Leaf sections were infected with the *Pto* WT strain. The number of
1022 stomata analyzed per condition is written underneath each condition and statistical significance
1023 was assessed using a one-way ANOVA test (****: p-value < 0.0001). Similar results were
1024 obtained in three independent experiments and the data are pooled in a single plot. **e.** ProtK
1025 treatment alone does not affect P100-P40 pellet activity against *Pto* DC3000. The stomatal
1026 reopening assay was performed as described in d. Similar results were obtained in two
1027 independent experiments and the data are pooled in a single plot.
1028

1029 **Supplementary Figure 6. Characterization of the apoplastic SN fractions of IR-**
1030 ***CFA6*/*HRPL*#4 and IR-*CYP51* plants.**
1031 **a.** Size distribution and abundance of nanoparticles in IR-*CFA6/HRPL*#4 P40 pellets or SN
1032 fraction. The analyses were performed using Nanoparticle Tracking Analysis (NTA) method.
1033 Similar results were obtained in three independent experiments. This is one representative
1034 experiment out of the three independent experiments performed. **b.** Size distribution and
1035 abundance of sRNA reads from the SN fraction of the IR-*CFA6/HRPL*#4 transgenic line. Data
1036 from two biological replicates are presented, and the same replicates are used in Fig. 6c. **c.**
1037 Anti-*cfa6* and anti-*hrpL* sRNAs accumulation is reduced after ProtK but not after MNase
1038 treatments, at the resolution of northern analysis. Accumulation of sRNAs in IR-
1039 *CFA6/HRPL*#4- and IR-*CYP51*-derived SN fractions was detected by low molecular weight
1040 northern blot analysis. MicroRNA167 (miR167-5p) was used as an endogenous miRNA
1041 control. This is one experiment out of the two independent experiments performed. **d.** The
1042 sRNAs from the SN fraction of IR-*HRPL*#4 plants suppress *Pto* DC3000-triggered stomatal
1043 aperture in a sequence-specific manner. Stomatal aperture measurements were conducted on
1044 Col-0 leaf sections incubated with IR-*HRPL*#4 or IR-*CYP51*-derived SN fractions. Leaf
1045 sections were inoculated with indicated bacterial strains and the stomatal aperture
1046 measurements were performed as in Supplementary Fig. 3e. Similar results were obtained in
1047 three independent experiments and are pooled in a single plot. **e.** MNase treatments fully
1048 degrade anti-*cfa6* and anti-*hrpL* sRNAs from total RNA extracts from IR-*CFA6*/*HRPL*#4
1049 plants. Ten micrograms of IR-*CFA6/HRPL*#4 total RNAs were treated with MNase and anti-
1050 *cfa6/hrpL* sRNAs were further detected by low molecular weight northern blot analysis. This
1051 is one representative experiment out of the three independent experiments performed.
1052

1053 **Supplementary Figure 7. Effect of EDTA treatment on *Pto* DC3000, and internalized**
1054 **anti-*cfa6/hrpL* 21nt long sRNAs.**
1055 **a.** Treatment with EDTA effectively degrades the outer membrane of *Pto* DC3000. Membrane
1056 permeability was evaluated by measuring the internalization of propidium iodide (P. I) using
1057 fluorescence. The fluorescence signal was normalized to the optical density at OD at 600 nm
1058 (OD). **b.** *Pto* DC3000 exhibits impaired growth after treatment with EDTA. The bacteria were
1059 treated with EDTA to disrupt the outer membrane and periplasm, then cultured in NYGB
1060 medium for 24 hours. *In vitro* growth was monitored by measuring OD_{600}. **c.** Upper panels:
1061 representations of the sRNA duplex with 2-nt 3' overhangs for the WT *hrpL* duplex (*hrpL* WT
1062 sRNA duplex) depicted in green, and its cognate mutated version (*hrpL* mut sRNA duplex),
1063 depicted in purple. Anti-*hrpL* WT sRNA (shown in green) is 100% complementary to *HrpL*
1064 mRNA, whereas anti-*hrpL* mut sRNA (shown in purple) has been mutated to alter anti-*hrpL*
1065 sRNA pairing with the *HrpL* mRNA.
1066
1067 **Supplementary Figure 8. *HrpL* mRNAs are not consistently and significantly altered in**
1068 ***Pto* DC3000 cells in the presence of leaf sections from IR-*CFA6*/*HRPL*#4 and IR-*CYP51***
1069 **plants pretreated with salicylic acid.**
1070 RT-qPCR analyses depicting the levels of *HrpL* mRNAs in four independent experiments. The
1071 *HrpL* mRNA levels display slight or no significant changes in the presence of extra-
1072 cellular/organismal sRNAs from IR-*CFA6*/*HRPL*#4 leaf sections (with or without SA). Four
1073 independent biological replicates are represented. Levels of *HrpL* mRNAs in *Pto* DC3000 cells
1074 exposed to either IR-*CYP51* SA or IR-*CFA6*/*HRPL*#4 SA were normalized to IR-*CYP51* mock
1075 or IR-*CFA6*/*HRPL*#4 mock, respectively. Statistical significance was assessed using Student's
1076 t-test (ns: p-value ≥ 0.05; *: $0.05 >$ p-value ≥ 0.01).
1077

1078 **Materials & Methods**

1079

1080 **Plasmid construction**

1081 The IR-*CFA6/HRPL* construct is composed of 250 bp regions of *Pto* DC3000 genes, *cfa6* (1-
1082 250 nt) and *hrpL* (99-349 nt), aligned in sense and antisense directions, with the intron of the
1083 petunia chalcone synthase gene (*CHSA)* in between. The control vector construct IR-*CYP51* is
1084 designed to target conserved regions from *F. graminearum* that encompass *CYP51A*, *CYP51B*
1085 and *CYP51C* genes[6], with the same *CHSA* intron. The IR-*CFA6/HRPL* and IR-*CYP51*
1086 constructs containing EcoRI and SalI sites at both extremities were synthesized by GenScript®,
1087 and inserted by restriction enzyme digestion into a modified pDONR221-P5-P2 vector carrying
1088 additional EcoRI and SalI sites to facilitate the insertion of these long-inverted repeats. The
1089 plasmids containing the 35S::IR-*CFA6*/*HRPL* and 35S::IR-*CYP51* constructs were obtained by
1090 a double recombination between pDONR221-P5-P2 carrying the inverted repeat sequences and
1091 pDONR221-P1-P5r carrying the 35S promoter sequence, in the pB7WG Gateway destination
1092 vector using LR Clonase Plus (Life Technologies). These plasmids were then introduced into
1093 the *Agrobacterium tumefaciens* C58C1 strain. The IR-*HRPL* construct, which is composed of
1094 the same 250 bp region of *hrpL* as in the IR-*CFA6/HRPL* construct, was recombined using
1095 GreenGate technology[76] to generate the $35S_{pro}$:IR-*HRPL* plasmid, which was then transformed
1096 in the Agrobacterium C58C1 strain. To generate the WT *hrpL* and the mut *hrpL* plasmids, the
1097 wild type (WT) *hrpL* sequence was amplified from the genomic DNA isolated from *Pto*
1098 DC3000, while the mutant *hrpL* sequence was amplified from a mutated sequence synthesized
1099 by GenScript®. These two sequences were further cloned into pDONR207 vector using BP
1100 Clonase (Life Technologies) and then introduced by recombination using LR Clonase (Life
1101 Technologies) into the pBS0046 destination vector, which carries a constitutive *NPTII*
1102 promoter. Specific primers used for the purpose of cloning are listed in Supplementary table 5.
1103 The Ubi.U4::IR-*HRPL* construct, was generated the same way than 35S::IR-*HRPL* but using

1104 Ubi.U4 promoter instead of 35S promoter. The second control vector IR-*LUC* construct was
1105 also generated using the GreenGate technology[76], and is composed of a 250 bp region of the
1106 firefly luciferase under the control of 35S promoter.
1107

1108 **Plant material and growth conditions**

1109 Stable transgenic lines expressing 35S::IR-*CFA6/HRPL*, 35S::IR-*CYP51,* 35S::IR-*LUC* and
1110 35S::IR-*HRPL*, and UbiU4::IR-*HRPL* constructs were generated by transforming Arabidopsis
1111 (Columbia-0 accession, Col-0) plants using the Agrobacterium-mediated-floral dip method[77].
1112 Three independent Arabidopsis T4 transgenic lines expressing the IR-*CFA6/HRPL* hairpin, *#4*,
1113 *#5* and *#10*, two independent Arabidopsis T2 transgenic lines expressing the 35S::IR-*HRPL*
1114 hairpin, *#1* and *#4,* and one reference Arabidopsis T4 transgenic line expressing the IR-*CYP51*
1115 hairpin *#2*, one T3 IR-*LUC* line, one T3 Ubi.U4::IR-*HRPL* line and one Ubi.U4::IR-*HRPL*
1116 *dcl234* line, generated by crossing the Ubi.U4::IR-*HRPL* line with *dcl234* mutant were
1117 generated and used in our experiments. Sterilized seeds of Arabidopsis Col-0 and the selected
1118 homozygous transgenic lines were first grown for 12-14 days at 22°C/ 19°C (day/night) on
1119 plates containing ½ x MS medium (Duchefa), 1% sucrose and 0.8% agar (with or without
1120 antibiotic selection), or in soil, in an 8h photoperiod under a light intensity of 100 µE/m^2/s.
1121 Seedlings were then pricked out to individual soil pots and grown in the same environmentally
1122 controlled conditions described above. Four- to six-week-old plants were used for all the
1123 experiments.
1124

1125 **Bacterial strains**

1126 The *Pto*Δ*cfa6*-GFP (*Pto* DC3118-GFP) strain is a gift from S. Y. He, while the *Pto*Δ*hrpL* strain
1127 is a gift from C. Ramos[78]. The *Pto hrpL-FLAG* and *Pto* pBS181 strains are gifts from M. J.
1128 Filiatrault and S. Cartinhour, respectively[44]. The *Pto*Δ*hrpL* strain expressing the *GFP* reporter

1129 gene was generated by transforming the bacterial mutant strain with the GFP-pPNpt Green
1130 plasmid by electroporation and then plating at 28°C on NYGA medium (5 g L^{-1} bactopeptone,
1131 3 g L^{-1} yeast extract, 20 ml L^{-1} glycerol, 15 g L^{-1} Agar) containing gentamycin (1 µg mL^{-1}) for
1132 selection. To generate the *Pto*Δ*hrpL* expressing WT *HrpL* or mut *HrpL* constructs, the
1133 *Pto*Δ*hrpL* strain was transformed by electroporation with the NPTII::WT-*HrpL* or NPTII::mut-
1134 *HrpL* plasmids. The bacteria were then plated at 28°C on NYGA medium with gentamycin (1
1135 µg mL^{-1}), to select the transformants that were confirmed by PCR using primers specific to
1136 *HrpL* gene.

1137 **Stomatal aperture measurements**

1138 For each indicated genotype, 0.5 cm^2 square sections were dissected from unpeeled leaves of
1139 3 plants and immersed in mock solution (water) or in bacterial suspension at 10^8 cfu mL^{-1}.
1140 After 3 hours, unpeeled leaf sections were stained with 10 µg mL^{-1} propidium iodide (Sigma)
1141 and the abaxial surface was observed with a SP5 or SP8 laser scanning confocal microscope.
1142 The stomatal aperture (width relative to length ratio) was measured using ImageJ software for
1143 at least 90-110 stomata per condition. For RNA and vesicles treatments, the leaf sections were
1144 incubated for one hour with total RNAs (20 ng $µl^{-1}$), P40 pellets, P100-P40 pellets and SN
1145 fractions extracted from specified genotypes, before incubation with the bacteria. In specified
1146 experiments, 1 µM of Coronatine (COR; Sigma) or *in vitro* synthesized sRNAs or long dsRNAs
1147 were supplemented to the bacterial suspension. Two to 5 independent experiments were pooled
1148 in each plot.

1149

1150 **Bacterial dipping assay**

1151 Three hours after the beginning of the night cycle in a growth chamber, three plants per
1152 condition were dip-inoculated with *Pto* DC3000 at 5 x 10^7 cfu mL^{-1} supplemented with 0.02
1153 % Silwet L-77 (Lehle seeds). Plants were then immediately placed in chambers with high

1154 humidity. At two day-post-inoculation, bacterial titers were measured for individual infected
1155 leaves (n=8), using a classical serial dilution method[79].Three independent experiments were
1156 pooled in the same plot.
1157
1158 **Purification of Apoplastic Fluid (APF), Extracellular Vesicles (EVs) and Supernatant**
1159 **Fraction (SN)**
1160 APF extraction was done as previously described[31]. Briefly, 12 to 24 rosettes from 5 to 7-week-
1161 old IR-*CYP51*, IR-*LUC*, IR-*CFA6/HRPL*#4 or IR-*HRPL*#4 plants were vacuum-infiltrated
1162 with vesicle isolation buffer (VIB; 20 mM MES, 2 mM $CaCl_2$, 0.1 M NaCl, pH 6.0). Rosettes
1163 were then placed inside a 20 mL needleless syringe that was inserted in a 50 mL Falcon tube
1164 and centrifuged at 900 g for 15 minutes at 4°C. The apoplastic fluid (APF) was collected and
1165 filtered through a 0.2 µm filter to discard cell debris. The APF was subjected to an
1166 ultracentrifugation step at 40,000 g for 60 min at 4°C giving rise to P40 pellets containing EVs.
1167 The supernatant from P40 pellets was subjected to another ultracentrifugation step at 100,000
1168 g for 60 min at 4°C to collect the P100 pellet. At this step the supernatant contains the lowest
1169 amount of canonical EVs and is named the SN fraction. The P100 pellet, referred to as P100-
1170 P40, was resuspended in VIB for washing and then ultracentrifuged at 100,000g for 60 minutes
1171 at 4°C, and used for further analyses. The size and concentration of EVs from P40 or P100-
1172 P40 pellets and SN fractions were analyzed using the ZetaView NTA instrument (Particle
1173 Metrix). All ultracentrifugations were performed using a swing-out rotor (TST41.14).
1174
1175 **Treatments of P40, P100-P40 pellets and SN fractions**
1176 When indicated, the P40 pellets, the P100-P40 pellets or the SN fractions were treated with
1177 enzymes to digest either RNAs and/or proteins that were not protected by EVs. To eliminate
1178 RNAs, Micrococcal Nuclease (MNase) (Thermo Fisher Scientific) was used at 0.2 U μL^{-1} at

1179 37°C for 15 min. The reaction was stopped with 20 mM EGTA. To digest proteins, Proteinase
1180 K (Thermo Fisher Scientific) was used at 2 U μL^{-1} at 37°C for 15 min. To digest both RNAs
1181 and proteins, MNase was first added to the sample for 15 min at 37°C, inactivated by addition
1182 of EGTA, and then Proteinase K was added for 15 min at 37°C. To disrupt EVs, they were
1183 incubated with 1% of Triton X-100 at room temperature for 1 hour, prior to enzymatic
1184 treatments. For all experiments, a negative control was performed by incubating samples at
1185 37°C without enzyme during the same timeframe as for the enzymatic treatments.
1186
1187 **Extracellular Vesicles observation by Transmission Electron Microscopy (TEM)**
1188 Five µL of P40, P100-P40 pellets or SN fraction were deposited on copper formvar coated,
1189 carbonated grids (Electron Microscopy Sciences - EM-FCF200-CU-SB) and incubated for 20
1190 min at room temperature. Grids were fixed afterwards in 2% paraformaldehyde/ 1%
1191 glutaraldehyde in 100 mM phosphate buffer pH 7.4 for 20 min at room temperature. The grids
1192 were washed 6 times in distilled water for 2 min. For embedding and contrast, grids were next
1193 incubated in a solution of 2% methylcellulose/ 1% uranyl acetate mixed at a 9:1 ratio for 7 min
1194 on ice in the dark. The excess of fluid from the grids was absorbed on a Whatman filter paper
1195 n°1. Grids were air-dried for 1 hour before storage. Observations were performed on a
1196 Transmission Electron Microscope (TEM) TECNAI 12BT 120 kV (ThermoFisher/FEI)
1197 equipped with a CCD Orius 1000 (Gatan) camera. Image acquisition was performed with
1198 DigitalMicrograph. EV diameters were measured using ImageJ software.
1199
1200 **Immunolabelling for Transmission Electron Microscopy (TEM)**
1201 Five µL of P100-P40 pellets were deposited on copper formvar coated, carbonated grids
1202 (Electron Microscopy Sciences - EM-FCF200-CU-SB) and incubated for 20 min at room
1203 temperature. Grids were fixed afterwards in 2% paraformaldehyde in 100 mM phosphate buffer

1204 pH 7.4 for 5 min at room temperature. The grids were washed 3 times in distilled water for 2
1205 min, and next incubated in a solution of 50 mM ammonium chloride in 100 mM phosphate
1206 buffer pH 7.4 for 30 min at room temperature. The grids were washed 3 times in 0.1 % BSA-c
1207 (AURION) in 100 mM phosphate buffer pH 7.4 for 2 min each, and next incubated in the same
1208 buffer supplemented with primary antibody (either antibody against TET8 purchased from
1209 PhytoAB (PHY2750A), or anti-UGPase, purchased from Agrisera) at a 1:50 ratio for 60 min
1210 in a humid chamber at room temperature. The grids were washed 6 times in 0.1 % BSA-c in
1211 100 mM phosphate buffer pH 7.4 for 2 min, then incubated in the same buffer with a 1:20 ratio
1212 of Goat anti-Rabbit (GAR) gold conjugate reagent (6 nm, AURION) for 60 min in a humid
1213 chamber at room temperature in the dark. The grids were washed 6 times in 0.1 % BSA-c in
1214 100 mM phosphate buffer pH 7.4 for 2 min, then washed 3 times in 100 mM phosphate buffer
1215 pH 7.4 for 2 min. Grids were fixed afterwards in 2% glutaraldehyde in 100 mM phosphate
1216 buffer pH 7.4 for 5 min at room temperature. The grids were washed 6 times in distilled water
1217 for 2 min, and next incubated in a solution of 2% Methylcellulose/ 1% uranyl acetate mixed at
1218 a 9:1 ratio for 7 min on ice in the dark for embedding and contrast. The excess of fluid from
1219 the grids was absorbed on a Whatman filter paper °1. Grids were air dried for 3 hours before
1220 storage. Observations were performed on a Transmission Electron Microscope (TEM)
1221 TECNAI 12BT 120 kV (ThermoFisher/FEI) equipped with a CCD Orius 1000 (Gatan) camera.
1222 Image acquisition was performed with DigitalMicrograph.
1223

1224 **Separation of long and small RNA fractions**

1225 From 100 µg of total RNAs extracted with the Tri-reagent (Sigma, St. Louis, MO), long and
1226 small RNA fractions were separated using the mirVana miRNA isolation kit (Ambion®)
1227 according to the manufacturer's instructions. The long and small RNA fractions were

1228 visualized by agarose gel electrophoresis and further analyzed using a Bioanalyzer 2100
1229 (Agilent Technologies).
1230
1231 ***In vitro* synthesis of Inverted Repeat RNAs**
1232 *In vitro* synthesized RNAs were generated following the instructions of the MEGAscript®
1233 RNAi Kit (Life Technologies, Carlsbad, CA). Templates were amplified by PCR using gene
1234 specific primers containing the T7 promoter. PCR amplification was done in two steps with
1235 two different annealing temperatures to increase the specificity of primer annealing. After the
1236 amplification step, PCR products were purified by gel extraction using the PCR Clean-up kit
1237 (Macherey-Nagel) to eliminate any unspecific PCR products. To produce dsRNAs, the purified
1238 PCR products were used as templates for *in vitro* transcription performed according to the
1239 MEGAscript® RNAi Kit instructions. After purification with the filter cartridges, the
1240 corresponding dsRNAs were processed in 18-25 nt sRNA duplexes by incubation with
1241 ShortCut® RNase III (NEB, Ipswich, MA) for 20 min at 37°C. Small RNAs were then
1242 precipitated overnight at -20°C in presence of 3 volumes of 100% EtOH and 0.1 volume of 3
1243 M NaCl, and then were washed once with 70% EtOH. Each step of this process was followed
1244 by gel electrophoresis (TAE 1X, 1% agarose gel for DNA amplification and 2% agarose gel
1245 for RNAs) to verify the quality of RNAs.
1246
1247 **RNA Gel Blot Analyses**
1248 Accumulation of low molecular weight RNAs was assessed by Northern blot analysis as
1249 previously described[80]. Total RNA was extracted using Tri-reagent (Sigma, St. Louis, MO)
1250 according to the manufacturer's instructions and stabilized in 50% formamide. RNA gel blot
1251 analysis of low molecular weight RNAs was performed on 30 µg of total RNAs and as
1252 described previously[80]. Prior to RNA extraction from P40 or P100-P40 pellets, 600 to 700 µL

1253 of those fractions were separated in equal volumes, and each fraction was further treated (with
1254 mock or the enzyme of interest). The corresponding total RNAs were subsequently extracted
1255 as described for total RNA fraction. All the extracted RNAs were loaded on gel for further low
1256 molecular weight northern blot analyses as previously described[80]. Prior to RNA extraction
1257 from SN fraction, 12 mL of SN fraction were separated in 3 equal volumes, each fraction (4
1258 mL) was further treated (with mock or the enzyme(s) of interest), and the corresponding RNAs
1259 were precipitated overnight at -20 °C using 400 µL NaCl 5 M, 12 mL EtOH 100%. RNAs from
1260 the resulting pellets were extracted as described before and loaded on gel for further low
1261 molecular weight northern blot analyses as previously described[80]. Two hundreds nanograms
1262 of total RNAs from IR-*CFA6*/*HRPL*#4 plants were also used as control in the northern blot
1263 experiments in parallel of the SN samples (as shown for instance in Fig. 4e). Detection of U6
1264 RNA was used to confirm equal loading of intracellular RNAs. DNA oligonucleotides
1265 complementary to miR167-5p and U6 sequences were end-labeled with γ-^{32}P-ATP using T4
1266 Polynucleotide Kinase (PNK) (Promega) following the manufacturer's instructions. To detect
1267 anti-*cfa6/hrpL* sRNAs, specific ^{32}P-radiolabeled probes were generated by amplifying regions
1268 of 150 bp to 300 bp with gene specific primers (see Supplementary Table 5) and the amplicons
1269 were labeled by random priming (Prime-a-Gene® Labeling System, Promega). The indicated
1270 probes were hybridized to the same membrane by sequential rounds of probing and stripping.
1271

1272 **P19 pull-down assays to purify sRNAs duplexes**

1273 To pull-down sRNA duplexes, purified MBP-p19 proteins associated with chitin beads were
1274 used. For this purpose, 40 µg of total RNAs, or 2 mL of SN fraction, were resuspended in
1275 binding buffer at a final concentration of: 20 mM Tris-HCl pH 7.0, 100 mM NaCl, 1 mM DTT,
1276 0.1 mg/mL BSA, 1X Protease Inhibitor Cocktail (Sigma Aldrich), and were then incubated
1277 with 100 units of purified MBP-p19-CBD proteins (gift from New England Biolabs) for 1 hour

1278 at room temperature. Forty µL of chitin magnetic beads (NEB) were first blocked overnight at
1279 4°C in 200 µL of pre-treatment buffer (20 mM Tris-HCl pH 7.0, 100 mM NaCl, 1 mM EDTA,
1280 1 mM DTT, 1 mg/mL BSA) before to be added to the sample and were then incubated with
1281 rotation for 1 hour at room temperature. To elute sRNA duplexes bound to p19, the beads were
1282 first washed 5 times in 500 µL of wash buffer (20 mM Tris-HCl pH 7.0, 100 mM NaCl, 1 mM
1283 DTT, 100 µg/mL BSA) and then resuspended in 30 µL of elution buffer (20 mM Tris-HCl pH
1284 7.0, 100 mM NaCl, 0.5% SDS) and incubated for 10 min at 37°C, followed by 10 min at RT
1285 under stirring. The elution step was repeated twice and both elution fractions were pooled. Each
1286 pooled elution fraction was divided into two for the detection of anti-*cfa6*/*hrpL* sRNAs
1287 (Northern blot analysis) and for activity test (stomatal reopening assay).
1288
1289 ***In vitro* bacterial incubation with ATTO 565-labeled anti-*hrpL* sRNA duplexes**
1290 A *Pto* DC3000-GFP culture was grown to OD600nm=0.6. Bacterial cells were harvested by
1291 centrifugation (4000 rpm, 5 min, same settings for all centrifugations in this section), washed
1292 with Milli-Q water, and diluted to OD600nm=0.2. A 200 µl aliquot of this bacterial suspension
1293 was then incubated with 2 µM of anti-*hrpL*-ATTO 565 duplexes in a 24 well-plate at room
1294 temperature on an orbital shaker (heidolph polymax 1040). The incubation was carried out for
1295 24 hours at 20 rpm. Following incubation, bacteria were collected by centrifugation and washed
1296 with Milli-Q water and resuspended in 500 µl of Milli-Q water. To cross-link the bacteria, 1%
1297 formaldehyde was added and incubated for 15 min at room temperature. The bacteria cells
1298 were again pelleted and washed with Milli-Q water and resuspended in 500 µL of Milli-Q
1299 water. A 1/10 dilution of the bacterial suspension was prepared for fluorescence analysis. GFP
1300 fluorescence was observed using a Leica SP8 laser scanning confocal microscope (excitation:
1301 488 nm; emission: 500-550 nm), and ATTO 565 fluorescence was detected (excitation: 565
1302 nm; emission: 580-630 nm).

1303 ***In vitro* bacterial incubation with Salicylic-Acid treated Arabidopsis leaves**

1304 Five-week-old IR-*CYP51* and IR-*CFA6/HRPL*#4 transgenic plants were sprayed with either
1305 water (mock) or SA (2 mM) solution supplemented with 0.02% Silwett. For each condition,
1306 48h after the spray, 8 pieces of 1 cm^2 were cut from 2-3 leaves and incubated in 6-well plates
1307 with 2 mL of *Pto* DC3000 *hrpL-FLAG* at 5 x 10^7 cfu mL^{-1} in *hrpL*-derepressing medium (HDM,
1308 10 mM fructose, 50 mM potassium phosphate buffer, 7.6 mM $(NH_4)_2SO_4$, 1.7 mM NaCl, pH
1309 6.0)[81,82] for 2 hours. Bacterial cells were then collected and *hrpL-FLAG* expression was
1310 assessed at the RNA level, by RT-qPCR analysis, and at the protein level, by western blot
1311 analysis.

1312

1313 **Incubation of bacteria with SN fraction and EDTA treatment**

1314 One mL of *Pto* DC3000 bacteria at OD600nm = 0.4 was incubated with 1 mL of SN from IR-
1315 *CFA6/HRPL#4* plants for 2 hours at room temperature. Then, bacteria were pelleted, washed
1316 with PBS, and resuspended in 400 µL of TSE buffer (0.2 M Tris-HCl pH 8.0, 0.5 M sucrose,
1317 1 mM EDTA) + 100 µL of 0.5 M EDTA to lyse the outer membrane. After a 15 min incubation
1318 at room temperature, bacteria were pelleted and washed with PBS again before RNA
1319 extraction. To assess the effectiveness of EDTA treatment in disrupting the outer membrane,
1320 20 µL of EDTA-treated bacterial suspension were diluted in a final volume of 200 µL H_2O,
1321 containing 1 µL of propidium iodide. The fluorescence of the propidium iodide, bound to
1322 bacterial DNA, was measured using an excitation wavelength of 535 nm and an emission
1323 wavelength of 617 nm. To evaluate the effect of EDTA treatment on bacterial viability, the
1324 treated bacteria were resuspended in 500 µL of H_2O. A 100 µL aliquot of the EDTA-treated
1325 bacteria was inoculated into 500 µL of NYGB medium in a 96-well plate, and optical density
1326 (OD600nm) was recorded 24 hours after inoculation.

1327

1328 **Bacterial RNA extraction and Real Time Quantitative PCR analysis**

1329 Total RNAs from bacterial cells were extracted with Tri-Reagent (Sigma, St. Louis, MO)
1330 according to the manufacturer's instructions, followed by DNAse (RQ1, Promega) digestion
1331 at 37°C to remove the genomic DNA. One µg of total RNA was reverse-transcribed using
1332 RevertAid H minus Reverse Transcriptase (Thermo Fisher Scientific) and random hexamers
1333 according to the manufacturer's instructions. Gene expression was quantified by Real Time-
1334 qPCR, using Takyon SYBR Green Supermix and gene specific primers with the following
1335 parameters: a 384-well optical reaction plate was heated at 95°C for 10 min, followed by 45
1336 cycles of denaturation at 95°C for 10 s, annealing at 60°C for 20 s, and elongation at 72°C for
1337 40 s. A melting curve was performed at the end of the amplification by steps of 1°C (from 95°C
1338 to 50°C). Expression was normalized to that of the bacterial gene *gyrA*. Primer sequences are
1339 listed in Supplementary table 5.

1340

1341 **Protein extraction and western blot analysis**

1342 Total protein extraction from bacterial cells or plant vesicles was done according to Hurckman
1343 & Tanaka[83]. Equal amounts of proteins were resolved on SDS-PAGE in Laemmli buffer and
1344 were then electroblotted on Immobilon®-P PVDF Membrane (Millipore). Membranes were
1345 blocked during 1 hour in a 5% milk solution in 1X PBS-Tween 0.1%, then incubated overnight
1346 at 4°C with specific antibodies. Antibodies against PEN3, UGPase and EF-Tu were purchased
1347 respectively from Agrisera and Hycult Biotech. Antibody against PEN1 was a gift from Prof.
1348 Thordal-Christensen. The next day, membranes were washed 3 times for 10 minutes in PBS-
1349 Tween 0.1% then incubated 2 hours at room temperature in PBS-Tween milk 5% with the
1350 secondary antibody. Membranes were washed again 3 times for 10 minutes in PBS-Tween
1351 0.1% and revelation was performed with Chemicapt ImageQuant400 with Immobilon forte
1352 HRP substrate (Sigma).

1353

1354 **Bioinformatic analysis – Thermodynamic energy analysis**

1355 Unique reads mapping to *cfa6* and *hrpL* genes of *Pto* DC3000 from two sRNA libraries were
1356 used for all BLAST analyses (Supplementary Fig. 1e). The 500 most abundant anti-*cfa6* and
1357 anti-*hrpL* sRNA reads were selected and blasted against annotated Arabidopsis genes
1358 (TAIR10) and *Pto* DC3000 coding sequences (CDS) (-e-value 10, -word_size 4, -ungapped, -
1359 reward 1, -penalty -1)[84]. The free energy of binding for each read paired with its top target was
1360 calculated using RNAup[85]. In Fig. 3c unique reads mapping to the *HrpL* gene of *Pto* DC3000
1361 in the two sRNA libraries presented in Fig. 1d were used for BLAST analysis against the
1362 sequences in Fig. 1c, and the thermodynamic energy analysis was performed as described
1363 earlier. Target prediction was made by aligning the reverse complement of each sRNA against
1364 the *Pto* DC3000 genome using blastn[86] (version 2.12.0+, Parameters: -outfmt 6 -evalue 20 - -
1365 max_hsps 10000 -max_target_seqs 1000 -word_size 4 -ungapped -reward 1 -penalty -1).
1366 Alignments were processed to keep up to 5 mismatches, where wobble pairs (G-U) matches
1367 were considered as a partial (0.5) mismatch. Predicted energy of the RNA-RNA pair between
1368 the sRNA and the target sequence was calculated using RNAup [85].

1369

1370 **Small RNA sequencing**

1371 Small RNA libraries were constructed and sequenced from four- to five-week-old leaves of IR-
1372 *CFA6/HRPL*#4 plants. Raw reads have been deposited at the NCBI SRA under Bioproject
1373 (PRJNA587213). Libraries were mapped against the *Arabidopsis thaliana* genome (v
1374 TAIR10.1 GCF_000001735.4), the IR-*CFA6/HRPL* sequence, and the *Pto* DC3000 genome
1375 using ShortStack (v 3.8.4) and Bowtie2 (v 2.3.4) with parameters --mismatches 0 --dicermin
1376 15 --dicermax 30 --bowtie_m 20 --mmap f[87]. Coverage of mapped loci was obtained with the
1377 Genomic Alignments package in R[88]. Unique reads mapping to *Cfa6* and *HrpL* in both

1378 replicates were extracted and quantified from ShortStack, and results were mapped using
1379 samtools[89].
1380

1381 **References**

1382 1. Cai, Q. *et al.* Plants send small RNAs in extracellular vesicles to fungal pathogen to
1383 silence virulence genes. *Science* **360**, 1126–1129 (2018).
1384 2. Zhang, T. *et al.* Cotton plants export microRNAs to inhibit virulence gene expression
1385 in a fungal pathogen. *Nature Plants* **2**, (2016).
1386 3. Wang, M. *et al.* Bidirectional cross-kingdom RNAi and fungal uptake of external
1387 RNAs confer plant protection. *Nat Plants* **2**, 16151 (2016).
1388 4. Hou, Y. *et al.* A Phytophthora Effector Suppresses Trans-Kingdom RNAi to Promote
1389 Disease Susceptibility. *Cell Host Microbe* (2018) doi:10.1016/j.chom.2018.11.007.
1390 5. He, B. *et al.* RNA-binding proteins contribute to small RNA loading in plant
1391 extracellular vesicles. *Nat. Plants* **7**, 342–352 (2021).
1392 6. Koch, A. *et al.* Host-induced gene silencing of cytochrome P450 lanosterol C14α-
1393 demethylase–encoding genes confers strong resistance to Fusarium species. *PNAS* **110**,
1394 19324–19329 (2013).
1395 7. Koch, A. *et al.* An RNAi-Based Control of Fusarium graminearum Infections
1396 Through Spraying of Long dsRNAs Involves a Plant Passage and Is Controlled by the Fungal
1397 Silencing Machinery. *PLoS Pathog* **12**, (2016).
1398 8. Lopez-Gomollon, S. & Baulcombe, D. C. Roles of RNA silencing in viral and non-
1399 viral plant immunity and in the crosstalk between disease resistance systems. *Nat Rev Mol*
1400 *Cell Biol* **23**, 645–662 (2022).
1401 9. Staiger, D., Korneli, C., Lummer, M. & Navarro, L. Emerging role for RNA-based
1402 regulation in plant immunity. *New Phytologist* **197**, 394–404 (2013).
1403 10. Pumplin, N. & Voinnet, O. RNA silencing suppression by plant pathogens: defence,
1404 counter-defence and counter-counter-defence. *Nat Rev Microbiol* **11**, 745–760 (2013).
1405 11. Bologna, N. G. & Voinnet, O. The Diversity, Biogenesis, and Activities of
1406 Endogenous Silencing Small RNAs in *Arabidopsis*. *Annu. Rev. Plant Biol.* **65**, 473–503
1407 (2014).
1408 12. Liu, L. & Chen, X. Intercellular and systemic trafficking of RNAs in plants. *Nature*
1409 *Plants* **4**, 869–878 (2018).
1410 13. Melnyk, C. W., Molnar, A. & Baulcombe, D. C. Intercellular and systemic movement
1411 of RNA silencing signals. *EMBO J* **30**, 3553–3563 (2011).
1412 14. Guo, Z., Li, Y. & Ding, S.-W. Small RNA-based antimicrobial immunity. *Nat Rev*
1413 *Immunol* **19**, 31–44 (2019).
1414 15. Weiberg, A. *et al.* Fungal Small RNAs Suppress Plant Immunity by Hijacking Host
1415 RNA Interference Pathways. *Science* **342**, 118–123 (2013).
1416 16. Dunker, F. *et al.* Oomycete small RNAs bind to the plant RNA-induced silencing
1417 complex for virulence. *eLife* **9**, e56096 (2020).
1418 17. Ren, B., Wang, X., Duan, J. & Ma, J. Rhizobial tRNA-derived small RNAs are signal
1419 molecules regulating plant nodulation. *Science* **365**, 919–922 (2019).
1420 18. Baulcombe, D. C. VIGS, HIGS and FIGS: small RNA silencing in the interactions of
1421 viruses or filamentous organisms with their plant hosts. *Current Opinion in Plant Biology* **26**,
1422 141–146 (2015).
1423 19. Xin, X.-F., Kvitko, B. & He, S. Y. Pseudomonas syringae: what it takes to be a

1424 pathogen. *Nat Rev Microbiol* **16**, 316–328 (2018).
1425 20. Melotto, M., Underwood, W., Koczan, J., Nomura, K. & He, S. Y. Plant Stomata
1426 Function in Innate Immunity against Bacterial Invasion. *Cell* **126**, 969–980 (2006).
1427 21. Melotto, M., Underwood, W. & He, S. Y. Role of Stomata in Plant Innate Immunity
1428 and Foliar Bacterial Diseases. *Annu Rev Phytopathol* **46**, 101–122 (2008).
1429 22. Bender, C. L., N-Chaidez, F. A. & Gross, D. C. Pseudomonas syringae Phytotoxins:
1430 Mode of Action, Regulation, and Biosynthesis by Peptide and Polyketide Synthetases.
1431 *MICROBIOL. MOL. BIOL. REV.* **63**, 27 (1999).
1432 23. Brooks, D. M. *et al.* Identification and characterization of a well-defined series of
1433 coronatine biosynthetic mutants of Pseudomonas syringae pv. tomato DC3000. *Mol Plant*
1434 *Microbe Interact* **17**, 162–174 (2004).
1435 24. Sreedharan, A., Penaloza-Vazquez, A., Kunkel, B. N. & Bender, C. L. CorR regulates
1436 multiple components of virulence in Pseudomonas syringae pv. tomato DC3000. *Mol Plant*
1437 *Microbe Interact* **19**, 768–779 (2006).
1438 25. Fouts, D. E. *et al.* Genomewide identification of Pseudomonas syringae pv. tomato
1439 DC3000 promoters controlled by the HrpL alternative sigma factor. *Proceedings of the*
1440 *National Academy of Sciences* **99**, 2275–2280 (2002).
1441 26. Plesse, B. *et al.* Effects of the polyubiquitin gene Ubi. U4 leader intron and first
1442 ubiquitin monomer on reporter gene expression in Nicotiana tabacum. *Plant Mol Biol* **45**,
1443 655–667 (2001).
1444 27. Daxinger, L. *et al.* Unexpected silencing effects from T-DNA tags in Arabidopsis.
1445 *Trends Plant Sci* **13**, 4–6 (2008).
1446 28. Mlotshwa, S. *et al.* Transcriptional silencing induced by Arabidopsis T-DNA mutants
1447 is associated with 35S promoter siRNAs and requires genes involved in siRNA-mediated
1448 chromatin silencing. *Plant J* **64**, 699–704 (2010).
1449 29. Vargason, J. M., Szittya, G., Burgyán, J. & Hall, T. M. T. Size Selective Recognition
1450 of siRNA by an RNA Silencing Suppressor. *Cell* **115**, 799–811 (2003).
1451 30. Ye, K., Malinina, L. & Patel, D. J. Recognition of small interfering RNA by a viral
1452 suppressor of RNA silencing. *Nature* **426**, 874–878 (2003).
1453 31. Rutter, B. D. & Innes, R. W. Extracellular Vesicles Isolated from the Leaf Apoplast
1454 Carry Stress-Response Proteins. *Plant Physiol.* **173**, 728–741 (2017).
1455 32. Théry, C., Amigorena, S., Raposo, G. & Clayton, A. Isolation and Characterization of
1456 Exosomes from Cell Culture Supernatants and Biological Fluids. *CP Cell Biology* **30**, (2006).
1457 33. Baldrich, P. *et al.* Plant Extracellular Vesicles Contain Diverse Small RNA Species
1458 and Are Enriched in 10- to 17-Nucleotide "Tiny" RNAs. *The Plant Cell* **31**, 315–324 (2019).
1459 34. Zand Karimi, H. *et al.* Arabidopsis apoplastic fluid contains sRNA- and circular
1460 RNA–protein complexes that are located outside extracellular vesicles. *The Plant Cell* **34**,
1461 1863–1881 (2022).
1462 35. Zhang, K., Hodge, J., Chatterjee, A., Moon, T. S. & Parker, K. M. Duplex Structure
1463 of Double-Stranded RNA Provides Stability against Hydrolysis Relative to Single-Stranded
1464 RNA. *Environ. Sci. Technol.* **55**, 8045–8053 (2021).
1465 36. Koeppen, K. *et al.* Let-7b-5p in vesicles secreted by human airway cells reduces
1466 biofilm formation and increases antibiotic sensitivity of *P. aeruginosa*. *Proc. Natl. Acad. Sci.*
1467 *U.S.A.* **118**, e2105370118 (2021).
1468 37. Alamillo, J. M., Saénz, P. & García, J. A. Salicylic acid-mediated and RNA-silencing
1469 defense mechanisms cooperate in the restriction of systemic spread of plum pox virus in
1470 tobacco. *The Plant Journal* **48**, 217–227 (2006).
1471 38. Campos, L. *et al.* Salicylic acid and gentisic acid induce RNA silencing-related genes
1472 and plant resistance to RNA pathogens. *Plant Physiol Biochem* **77**, 35–43 (2014).
1473 39. Diao, P. *et al.* miR403a and SA Are Involved in NbAGO2 Mediated Antiviral

1474 Defenses Against TMV Infection in Nicotiana benthamiana. *Genes (Basel)* **10**, 526 (2019).
1475 40. Alazem, M., Kim, K.-H. & Lin, N.-S. Effects of Abscisic Acid and Salicylic Acid on
1476 Gene Expression in the Antiviral RNA Silencing Pathway in Arabidopsis. *Int J Mol Sci* **20**,
1477 2538 (2019).
1478 41. Xie, Z., Fan, B., Chen, C. & Chen, Z. An important role of an inducible RNA-
1479 dependent RNA polymerase in plant antiviral defense. *Proc Natl Acad Sci U S A* **98**, 6516–
1480 6521 (2001).
1481 42. Carr, J. P., Lewsey, M. G. & Palukaitis, P. Signaling in induced resistance. *Adv Virus*
1482 *Res* **76**, 57–121 (2010).
1483 43. Lee, W.-S. *et al.* Salicylic acid treatment and expression of an RNA-dependent RNA
1484 polymerase 1 transgene inhibit lethal symptoms and meristem invasion during tobacco
1485 mosaic virus infection in Nicotiana benthamiana. *BMC Plant Biol* **16**, 15 (2016).
1486 44. Lam, H. N. *et al.* Global Analysis of the HrpL Regulon in the Plant Pathogen
1487 Pseudomonas syringae pv. tomato DC3000 Reveals New Regulon Members with Diverse
1488 Functions. *PLoS ONE* **9**, e106115 (2014).
1489 45. Montavon, T. *et al.* A specific dsRNA-binding protein complex selectively sequesters
1490 endogenous inverted-repeat siRNA precursors and inhibits their processing. *Nucleic Acids*
1491 *Res* **45**, 1330–1344 (2017).
1492 46. Max, K. E. A. *et al.* Human plasma and serum extracellular small RNA reference
1493 profiles and their clinical utility. *Proc Natl Acad Sci U S A* **115**, E5334–E5343 (2018).
1494 47. Tosar, J. P. & Cayota, A. Extracellular tRNAs and tRNA-derived fragments. *RNA*
1495 *Biol* **17**, 1149–1167 (2020).
1496 48. Koeppen, K. *et al.* A Novel Mechanism of Host-Pathogen Interaction through sRNA
1497 in Bacterial Outer Membrane Vesicles. *PLoS Pathog* **12**, e1005672 (2016).
1498 49. He, X. *et al.* Human tRNA-Derived Small RNAs Modulate Host–Oral Microbial
1499 Interactions. *J Dent Res* **97**, 1236–1243 (2018).
1500 50. Yang, M. *et al.* Targeting Fusobacterium nucleatum through chemical modifications
1501 of host-derived transfer RNA fragments. *ISME J* **17**, 880–890 (2023).
1502 51. Kusch, S., Singh, M., Thieron, H., Spanu, P. D. & Panstruga, R. Site-specific analysis
1503 reveals candidate cross-kingdom small RNAs, tRNA and rRNA fragments, and signs of
1504 fungal RNA phasing in the barley–powdery mildew interaction. *Molecular Plant Pathology*
1505 **24**, 570–587 (2023).
1506 52. Panstruga, R. & Spanu, P. Transfer RNA and ribosomal RNA fragments - emerging
1507 players in plant-microbe interactions. *New Phytol* **241**, 567–577 (2024).
1508 53. Thompson, A. *et al.* tRex: A Web Portal for Exploration of tRNA-Derived Fragments
1509 in Arabidopsis thaliana. *Plant Cell Physiol* **59**, e1 (2018).
1510 54. Nobori, T. *et al.* Multidimensional gene regulatory landscape of a bacterial pathogen
1511 in plants. *Nat. Plants* **6**, 883–896 (2020).
1512 55. Wang, M., Thomas, N. & Jin, H. Cross-kingdom RNA trafficking and environmental
1513 RNAi for powerful innovative pre- and post-harvest plant protection. *Current Opinion in*
1514 *Plant Biology* **38**, 133–141 (2017).
1515 56. Mi, S. *et al.* Sorting of Small RNAs into Arabidopsis Argonaute Complexes Is
1516 Directed by the 5′ Terminal Nucleotide. *Cell* **133**, 116–127 (2008).
1517 57. Montgomery, T. A. *et al.* Specificity of ARGONAUTE7-miR390 Interaction and
1518 Dual Functionality in TAS3 Trans-Acting siRNA Formation. *Cell* **133**, 128–141 (2008).
1519 58. Yan, Y., Ham, B.-K., Chong, Y. H., Yeh, S.-D. & Lucas, W. J. A Plant SMALL
1520 RNA-BINDING PROTEIN 1 Family Mediates Cell-to-Cell Trafficking of RNAi Signals.
1521 *Mol Plant* **13**, 321–335 (2020).
1522 59. Lühmann, K. L., Seemann, S., Martinek, N., Ostendorp, S. & Kehr, J. The glycine-
1523 rich domain of GRP7 plays a crucial role in binding long RNAs and facilitating phase

separation. *Sci Rep* **14**, 16018 (2024).
60. Buzás, E. I., Tóth, E. Á., Sódar, B. W. & Szabó-Taylor, K. É. Molecular interactions at the surface of extracellular vesicles. *Semin Immunopathol* **40**, 453–464 (2018).
61. Sundaram, K. *et al.* Plant-Derived Exosomal Nanoparticles Inhibit Pathogenicity of Porphyromonas gingivalis. *iScience* **21**, 308–327 (2019).
62. Teng, Y. *et al.* Plant-Derived Exosomal MicroRNAs Shape the Gut Microbiota. *Cell Host Microbe* **24**, 637-652.e8 (2018).
63. Dalakouras, A. *et al.* Delivery of Hairpin RNAs and Small RNAs Into Woody and Herbaceous Plants by Trunk Injection and Petiole Absorption. *Front Plant Sci* **9**, 1253 (2018).
64. Koch, B. L., Rutter, B. D. & Innes, R. W. Arabidopsis produces distinct subpopulations of extracellular vesicles that respond differentially to biotic stress. 2024.04.18.589804 Preprint at https://doi.org/10.1101/2024.04.18.589804 (2024).
65. Li, S. *et al.* MicroRNAs inhibit the translation of target mRNAs on the endoplasmic reticulum in Arabidopsis. *Cell* **153**, 562–574 (2013).
66. Brodersen, P. *et al.* Widespread Translational Inhibition by Plant miRNAs and siRNAs. **320**, 7 (2008).
67. Iwakawa, H. & Tomari, Y. Molecular Insights into microRNA-Mediated Translational Repression in Plants. *Molecular Cell* **52**, 591–601 (2013).
68. Holmqvist, E. & Vogel, J. RNA-binding proteins in bacteria. *Nat Rev Microbiol* **16**, 601–615 (2018).
69. Horman, S. R. *et al.* Akt-mediated phosphorylation of argonaute 2 downregulates cleavage and upregulates translational repression of MicroRNA targets. *Mol Cell* **50**, 356–367 (2013).
70. Jonas, S. & Izaurralde, E. Towards a molecular understanding of microRNA-mediated gene silencing. *Nat Rev Genet* **16**, 421–433 (2015).
71. Mishima, Y. *et al.* Translational inhibition by deadenylation-independent mechanisms is central to microRNA-mediated silencing in zebrafish. *Proc Natl Acad Sci U S A* **109**, 1104–1109 (2012).
72. Larivera, S., Neumeier, J. & Meister, G. Post-transcriptional gene silencing in a dynamic RNP world. *Biol Chem* **404**, 1051–1067 (2023).
73. Dutta, T. & Srivastava, S. Small RNA-mediated regulation in bacteria: A growing palette of diverse mechanisms. *Gene* **656**, 60–72 (2018).
74. Lalaouna, D., Simoneau-Roy, M., Lafontaine, D. & Massé, E. Regulatory RNAs and target mRNA decay in prokaryotes. *Biochimica et Biophysica Acta (BBA) - Gene Regulatory Mechanisms* **1829**, 742–747 (2013).
75. Shen, X. & Corey, D. R. Chemistry, mechanism and clinical status of antisense oligonucleotides and duplex RNAs. *Nucleic Acids Research* **46**, 1584–1600 (2018).
76. Lampropoulos, A. *et al.* GreenGate - A Novel, Versatile, and Efficient Cloning System for Plant Transgenesis. *PLoS ONE* **8**, e83043 (2013).
77. Clough, S. J. & Bent, A. F. Floral dip: a simplified method for Agrobacterium-mediated transformation of Arabidopsis thaliana. *Plant J* **16**, 735–743 (1998).
78. Castillo-Lizardo, M. G. *et al.* Contribution of the non-effector members of the HrpL regulon, iaaL and matE, to the virulence of Pseudomonas syringae pv. tomato DC3000 in tomato plants. *BMC Microbiol* **15**, 165 (2015).
79. Halter, T. *et al.* The Arabidopsis active demethylase ROS1 cis-regulates defense genes by erasing DNA methylation at promoter-regulatory regions. *eLife* https://elifesciences.org/articles/62994 (2021) doi:10.7554/eLife.62994.
80. Navarro, L., Jay, F., Nomura, K., He, S. Y. & Voinnet, O. Suppression of the microRNA pathway by bacterial effector proteins. *Science* **321**, 964–967 (2008).

1574 81. Huynh, T. V., Dahlbeck, D. & Staskawicz, B. J. Bacterial blight of soybean:
1575 regulation of a pathogen gene determining host cultivar specificity. *Science* **245**, 1374–1377
1576 (1989).
1577 82. Peñaloza-Vázquez, A., Preston, G. M., Collmer, A. & Bender, C. L. Regulatory
1578 interactions between the Hrp type III protein secretion system and coronatine biosynthesis in
1579 Pseudomonas syringae pv. tomato DC3000. *Microbiology (Reading)* **146 (Pt 10)**, 2447–2456
1580 (2000).
1581 83. Hurkman, W. J. & Tanaka, C. K. Solubilization of plant membrane proteins for
1582 analysis by two-dimensional gel electrophoresis. *Plant Physiol* **81**, 802–806 (1986).
1583 84. Altschul, S. F. *et al.* Gapped BLAST and PSI-BLAST: a new generation of protein
1584 database search programs. *Nucleic Acids Res* **25**, 3389–3402 (1997).
1585 85. Lorenz, W. A. & Clote, P. Computing the partition function for kinetically trapped
1586 RNA secondary structures. *PLoS One* **6**, e16178 (2011).
1587 86. Camacho, C. *et al.* BLAST+: architecture and applications. *BMC Bioinformatics* **10**,
1588 421 (2009).
1589 87. Axtell, M. J. ShortStack: comprehensive annotation and quantification of small RNA
1590 genes. *RNA* **19**, 740–751 (2013).
1591 88. Lawrence, M. *et al.* Software for computing and annotating genomic ranges. *PLoS*
1592 *Comput Biol* **9**, e1003118 (2013).
1593 89. Li, H. A statistical framework for SNP calling, mutation discovery, association
1594 mapping and population genetical parameter estimation from sequencing data. *Bioinformatics*
1595 **27**, 2987–2993 (2011).
1596

1597
1598 **Acknowledgements**
1599
1600 We thank S.-H. He for providing the *Pto* DC3118-GFP strain, C. Ramos for providing the *Pto*
1601 DC3000 *hrpL* mutant strain, M. J. Filiatrault and S. Cartinhour for providing the *Pto* DC3000
1602 *hrpL-FLAG* strain and *Pto* pBS181, H. Thordal-Christensen for providing PEN1 antibody, L.
1603 Martin-Jaular and F. Cocozza from C. Théry Lab for their help on the use of the NTA, H. Jin
1604 for providing an anti-TET8 antibody, J. Alfano for providing the anti-EF-Tu antibody,
1605 BioRender.com for some illustrations shown in the figures of this article, and members of the
1606 Navarro laboratory for critical reading of the manuscript.

1607 **Funding**

1608 This work was supported by the French funding research agency "L'Agence nationale de la
1609 recherche" ANR-18-CE200020-NEPHRON (to L.N.), ANR-21-CE20-0039-02-SYMBISIL
1610 (to L.N.), European Research Council (ERC) "Silencing & Immunity", grant no. 281749 (to

L.N), A.R. received Ph.D. funding support from CNRS, A.R. and M. S-R received Ph.D. funding supports under the program “Investissements d'Avenir” and implemented by ANR (ANR-10-LABX-54 MEMO LIFE, ANR-10-IDEX-0001-02PSL). O.T., J. Z, and A.E.F. received support from the French programs “Jeune Entreprise Innovante” (JEI) and “Crédit Impôt Recherche” (CIR).

Author contributions

A.R., J.Z., M.S-R., O.T., L.N. designed research; A.R., J.Z., M.C., M.S-R., O.T., A.C. performed research; A.R., J.Z., M.C., M.S-R., O.T., A.E.F., V.M., L.L., generated resources; A.P-Q and L.C. conducted the bioinformatic analyses; A.R., J.Z., M.C., M.S-R., O.T., A.E.F., L.C., L.N. analyzed data; A.R. and L.N. wrote the manuscript; all the authors reviewed and edited the manuscript.

Competing Interest Statement

A.R., M.S-R, M.C., V.M., A.P-Q., A.C. declare no competing interests. J.Z., O.T., A.E.F. were employees of the start-up IRT, and are now employees of ENGreen. L.N. is Research Director at CNRS and co-founder of IRT.

Figure 1

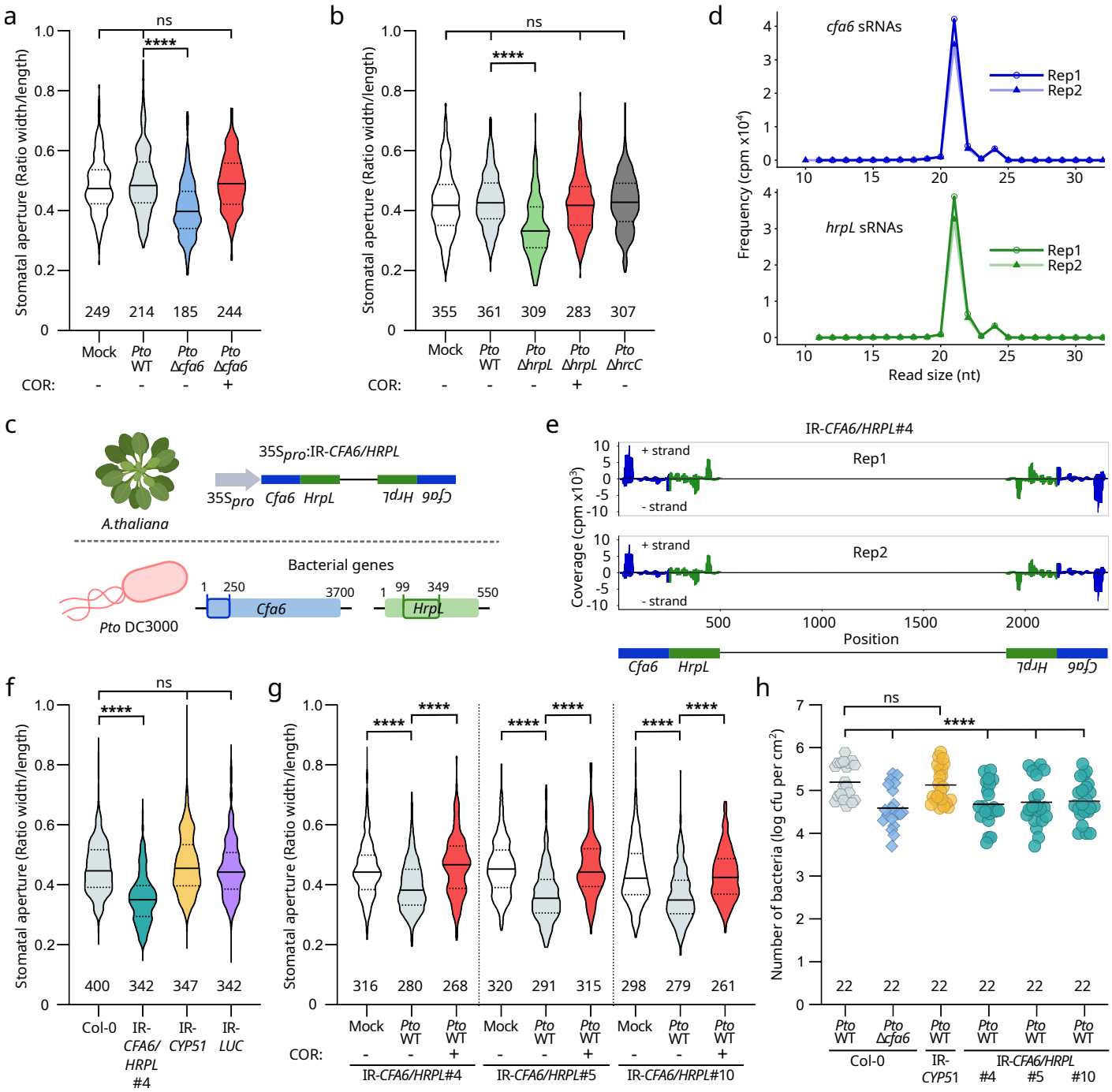
a
Stomatal aperture (Ratio width/length)
ns
****
249 214 185 244
Mock
Pto WT
Pto Δcfa6
Pto Δcfa6
COR: - - - +
b
Stomatal aperture (Ratio width/length)
ns
****
355 361 309 283 307
Mock
Pto WT
Pto ΔhrpL
Pto ΔhrpL
Pto ΔhrcC
COR: - - - + -
d
cfa6 sRNAs
hrpL sRNAs
Rep1
Rep2
Frequency (cpm x10^4)
Read size (nt)
c
A.thaliana
35Spro:IR-CFA6/HRPL
35Spro
Cfa6
HrpL
Pto DC3000
Bacterial genes
Cfa6
HrpL
e
IR-CFA6/HRPL#4
Rep1
Rep2
+ strand
- strand
Coverage (cpm x10^3)
Position
Cfa6
HrpL
f
Stomatal aperture (Ratio width/length)
ns
****
400 342 347 342
Col-0
IR-CFA6/HRPL #4
IR-CYP51
IR-LUC
g
Stomatal aperture (Ratio width/length)
****
316 280 268 320 291 315 298 279 261
Mock
Pto WT
Pto WT
COR: - - + - - + - - +
IR-CFA6/HRPL#4
IR-CFA6/HRPL#5
IR-CFA6/HRPL#10
h
Number of bacteria (log cfu per cm^2)
ns
****
22 22 22 22 22 22
Pto WT
Pto Δcfa6
Pto WT
Pto WT
Pto WT
Pto WT
Col-0
IR-CYP51
IR-CFA6/HRPL
#4
#5
#10

Figure 1. Stable expression of the IR-*CFA6/HRPL* transgene in Arabidopsis reduces *Pto* DC3000 virulence during infection.

a. The coronatine (COR)-defective *Pto*Δ*cfa6* strain is impaired in its ability to reopen stomata and this phenotype is rescued upon exogenous application of COR. Leaf sections of Col-0 plants were treated with mock (water), WT *Pto* DC3000 (*Pto* WT) or *Pto*Δ*cfa6* –with or without COR– and the stomatal aperture response was analyzed at 3 hours post-inoculation (hpi). The concentrations of bacterial strains and of COR were of 10^8 cfu mL^{-1} and 1μM, respectively. The number of stomata analyzed per condition is written underneath each condition and statistical significance was assessed using a one-way ANOVA test (ns: p-value ≥ 0.05; ****: p-value < 0.0001). Similar results were obtained in three independent experiments and are pooled in a single plot. **b.** The *Pto*Δ*hrpL* strain, but not the *Pto*Δ*hrcC* strain, is impaired in its ability to reopen stomata and this phenotype is rescued upon exogenous application of COR. The stomatal aperture assay was conducted as in a. with leaf sections of Col-0 inoculated with *Pto* WT, Δ*hrpL* –with or without COR– and Δ*hrcC* strains. **c.** Schematic representations of the IR-*CFA6*/*HRPL* chimeric hairpin construct stably expressed in Arabidopsis transgenic plants (upper panel), and of the 250 bp regions of the *Cfa6* (1-250 nt, blue box) and *HrpL* (99-349 nt, green box) genes that are targeted by sRNAs in *Pto* DC3000 (bottom panel). **d.** Size distribution and abundance of anti-*cfa6*/*hrpL* sRNA reads along the *CFA6/HRPL* inverted repeat, sequenced from the IR-*CFA6*/*HRPL*#4 plants. **e.** Total sRNA reads that map to the IR-*CFA6*/*HRPL* inverted repeat are depicted. Anti-*cfa6* and anti-*hrpL* sRNAs are shown in blue and green, respectively. **f.** *Pto* DC3000 WT no longer induces stomatal reopening in Arabidopsis IR-*CFA6*/*HRPL* transgenic lines. Stomatal aperture measurements were conducted on leaf sections of IR-*CFA6/HRPL*#4, IR-*CYP51* and IR-*LUC* lines infected with *Pto* WT, as described in a. **g.** The impaired stomatal reopening phenotypes observed in IR-*CFA6*/*HRPL* lines are rescued upon application of exogenous COR. Stomatal aperture measurements were conducted on leaf sections of IR-*CFA6/HRPL*#4, #5, #10 lines infected with *Pto* WT, as described in a., with or without COR. **h.** Arabidopsis IR-*CFA6/HRPL* lines exhibit reduced *Pto* WT titers when compared to Col-0 and IR-*CYP51*-infected plants at 2 days post-infection (dpi). Five to six-week-old Col-0, IR-*CYP51* and IR-*CFA6/HRPL*#4, #5 and #10 plants were dip-inoculated, at a concentration of 5 x 10^7 cfu mL^{-1}, with *Pto* WT-GFP. As a control condition, Col-0 plants were treated at the same concentration with *Pto*Δ*cfa6*-GFP. Number of leaf disc analyzed is written underneath each condition. Data from three independent experiments are pooled in a single plot. Statistical significance was assessed using a two-way ANOVA test (ns: p-value>0.05; ****: p-value<0.0001).

Figure 2

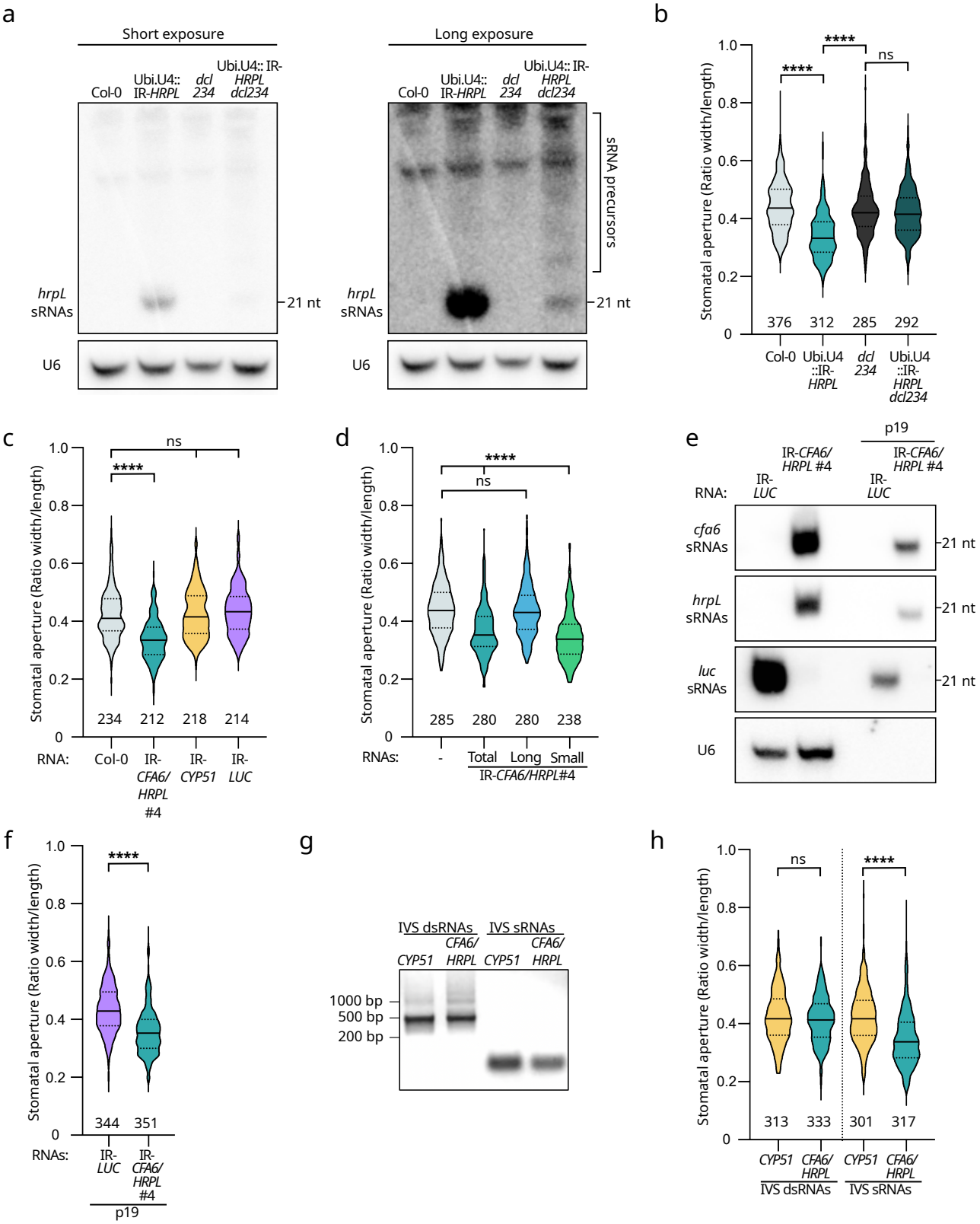
a
Short exposure
Long exposure
Col-0
Ubi.U4:: IR-HRPL
dcl 234
Ubi.U4:: IR-HRPL dcl234
hrpL sRNAs
21 nt
U6
sRNA precursors
b
Stomatal aperture (Ratio width/length)
****
ns
376 312 285 292
Col-0 Ubi.U4 ::IR-HRPL dcl 234 Ubi.U4 ::IR-HRPL dcl234
c
234 212 218 214
RNA: Col-0 IR-CFA6/HRPL #4 IR-CYP51 IR-LUC
d
285 280 280 238
RNAs: - Total Long Small
IR-CFA6/HRPL#4
e
p19
IR-CFA6/HRPL #4
RNA: IR-LUC
cfa6 sRNAs
hrpL sRNAs
luc sRNAs
f
344 351
RNAs: IR-LUC IR-CFA6/HRPL #4
g
IVS dsRNAs
IVS sRNAs
CYP51 CFA6/HRPL
1000 bp
500 bp
200 bp
h
313 333 301 317
CYP51 CFA6/HRPL
IVS dsRNAs
IVS sRNAs

Figure 2. Antibacterial sRNA species, but not unprocessed dsRNAs, are causal for the suppression of *Pto* DC3000-triggered stomatal aperture.

a. Accumulation level of anti-*hrpL* sRNAs in Col-0, Ubi.U4 IR-*HRPL*, *dcl2-1 dcl3-1 dcl4-2* (*dcl234*), and Ubi.U4 IR-*HRPL* in *dcl234* mutant background (Ubi.U4 IR-*HRPL dcl234*) was assessed by low molecular weight northern blot analysis. The northern blot results, obtained from the same membrane, are shown at two different expositions: short (left) and long (right). The long exposition was depicted to better visualize unprocessed forms of dsRNA precursors, referred to as "sRNA precursors" in the panel. Because the same membrane was used to obtain the results shown in panel a, the same U6 loading control This is one representative experiment out of the three independent experiments performed. **b.** Ubi.U4 IR-*HRPL dcl234* plants do not suppress *Pto* DC3000-induced stomatal reopening response. The stomatal reopening assay was conducted on leaf sections of the same genotypes detailed in a. and as described in Fig 1a. Similar results were obtained in three independent experiments and are pooled in a single plot. The number of stomata analyzed per condition is written underneath each condition and statistical significance was assessed using a one-way ANOVA test (ns: p-value ≥ 0.05; ****: p-value < 0.0001). **c.** Twenty ng μl^{-1} of total RNA from IR-*CFA6/HRPL#4* but not IR-*LUC* and IR-*CYP51* prevents stomatal reopening. Col-0 leaf sections were incubated with total RNA from Col-0, IR-*CFA6/HRPL#4,* IR-*LUC* or IR-*CYP51* and stomatal reopening assay was performed as in b. Similar results were obtained in two independent experiments and are pooled in a single plot. **d.** Small RNA species, but not corresponding long RNA species, from IR-*CFA6/HRPL*#4 plants suppress *Pto* DC3000-induced stomatal reopening. The stomatal reopening assay was conducted with *Pto* DC3000 and by incubating Col-0 leaf sections with total, long (> 200 nt) or small (< 200 nt) RNA fractions, separated from total RNAs of IR-*CFA6/HRPL*#4 plants. Similar results were obtained in three independent experiments and are pooled in a single plot. **e.** Accumulation of anti-*cfa6*/*hrpL* sRNAs in IR-*CFA6/HRPL*#4 and IR-*LUC* total RNAs before or after p19 pull-down was detected by low molecular weight northern blot analysis. U6 was used as a control of intracellular RNAs. This is one representative experiment out of the three independent experiments performed. **f.** P19 pulled-down sRNAs from the IR-*CFA6/HRPL*#4 total RNAs suppress the ability of *Pto* DC3000 to reopen stomata. Stomatal aperture assay was conducted as in b. Statistical significance was assessed using Student's *t*-test (****: p-value<0.0001). Similar results were obtained in three independent experiments and are pooled in a single plot. **g.** Agarose gel picture of ethidium bromide-stained *in vitro* synthesized (IVS) long dsRNAs and sRNA duplexes. **h.** *In vitro* synthesized anti-*cfa6*/*hrpL* sRNAs*,* but not cognate unprocessed dsRNA precursors, suppress *Pto* DC3000-triggered stomatal reopening. The stomatal reopening assay was conducted as in b. Similar results were obtained in three independent experiments and are pooled in a single plot.

Figure 3

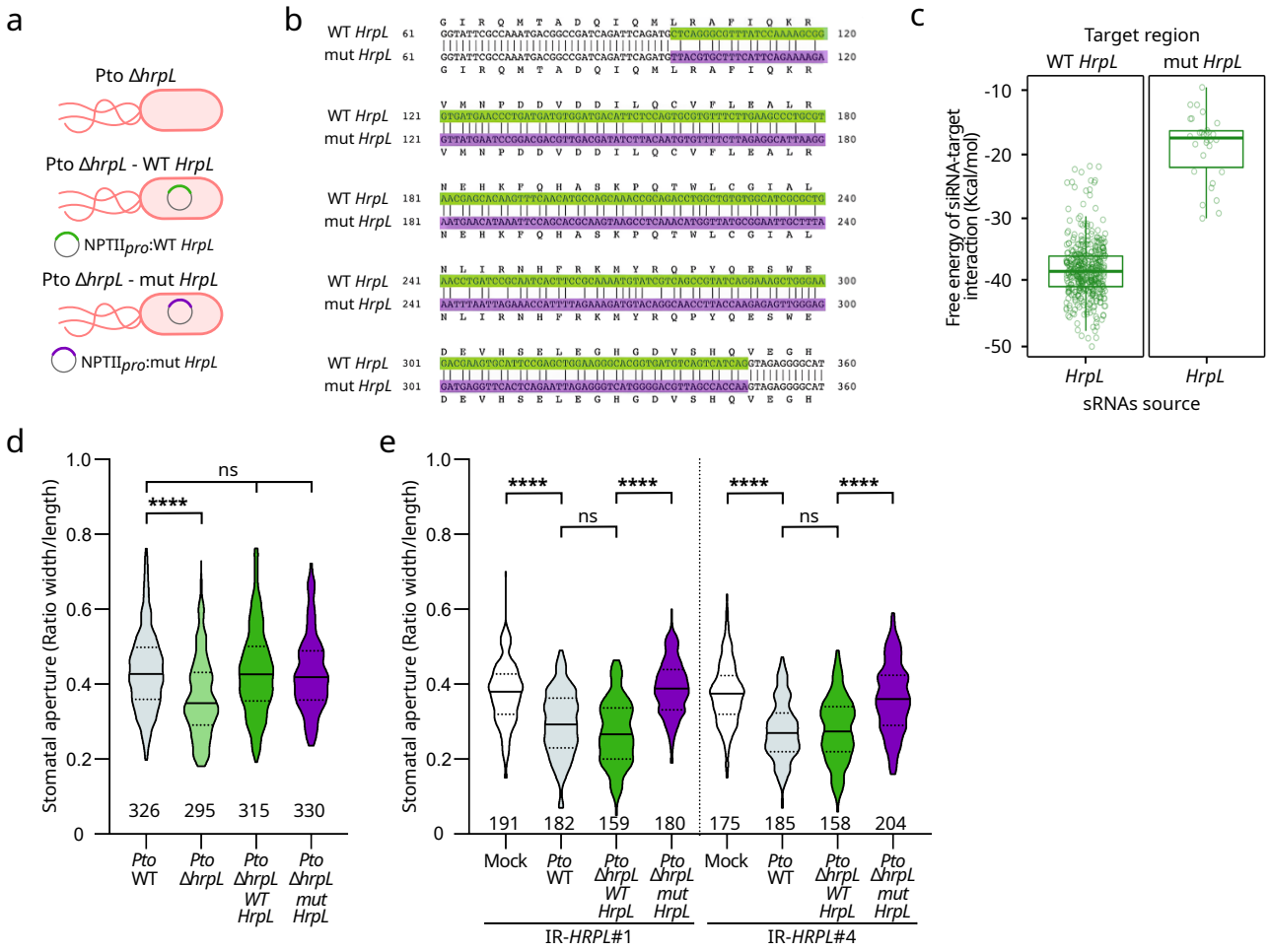
a
Pto ΔhrpL
Pto ΔhrpL - WT HrpL
NPTIIpro:WT HrpL
Pto ΔhrpL - mut HrpL
NPTIIpro:mut HrpL
b
WT HrpL
mut HrpL
c
Target region
WT HrpL
mut HrpL
Free energy of siRNA-target interaction (Kcal/mol)
HrpL
HrpL
sRNAs source
d
Stomatal aperture (Ratio width/length)
ns
****
326
295
315
330
Pto WT
Pto ΔhrpL
Pto ΔhrpL WT HrpL
Pto ΔhrpL mut HrpL
e
Stomatal aperture (Ratio width/length)
****
ns
191
182
159
180
175
185
158
204
Mock
Pto WT
Pto ΔhrpL WT HrpL
Pto ΔhrpL mut HrpL
IR-HRPL#1
IR-HRPL#4

Figure 3. Anti-*hrpL* sRNAs are causal for the suppression of stomatal reopening

a. Schematic representation of *Pto*Δ*hrpL* and of the recombinant strains expressing either the WT *HrpL* or mut *HrpL* constructs, under the control of the constitutive *NPTII* promoter. **b.** The sequence of WT *HrpL* (99-349 nt) selected to generate the inverted repeat transgene (highlighted in green) was aligned with the sequence of mutated *HrpL* (mut *HrpL*) designed to contain as many silent mutations as possible in the sRNA targeted region (highlighted in purple). **c.** Thermodynamic energy analysis of sRNA-target interactions between anti-*hrpL* sRNAs and the WT or mutated *HrpL* sequence versions. **d.** Both the WT *HrpL* and mut *HrpL* constructs fully complemented *PtoΔhrpL* for its ability to reopen stomata. Col-0 leaves were incubated with *PtoΔhrpL*, *PtoΔhrpL* WT *HrpL* and *PtoΔhrpL* mut *HrpL* bacterial strains. Stomatal reopening response was assessed as described previously. Statistical significance was assessed using a one-way ANOVA test (ns: p-value ≥ 0.05; ****: p-value < 0.0001). Similar results were obtained from three independent experiments and the data are pooled in a single plot. **e.** The *Pto*Δ*hrpL* mut *HrpL* strain is refractory to anti-*hrpL* sRNAs action at 3 hpi. The stomatal reopening assay was conducted as in d., IR-*HRPL*#1 and #4 leaf sections were treated with mock (water) or the indicated bacteria at a concentration of 10^8 cfu mL^{-1}. Results of two independent experiments are pooled in a single plot. Statistical significance was assessed using a one-way ANOVA test (ns: p-value>0.05; ****: p-value<0.0001).

Figure 4

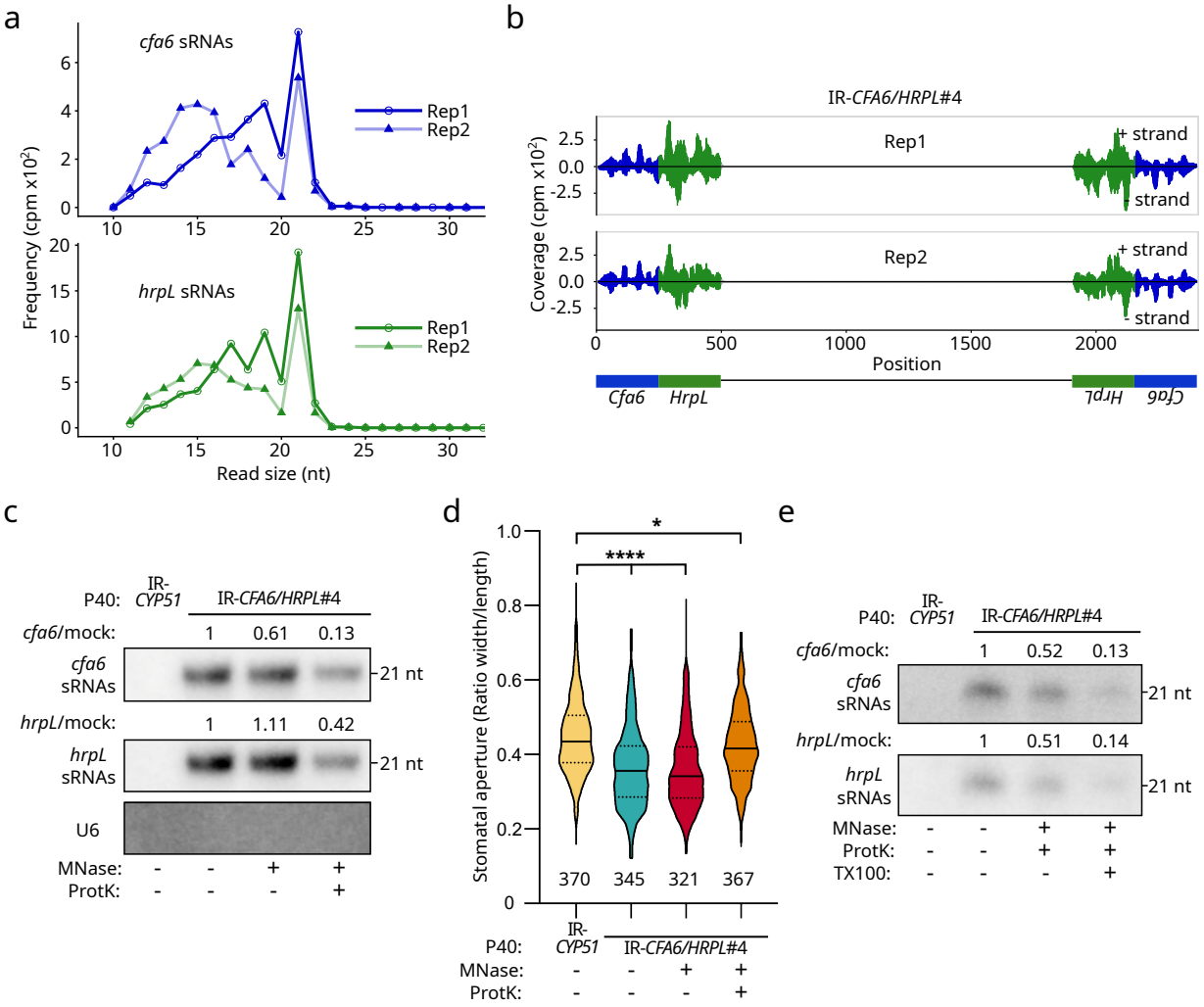
a
cfa6 sRNAs
Rep1
Rep2
hrpL sRNAs
Rep1
Rep2
Frequency (cpm x10²)
Read size (nt)
b
IR-CFA6/HRPL#4
Rep1
Rep2
+ strand
- strand
Coverage (cpm x10²)
Position
Cfa6
HrpL
c
P40: IR-CYP51 IR-CFA6/HRPL#4
cfa6/mock: 1 0.61 0.13
cfa6 sRNAs
21 nt
hrpL/mock: 1 1.11 0.42
hrpL sRNAs
21 nt
U6
MNase: - - + +
ProtK: - - - +
d
Stomatal aperture (Ratio width/length)
*
****
370 345 321 367
P40: IR-CYP51 IR-CFA6/HRPL#4
MNase: - - + +
ProtK: - - - +
e
P40: IR-CYP51 IR-CFA6/HRPL#4
cfa6/mock: 1 0.52 0.13
cfa6 sRNAs
21 nt
hrpL/mock: 1 0.51 0.14
hrpL sRNAs
21 nt
MNase: - - + +
ProtK: - - + +
TX100: - - - +

Figure 4. A pool of anti-*cfa6*/*hrpL* sRNAs, associated to proteins that are located outside EVs, suppresses *Pto* DC3000-triggered stomatal reopening.

a. Size distribution and abundance of anti-*cfa6*/*hrpL* sRNA reads from MNase-treated P40 pellets of IR-*CFA6/HRPL*#4 plants. **b.** Small RNA reads from the P40 pellets of IR-*CFA6*/*HRPL*#4 plants that map to the *CFA6*/*HRPL* inverted repeat are depicted. Anti-*cfa6* and anti-*hrpL* sRNAs are shown in blue and green, respectively. **c.** Anti-*cfa6*/*hrpL* sRNAs accumulation is reduced when the P40 pellets of IR-*CFA6*/*HRPL*#4 plants were treated with MNase and ProtK. The P40 pellets from IR-*CFA6*/*HRPL*#4 plants were treated with mock, MNase or MNase plus ProtK, and the accumulation of anti-*cfa6*/*hrpL* sRNAs was analyzed by northern blot analysis. P40 pellets from untreated IR-*CYP51* plants were used as a negative control. The membrane was also probed with U6 to make sure that the P40 fractions were not contaminated by intracellular RNAs. The band intensities of *cfa6 /hrpL* siRNAs were quantified using ImageJ. Band intensities were normalized to the expression level of the mock condition. The results are shown above each blot. This is one representative experiment out of the three independent experiments performed. **d.** The ability of *Pto* DC3000 to reopen stomata is impaired in response to P40 pellets from IR-*CFA6*/*HRPL*#4 plants, and this effect is compromised in the presence of P40 pellets treated with MNase and Proteinase K (ProtK). The stomatal reopening assay was performed on Col-0 leaf sections incubated with IR-*CFA6/HRPL*#4 or IR-*CYP51*-derived P40 pellets that were subjected to different enzymatic treatments. Statistical significance was analyzed using a one-way ANOVA test (ns: p-value ≥ 0.05; *: $0.05 >$ p-value ≥ 0.01; ****: p-value < 0.0001). Similar results were obtained in three independent experiments and are pooled in a single plot. **e.** Anti-*cfa6* and anti-*hrpL* sRNAs accumulation is significantly reduced after MNase, ProtK and Triton X100 (TX100) treatments. Accumulation of sRNAs in IR-*CFA6/HRPL*#4- and IR-*CYP51*-derived P40 pellets was detected by northern blot analysis. The band intensities of *cfa6/hrpL* siRNAs were quantified using ImageJ. Band intensities were normalized to the expression level of the mock condition. The results are shown above each blot. This is one representative experiment out of the two independent experiments performed.

Figure 5

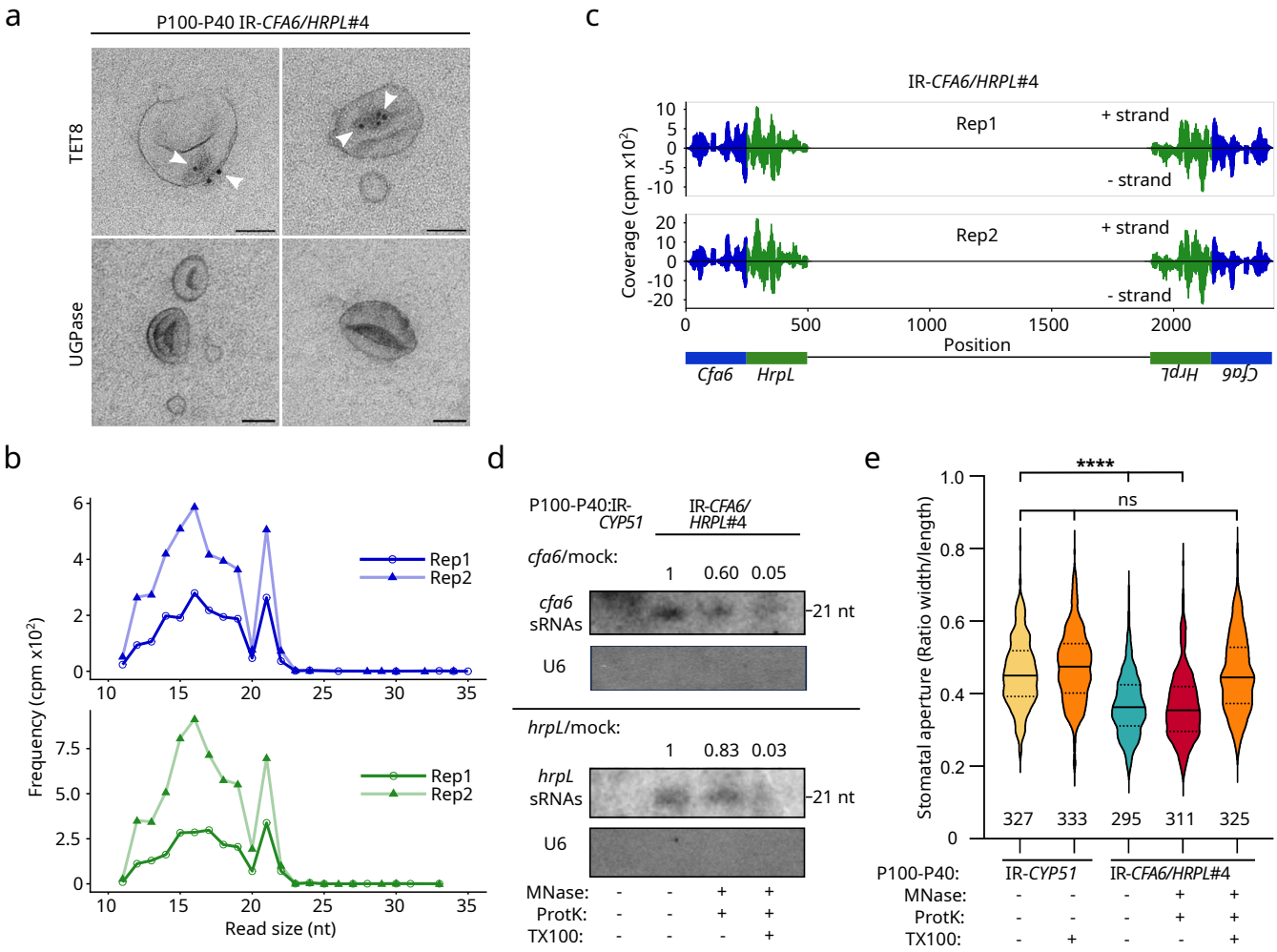
a
P100-P40 IR-CFA6/HRPL#4
TET8
UGPase
c
IR-CFA6/HRPL#4
Rep1
Rep2
+ strand
- strand
Coverage (cpm x10²)
Position
Cfa6
HrpL
b
Rep1
Rep2
Frequency (cpm x10²)
Read size (nt)
d
P100-P40:IR-CYP51
IR-CFA6/HRPL#4
cfa6/mock:
1 0.60 0.05
cfa6 sRNAs
21 nt
U6
hrpL/mock:
1 0.83 0.03
hrpL sRNAs
MNase:
ProtK:
TX100:
e
****
ns
Stomatal aperture (Ratio width/length)
327 333 295 311 325
P100-P40:
IR-CYP51
IR-CFA6/HRPL#4
MNase:
ProtK:
TX100:

Figure 5. A pool of anti-*cfa6*/*hrpL* sRNAs, likely located inside TET8-positive EVs, suppresses *Pto* DC3000-triggered stomatal aperture

a. P100-P40 pellets contain TET8-positive EVs. EVs were visualized through TEM analysis, using native anti-TET8 (PhytoAB, PHY2750A) or UGPase (Agrisera) primary antibodies, followed by detection with a gold-conjugated secondary antibody. White arrows indicate the presence of gold beads. Scale bar: 50 nm. **b.** Size distribution and abundance of anti-*cfa6*/*hrpL* sRNA reads from MNase-treated P100-P40 pellets of IR-*CFA6/HRPL*#4 plants. **c.** Small RNA reads from the P100-P40 pellets of IR-*CFA6*/*HRPL*#4 plants that map to the *CFA6*/*HRPL* inverted repeat are depicted. Anti-*cfa6* and anti-*hrpL* sRNAs are shown in blue and green, respectively. **d.** Anti-*cfa6*/*hrpL* sRNAs accumulation is reduced when P100-P40 pellets of IR-*CFA6*/*HRPL*#4 plants were treated with TX100, MNase and ProtK. The P100-P40 pellets from IR-*CFA6*/*HRPL*#4 plants were treated with mock, MNase plus ProtK, or TX100 plus MNase plus ProtK and the accumulation of anti-*cfa6*/*hrpL* sRNAs was detected by northern blot analysis. P40 pellets from untreated IR-*CYP51* plants were used as a negative control. The membranes used were hybridized with either the *cfa6* probe (upper panel) or the *hrpL* probe (bottom panel). Of note, it was not possible to sequentially probe the same membrane with the *cfa6* and *hrpL* probes because of low abundance of these sRNAs from P100-P40 pellets. The band intensities of *cfa6/hrpL* sRNAs were quantified using ImageJ. Band intensities were normalized to the expression level of the mock condition. The results are shown above each blot. The membranes were also probed with U6 to make sure that the P100-P40 fractions were not contaminated by intracellular RNAs. **e.** The ability of *Pto* DC3000 to reopen stomata is impaired in response to P100-P40 pellets from IR-*CFA6*/*HRPL*#4 plants, and this effect is compromised when these P100-P40 pellets were treated with MNase, ProtK and TX100. Stomatal aperture measurements were performed on Col-0 leaf sections incubated with IR-*CFA6/HRPL*#4 or IR-*CYP51*-derived P100-P40 pellets that were subjected to different enzymatic treatments. Statistical significance was analyzed using a one-way ANOVA test (ns: p-value ≥ 0.05; ****: p-value < 0.0001). Similar results were obtained in three independent experiments and are pooled in a single plot.

Figure 6

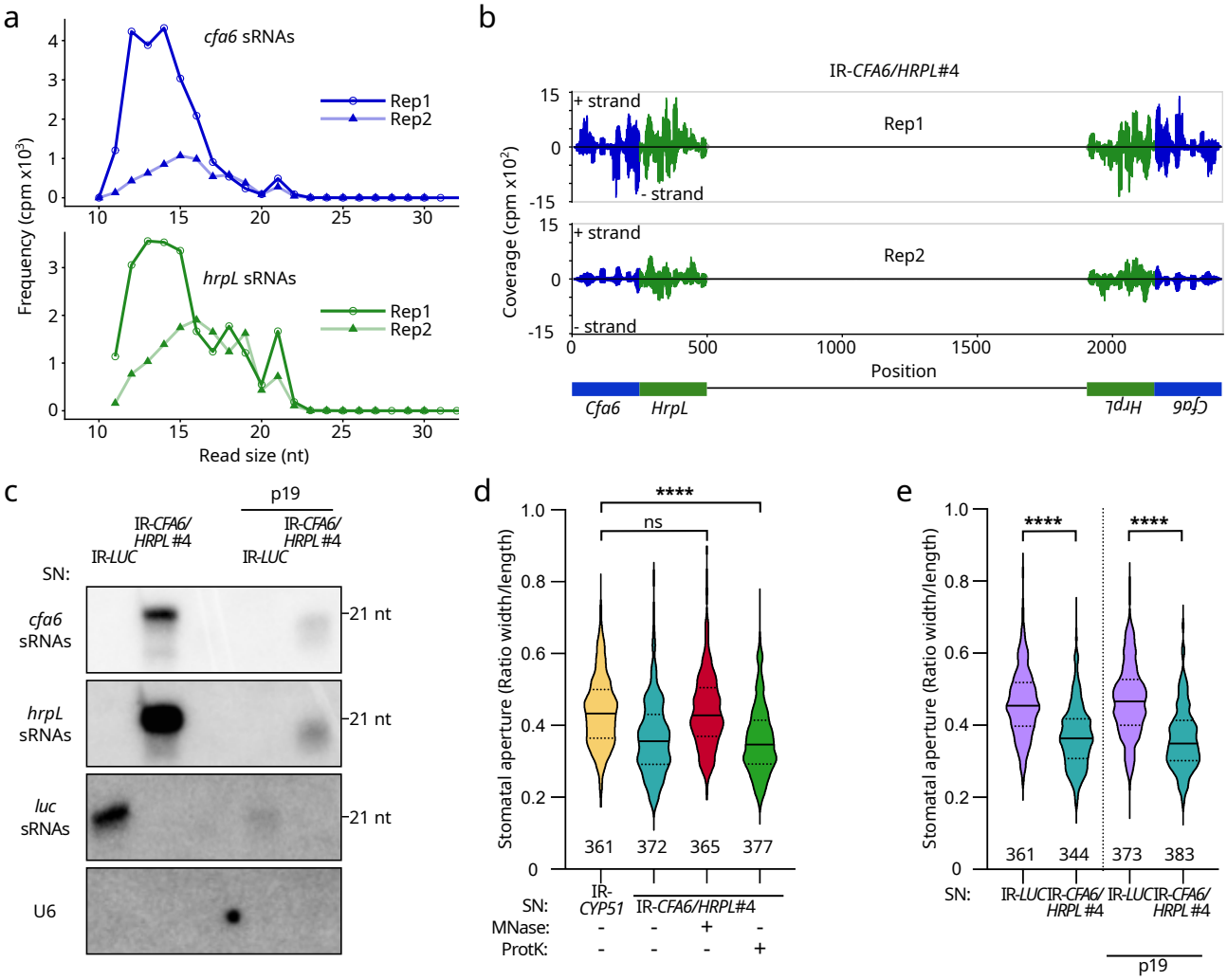
a
cfa6 sRNAs
Rep1
Rep2
hrpL sRNAs
Frequency (cpm x10³)
Read size (nt)
b
IR-CFA6/HRPL#4
+ strand
- strand
Rep1
Rep2
Coverage (cpm x10²)
Position
Cfa6
HrpL
c
p19
IR-CFA6/ HRPL #4
IR-LUC
SN:
cfa6 sRNAs
hrpL sRNAs
luc sRNAs
U6
21 nt
d
****
ns
Stomatal aperture (Ratio width/length)
361
372
365
377
IR-CYP51
IR-CFA6/HRPL#4
MNase:
ProtK:
e
****
361
344
373
383
IR-LUC
IR-CFA6/ HRPL #4
p19

Figure 6. Extracellular free anti-*cfa6*/*hrpL* sRNA duplexes are recovered from SN fraction and harbour anti-virulence activity

a. Size distribution and abundance of anti-*cfa6*/*hrpL* sRNA reads from the SN fraction of IR-*CFA6/HRPL*#4 plants. **b.** Accumulation of anti-*cfa6*/*hrpL* sRNAs in IR-*CFA6/HRPL*#4 and IR-*LUC*-derived SN fractions before or after p19 pull-down assay was detected by northern blot analysis. U6 was used as a control of intracellular RNA. The membrane was also probed with U6 to make sure that the SN fractions were not contaminated with intracellular RNAs. This is one representative experiment out of the two independent experiments performed. **c.** Small RNA reads from the SN fraction of IR-*CFA6*/*HRPL*#4 plants that map to the *CFA6*/*HRPL* inverted repeat are depicted. Anti-*cfa6* and anti-*hrpL* sRNAs are shown in blue and green, respectively. **d.** The SN fraction from IR-*CFA6*/*HRPL*#4 plants prevents *Pto* DC3000-induced stomatal reopening, and this effect is abolished upon treatment of this APF fraction with MNase. Statistical significance was assessed using a one-way ANOVA test (ns: p-value ≥ 0.05; ****: p-value < 0.0001). Similar results were obtained in three independent experiments and are pooled in a single plot. **e.** P19 pulled-down sRNAs from the IR-*CFA6/HRPL*#4 SN fraction suppress *Pto* DC3000-induced stomatal reopening. The stomatal reopening assay was conducted as in c. Statistical significance was assessed using Student's t-test (****: p-value<0.0001). Similar results were obtained in three independent experiments and are pooled in a single plot.

Figure 7

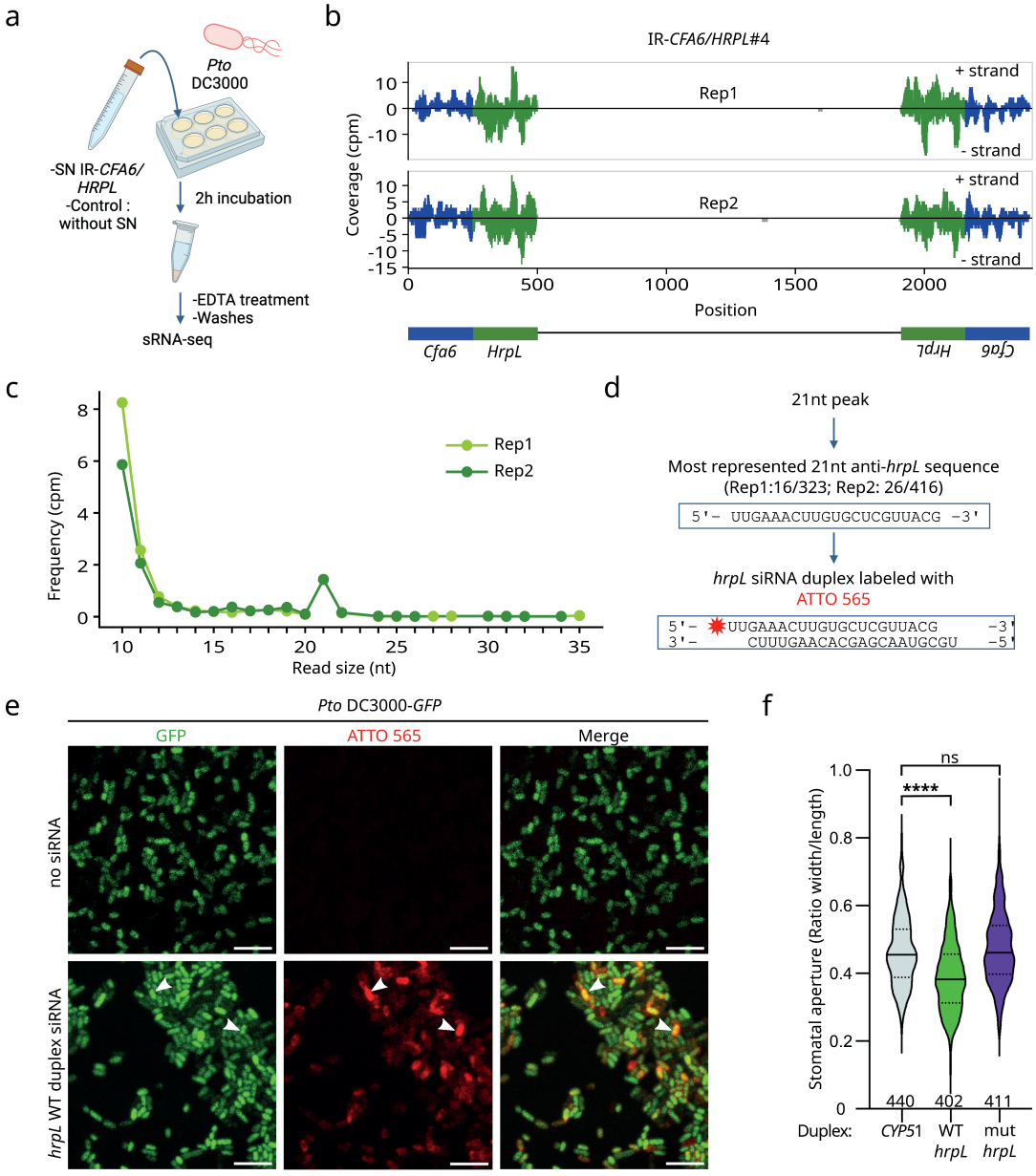
a
Pto
DC3000
-SN IR-CFA6/
HRPL
-Control :
without SN
2h incubation
-EDTA treatment
-Washes
sRNA-seq
b
IR-CFA6/HRPL#4
Rep1
Rep2
+ strand
- strand
Coverage (cpm)
Position
Cfa6
HrpL
c
Rep1
Rep2
Frequency (cpm)
Read size (nt)
d
21nt peak
Most represented 21nt anti-hrpL sequence
(Rep1:16/323; Rep2: 26/416)
5'- UUGAAACUUGUGCUCGUUACG -3'
hrpL siRNA duplex labeled with
ATTO 565
5'- UUGAAACUUGUGCUCGUUACG -3'
3'- CUUUGAACACGAGCAAUGCGU -5'
e
Pto DC3000-GFP
GFP
ATTO 565
Merge
no siRNA
hrpL WT duplex siRNA
f
ns
****
Stomatal aperture (Ratio width/length)
440
402
411
Duplex:
CYP51
WT hrpL
mut hrpL

Figure 7. A subset of SN-derived anti-*hrpL* sRNAs is internalized by *Pto* DC3000 cells

a. Schematic representation of the experimental set-up employed to sequence sRNAs that are internalized by *Pto* DC3000. Bacterial cells were either incubated in VIB or in SN, derived from SA-treated IR-*CFA6/HRPL*#4 plants (see methods), for two hours before collection of the cells and washing with EDTA. Total RNAs were further extracted and used for sRNA-seq. **b.** Internalized sRNA reads that map to the *CFA6*/*HRPL* inverted repeat are depicted. Anti-*cfa6* and anti-*hrpL* sRNAs are shown in blue and green, respectively. **c.** Size distribution and abundance of anti-*cfa6*/*hrpL* sRNA reads. **d.** The most represented 21nt anti-*hrpL* sequence is framed in blue on top of the panel, with occurrence numbers for both replicates shown above it. Below is depicted the corresponding duplex version labeled with ATTO 565 (red star) in the 5' end of the anti-*hrpL* sRNA strand that is complementary to *HrpL* mRNAs. **e.** Imaging of *Pto* DC3000-*GFP (*green) incubated with the *hrpL* duplex labeled with ATTO 565 (red). White arrows highlight examples of signals co-localization between ATTO 565 and GFP. Scale bar: 5 µm. **f.** WT *hrpL* duplexes but not *CYP51*, nor mut *hrpL* duplexes, suppress *Pto* DC3000-induced stomatal reopening. The stomatal aperture measurements were performed on Col-0 leaf sections incubated with sRNA duplexes. Statistical significance was analyzed using a one-way ANOVA test (ns: p-value ≥ 0.05; ****: p-value < 0.0001). Similar results were obtained in three independent experiments and are pooled in a single plot.

Figure 8

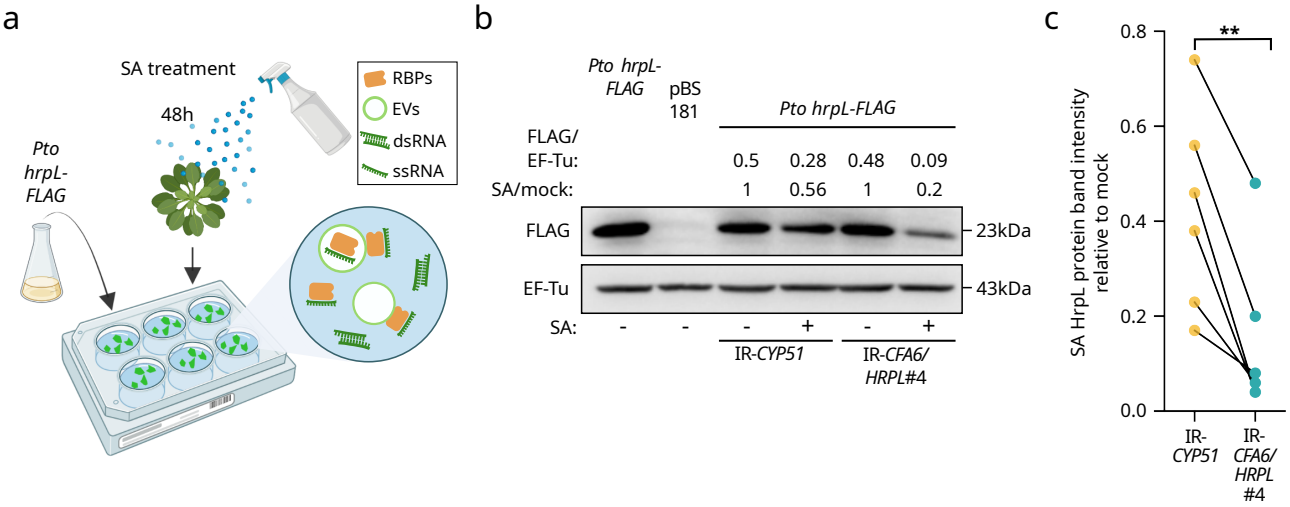
a
SA treatment
48h
Pto hrpL-FLAG
RBPs
EVs
dsRNA
ssRNA
b
Pto hrpL-FLAG
pBS 181
Pto hrpL-FLAG
FLAG/ EF-Tu:
0.5
0.28
0.48
0.09
SA/mock:
1
0.56
1
0.2
FLAG
23kDa
EF-Tu
43kDa
SA:
-
-
-
+
-
+
IR-CYP51
IR-CFA6/ HRPL#4
c
SA HrpL protein band intensity relative to mock
0.8
0.6
0.4
0.2
0.0
**
IR-CYP51
IR-CFA6/ HRPL #4

Figure 8. The accumulation of HrpL proteins is reduced in *Pto* DC3000 cells incubated with leaf sections of salicylic acid-treated IR-*CFA6*/*HRPL*#4 plants

a. Schematic representation of the experimental set-up employed to expose *Pto* DC3000 cells to plant-derived extra-cellular/organismal sRNAs. IR-*CFA6/HRPL*#4 or IR-*CYP51* plants were sprayed with SA (2 mM) for 48 hours prior to the experiment, and leaf sections from those plants were further incubated with a *Pto* DC3000 strain expressing a Flag-tagged version of *HrpL*, namely the *Pto* DC3000 *hrpL-FLAG* strain[44]. Some possible extra-cellular/organismal sRNA populations are illustrated in the circle. RBPs, EVs, dsRNA and ssRNA, stand for RNA-Binding Proteins, Extracellular Vesicles, double-stranded RNA and single-stranded RNA, respectively. **b**. Western blot analysis showing the reduction in the accumulation of HrpL proteins upon incubation of the *Pto* DC3000 *hrpL-FLAG* strain with leaf sections of SA-treated IR-*CFA6/HRPL*#4 plants, compared to leaf sections of IR-*CYP51* plants treated in the same condition. The accumulation of the elongation factor EF-Tu served as loading control. *Pto* DC3000 pBS181 contains the empty expression vector pBS181 and served as a negative control. This is one representative experiment out of the six independent experiments performed. **c.** Plot depicting the band intensity of *Pto* DC3000 *hrpL-FLAG* protein levels normalized to corresponding EF-Tu bands. IR-*CYP51* or IR-*CFA6/HRPL*#4 SA-treated ratios were then further normalized to IR-*CYP51* and IR-*CFA6*/*HRPL*#4 mock condition ratios, respectively. Similar results were obtained in six independent experiments and the data are pooled in a single plot. Statistical significance was assessed using Student's paired t-test (ns: p-value ≥ 0.05).

Figure 9

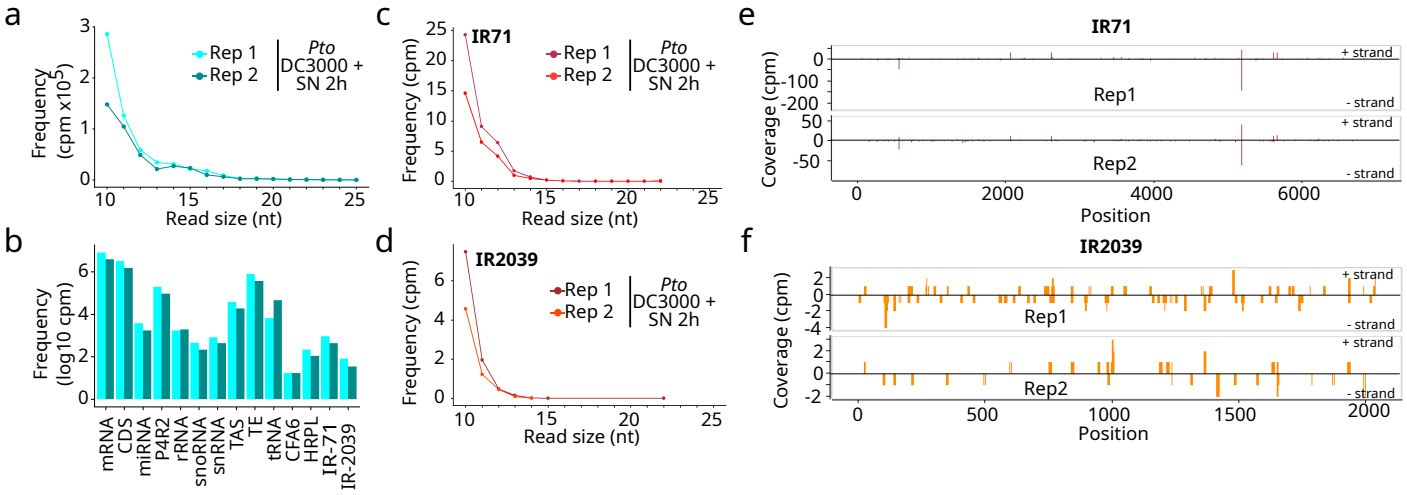

g

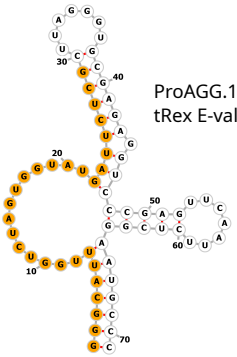

ProAGG.17
tRex E-value: 1e-11

h

	Minimal free energy (kcal/mol)	Putative targets
3'-gctcttagtatggtgatctggtttacggg-5' tRF ...|o.|..|o.||||o||.||||||||| 5'-GCUGGCUGCUGGCACUGGAGCAAAUGCCC-3' priA	-26.12	Primosomal protein N'
3'-gctcttagtatggtgatctggtttacggg-5' tRF .||.|...o||||||.o|||||||||o. 5'-GGAAAUCAGUACCACAGGACCAAAUGCUG-3' PSPTO_5016	-29.22	Proline permease
3'-gctcttagtatggtgatctggtttacggg-5' tRF o...|o||o||||||.||||.||..|| 5'-UACCAGUCGUACCACUCGACCAUAUUGCC-3' PSPTO_4296	-28.18	Metabolite-proton symporter

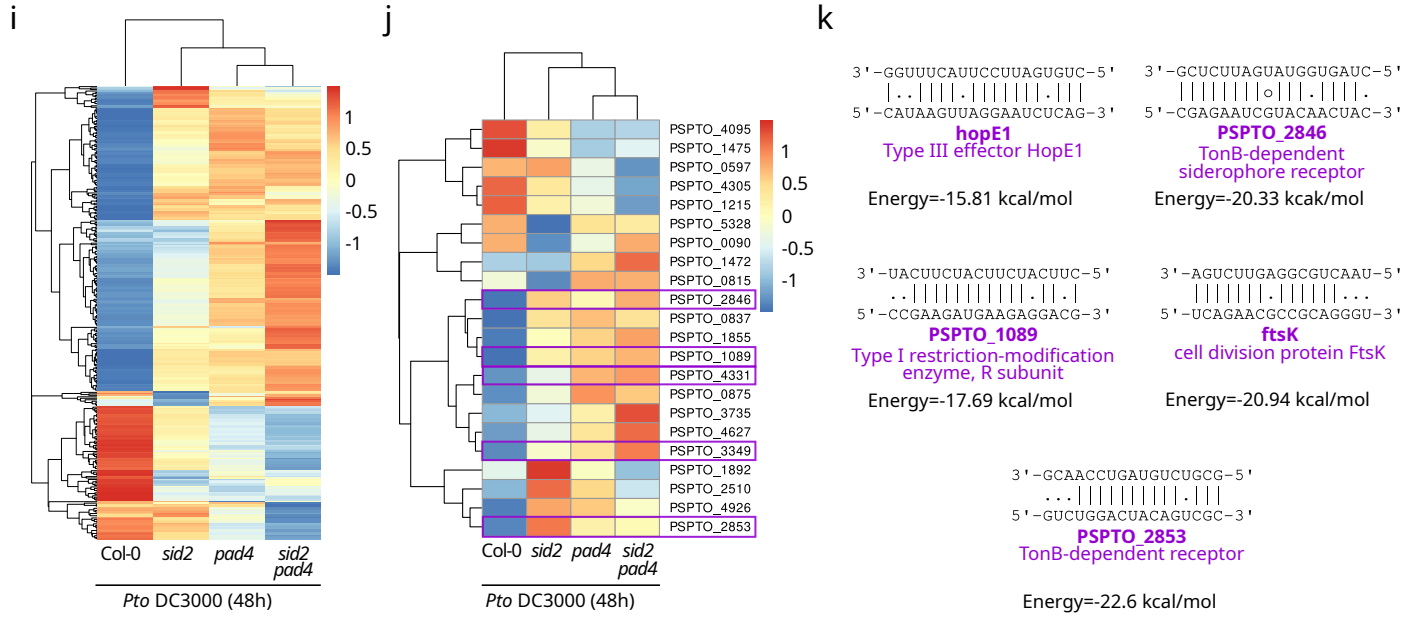

Figure 9. Endogenous sRNAs, from the SN of SA-treated IR-*CFA6/HRPL*#4 plants, are transferred into the cytoplasm of *Pto* DC3000 cells

a. Size distribution of all the endogenous sRNAs that were recovered in *Pto* DC3000 cells. SN fractions from SA-treated IR-*CFA6*/*HRPL*#4 plants were incubated for 2 hours with *Pto* DC3000 cells (*Pto* DC3000 + SN 2h), and the internalized endogenous sRNAs analyzed using the second stringent filter (see methods). **b.** Class repartition of reads after the second filtering step. **c.** Size distribution of reads mapping to IR71 after the second filtering step. **d.** Size distribution of reads mapping to IR2039 after the second filtering step. **e, f.** Coverage of sRNAs on IR71 (e) and IR2039 (f) after the second filtering step. **g.** RNA-fold structure of ProAGG.17. The most represented tRNA sequence from our filtered samples is highlighted in orange. **h.** Examples of predicted *Pto* DC3000 targets of the tRF highlighted in g. The three best predictions according to the minimal free energy value are represented. **i.** Three hundred seven *Pto* DC3000 SA-responsive proteins were predicted to be targets of internalized sRNAs. The heatmap depicts their accumulation in Col-0, *sid2*, *pad4* and *sid2 pad4* that were infected for 48 hours with *Pto* DC3000[54]. Z-score normalized (by row) values based on protein accumulation values reported in Nobori *et al*.[54] **j.** Twenty-two of the SA-responsive proteins corresponded to targets of the top 100 most represented internalized sRNA reads. Their accumulation in Col-0-, *sid2*-, *pad4*- and *sid2 pad4*-infected plants is shown in the heatmap. **k.** Representation of some candidate sRNA-Target pairings corresponding to internalized sRNAs predicted to target mRNAs, whose protein levels are down-regulated in Col-0-infected plants but no longer repressed in *sid2*-, *pad4*-, and/or *pad4*/*sid2*-infected plants (from the 5 purple framed candidates depicted in j.).

Figure 10

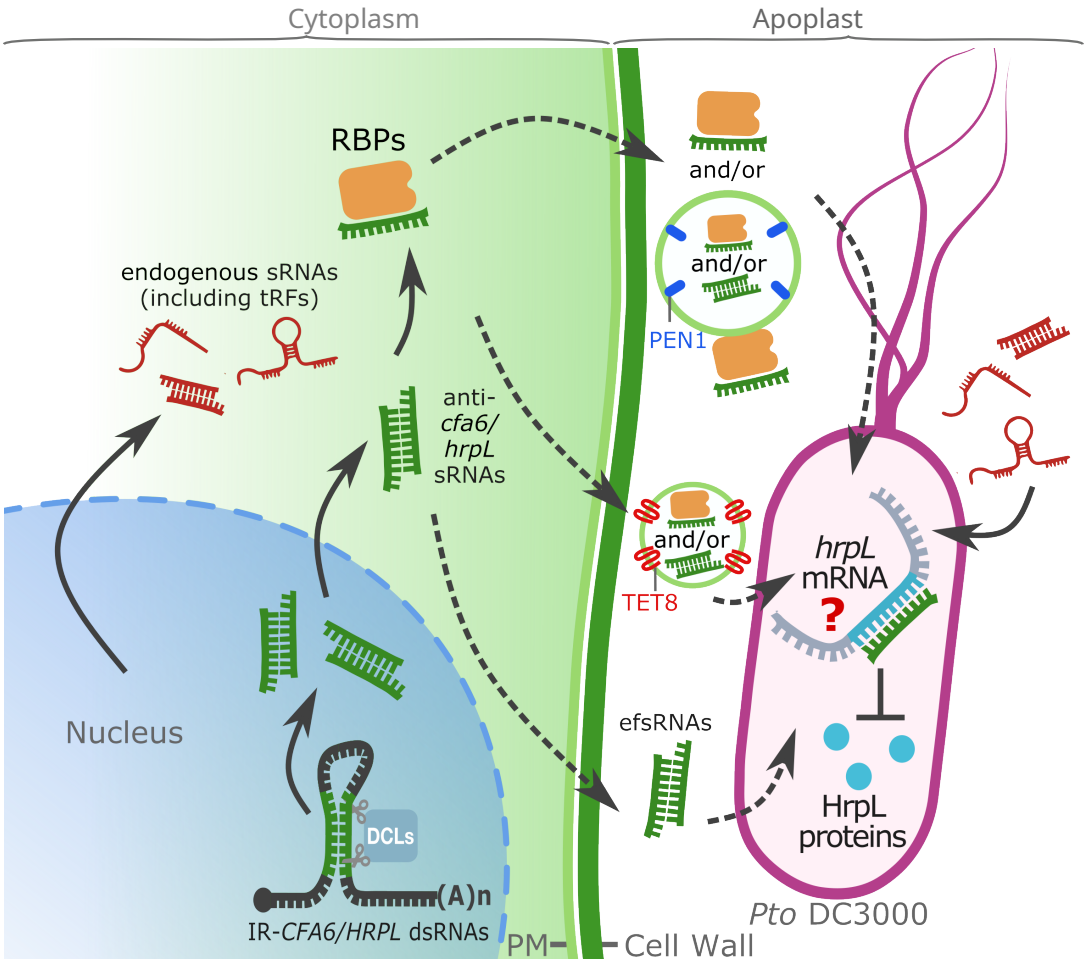
Cytoplasm
Apoplast
RBPs
endogenous sRNAs
(including tRFs)
anti-
cfa6/
hrpL
sRNAs
and/or
and/or
PEN1
and/or
TET8
hrpL
mRNA
?
efsRNAs
HrpL
proteins
Nucleus
DCLs
(A)n
IR-CFA6/HRPL dsRNAs
PM
Cell Wall
Pto DC3000

Figure 10. Model depicting the extracellular sRNA populations that are active against *Pto* DC3000 and/or internalized by these bacterial cells

Model depicting the characterized Arabidopsis-encoded artificial sRNA species directing gene silencing in interacting *Pto* DC3000 cells. The Arabidopsis IR-*CFA6/HRPL*#4 transgenic plants produce an inverted repeat transcript that is processed by DCL proteins into anti-*cfa6/hrpL* sRNAs (in green). The cytoplasmic anti-*cfa6/hrpL* sRNA species are further incorporated into protein complexes containing RNA Binding Proteins (RBPs), or potentially present in a free and dsRNA form in the cytosol, or in EVs. Both sRNA species are then exported in the apoplast through unknown mechanisms (dashed arrows). Three populations of active anti-*cfa6/hrpL* sRNAs have been characterized in this study: a first pool that is bound to proteins, which are either non-associated to PEN1-positive EVs, or potentially located on their surface. A second pool of sRNAs that is presumably located inside TET8-positive EVs, and a third pool that is unbound to proteins and in a free and dsRNA form, named efsRNAs. Active plant extracellular-sRNA species (*e.g.* anti-*hrpL* sRNAs), are subsequently transferred towards *Pto* DC3000 cells (dashed arrows), to direct sequence-specific gene silencing of *hrpL* through as-yet unknown mechanisms. Finally, the model depicts the endogenous sRNAs (in red), produced from various Arabidopsis endogenous genomic origins, including specific tRFs, which are internalized by *Pto* DC3000 cells.